Distribution Agreement

In presenting this thesis or dissertation as a partial fulfillment of the requirements for an advanced degree from Emory University, I hereby grant to Emory University and its agents the non-exclusive license to archive, make accessible, and display my thesis or dissertation in whole or in part in all forms of media, now or hereafter known, including display on the world wide web. I understand that I may select some access restrictions as part of the online submission of this thesis or dissertation. I retain all ownership rights to the copyright of the thesis or dissertation. I also retain the right to use in future works (such as articles or books) all or part of this thesis or dissertation. Signature:

_____ _____

Matthew T. Geballe Date

Part I: Structure and Function in the NMDA Ligand Binding Domain

Part II: Comparison of Paclitaxel Analogs through Molecular Dynamics Simulation; Solution Conformations of Cyclic Peptides

By

Matthew T. Geballe
Doctor of Philosophy

Chemistry

Dr. Dennis C. Liotta
Advisor

Dr. Justin P. Gallivan
Committee Member

Dr. James T. Kindt
Committee Member

Dr. David G. Lynn
Committee Member

Accepted:

Lisa A. Tedesco, Ph.D.
Dean of Graduate School

Date

Part I: Structure and Function in the NMDA Ligand Binding Domain

Part II: Comparison of Paclitaxel Analogs through Molecular Dynamics Simulation; Solution Conformations of Cyclic Peptides

By

Matthew T. Geballe
B.S., Pacific Lutheran University, 2002

Advisor: Dennis C. Liotta, Ph.D.

An abstract of
a dissertation submitted to the Faculty of the Graduate School of Emory University in partial fulfillment of the requirements for the degree of Doctor of Philosophy

Chemistry

2009

Abstract

Part I: Structure and Function in the NMDA Ligand Binding Domain

Part II: Comparison of Paclitaxel Analogs through Molecular Dynamics Simulation; Solution Conformations of Cyclic Peptides

By Matthew T. Geballe

Part I:

The NMDA receptor is an ionotropic glutamate receptor found throughout the CNS. The receptor functions as a tetramer comprised of two NR1 subunits and two NR2 subunits. There are four subtypes of NR2, NR2A through NR2D, and functional properties of the assembled receptor vary with the identity of the NR2 subunits. The ligand binding domain of this receptor binds either the agonist glutamate or co-agonist glycine, and triggers the gating process which allows ions to flow through the channel. Crystal structures of the ligand binding domain have recently been solved, and these structures provided the basis for molecular dynamics simulations of ligand binding domains of different NR2 subtypes. Structures of different NR2 ligand binding domains were prepared by homology modeling, and simulations were performed of just the NR2 ligand binding domain, as well as simulation of the ligand binding domain dimer of NR1/NR2. Comparison of simulations of different subtypes as well as the same subtype with different ligands bound reveal structural differences and changes that may shed light on how the receptor functions.

Part II:

The dynamic equilibrium between free α,β-tubulin and assembled microtubules plays a important role in cellular structure. Alteration of this equilibrium by paclitaxel (PTX) and other similar compounds is a critical method of anti-cancer treatment, and recently analogs were discovered that induce polymerization at levels much greater than paclitaxel. These analogs were placed into a crystal structure of α,β-tubulin with PTX and subjected to molecular dynamics simulation. Over the simulation the analogs induced changes in the critical M-loop and strengthened theories of how the M-loop facilitates tubulin polymerization.

A cyclic pentapeptide was analyzed using NAMFIS (NMR Analysis of Molecular Flexibility In Solution), a method which combines NMR data and modeling-based conformational searching. This peptide was well-studied in the literature, providing an opportunity to evaluate NAMFIS alongside other methods for predicting conformations of small molecules in solution. NAMFIS was able to identify the conformations previously found, as well as a few new conformations that may be necessary to recreate the NMR data accurately.

Part I: Structure and Function in the NMDA Ligand Binding Domain

Part II: Comparison of Paclitaxel Analogs through Molecular Dynamics Simulation; Solution Conformations of Cyclic Peptides

By

Matthew T. Geballe
B.S., Pacific Lutheran University, 2002

Advisor: Dennis C. Liotta, Ph.D.

A dissertation submitted to the Faculty of the Graduate School of Emory University in partial fulfillment of the requirements for the degree of Doctor of Philosophy

Chemistry

2009

Acknowledgements

I would like to begin by thanking Dr. Dennis Liotta and Dr. Jim Snyder for guiding me through my graduate career. They have given me guidance, scientific support, and direction while allowing me the freedom to pursue my interests and passions. I believe my scientific career will be influenced by the stimulating "initial conditions" I experienced here. Thanks are also owed to my committee members Dr. Justin Gallivan, Dr. James Kindt, and Dr. David Lynn, who provided scientific support and encouragement to think for myself and continue to push my research farther and do good science.

My appreciation goes out to my many collaborators as well, especially Dr. Stephen Traynelis, who in many ways has been an unofficial advisor to me. Every computational chemist needs collaborators with whom to work in synergy, and Dr. Traynelis has always been an eager and astute partner. I am also indebted to Dr. David Wyllie, Dr. Kevin Erreger, Dr. Shashank Dravid, Dr. Anders Kristensen, Dr. Kasper Hansen, Dr. Philip Chen, and Dr. Low as well as all the members of Dr. Traynelis' lab at Emory for their patience and support in collaborating with me, providing excellent data, and aiding in my education about the NMDA receptor. Additionally, I'd like to thank Dr. Susan Bane and Natasha Shanker for their collaboration on the tubulin work. Dr. Yesim Tahirovic, Rose Santangelo and Cara Mosley were wonderful synthetic collaborators that I was lucky to work with in our lab.

No one could survive graduate school without a strong support system of friends, and I have been fortunate to have wonderful friends within our lab. I need to thank previous members of the Liotta group such as Dr. Ben Cornett, Dr. Ami Shah, Dr. Jim Nettles, Dr. Pahk Thepchatri, and Serdar Kurtkaya for their friendship and guidance. Current members of the Modeling Lab have also been wonderful to work alongside, especially Ana Alcaraz, Ashutosh Jogalekar, Andy Prussia. My thanks also goes out to Mark Baillie for his continued friendship and support.

Lastly but most importantly, I would like to express my gratitude to my family, my parents and especially my wife Rebecca, whose love, support, dedication, and encouragement carried me through many a rough patch. You are an integral part in any of my success.

> "My most brilliant achievement was my ability to be able to persuade my wife to marry me."
>
> — Winston Churchill

Table of Contents

List of Figures

List of Tables

Chapter 1

Introduction

> "If you can find a path with no obstacles, it probably doesn't lead anywhere."
>
> — Frank A. Clark

The conformations that a protein takes in solution and the dynamic paths that allow conversion between these conformations are intimately tied to the biological function of any protein or peptide. Internal motions of proteins play a role in critical processes such as the binding and release of ligands, association and dissociation with other proteins, and catalysis of chemical reactions. The combination of structural information with understanding of the dynamics of a protein facilitate a fundamental insight into how a protein performs its biological function. This deep degree of knowledge can further future scientific pursuits and open the door to directed protein engineering or design.

The use of theory to predict, simulate, and drive understanding of the natural world can be applied to the realm of protein conformations in solution. This work focuses on the use of computational methods to simulate and predict how proteins and peptides exist in solution. Although different systems call for different methods, in each area of research the objective remains to understand how predicted conformations affect protein function. Every endeavor involving prediction or simulation necessitates a firm grounding in experiment, and in each case caution is applied to maintain a corroboration with experimental data.

Part 1 focuses on the use of molecular dynamics simulations to probe structural differences between different subtypes of NR2 ligand binding domains of the N-methyl-D-aspartate (NMDA) receptor, as well as evaluating the effects of different ligands on the structure of the ligand binding domain (LBD). Chapter 2 provides a functional

and structural introduction to this ligand-gated ion channel, and highlights recent advances in structural understanding that provide the starting point for our simulations. Published simulations of related proteins as well as potential drawbacks to a molecular dynamics approach are also discussed. Chapter 3 describes our initial simulations of only the NR2 LBD, both based on a homology model derived from the NR1 crystal structure and then subsequent simulations of models constructed from the NR2A crystal structure. These include the first simulations directly comparing two different subtypes, NR2A and NR2D, and identify a particular region of interest that varies between the simulations. The transition to simulations of the NR1/NR2 ligand binding domain dimer are covered in Chapter 4. With the adjacent NR1 ligand binding domain providing a stabilizing interface, structural distinctions between simulations of different NR2 subunits are evaluated with greater confidence. Additionally, placement of different ligands in both the NR1 or NR2 domain is observed to induce changes in the positioning of some structural elements of the protein. Finally, Chapter 5 summarizes the results of the simulations, examines experimental evidence for corroboration of the structural differences drawn from the models, and theorizes about how these differences may modulate the overall function of the receptor.

Part 2 covers two other projects involving conformations in solution. Chapter 6 details the molecular dynamics simulation of several different taxanes within the α,β-tubulin dimer. These simulations attempt to provide structural insight into the in-

creased ability of some of the compounds to induce tubulin polymerization. Finally, Chapter 7 details the application of NAMFIS (NMR Analysis of Molecular Flexibility In Solution), a method widely used in our lab over the years, to examine the predicted conformations of a cyclic pentapeptide. This particular peptide is of interest due to a extended debate in the literature regarding the presence of a particular conformation with a γ-turn. This debate spurred the collection of high quality NMR measurements as well as independent molecular dynamics simulations, providing an excellent opportunity to validate NAMFIS on a well-studied molecule.

Part I

Structure and Function in the
NMDA Ligand Binding Domain

Chapter 2

The NMDA Receptor

> "We occasionally stumble over the truth but most of us pick ourselves up and hurry off as if nothing had happened."
>
> — Winston Churchill

The NMDA receptor is a ligand-gated ion channel distributed throughout the central nervous system. A member of the family of ionotropic glutamate receptors which include the AMPA and kainate receptors, it derives its name from a selective agonist, N-methyl-D-aspartate, shown in Figure 2.1.[1] The receptor is activated by binding of both glutamate and glycine, which results in opening of the ion channel, allowing cations (predominantly calcium at the synapse) to flow through the channel, and is responsible for the slow component of excitatory postsynaptic current within the glutamatergic system. The NMDA receptor plays a critical role in synaptic plasticity, learning, motor coordination, and memory, and its disfunction has been implicated in a wide variety of neurologic conditions including epilepsy, ischemic stroke, schizophrenia, neuropathic pain, and neurodegenerative disorders such as Parkinson's, Huntington's and Alzheimer's disease.[2] This degree of involvement over so many functions and conditions make the NMDA receptor both a coveted and immensely challenging target for precise pharmaceutical modulation.

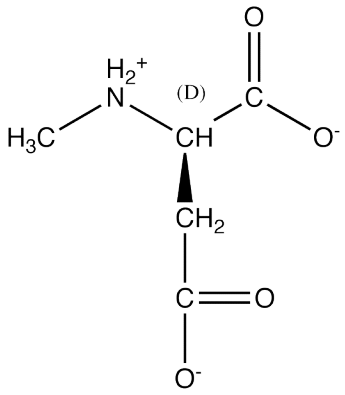

Figure 2.1 *N-methyl-D-aspartate*

The NMDA receptor functions as a tetramer comprised of different types of subunits.[1, 3] Seven subunits have been discovered: the NR1 subunit, four distinct NR2 subunits (subtypes NR2A through NR2D), and two NR3 subunits (NR3A and NR3B).

However, three distinct exons in the NR1 gene furnish eight different splice variants of the NR1 subunit. The NR2 subunits are relatively similar to each other, with over 50% sequence identity between them compared to about 20% identity to the NR1 subunit. Generally, two NR1 subunits and two NR2 subunits combine to form the functional heterotetramer, although NR3 can replace one or both NR2 subunits.[1, 4]

Unlike other ionotropic glutamate receptors, the NMDA receptor requires the presence of a co-agonist, glycine, in addition to glutamate to open the channel. Glycine binds to the NR1 subunit, while glutamate binds to NR2. Most receptors are formed with two units of the same NR2 subtype, along with the two NR1 subunits, but clear evidence exists for the formation *in vivo* of tri-heteromeric channels with two different NR2 subtypes (or an NR2 and NR3, as mentioned previously).[2, 5] The NR3 subunits bind glycine rather than glutamate, and recombinant receptors consisting only of NR1 and NR3 subunits have also been reported that are activated by glycine, do not bind glutamate, and have altered channel characteristics.[4]

Most of the receptor structure is external to the cell, with a membrane-bound pore region and a small domain internal to the cell. Electron microscopy reveals that while the pore region has four-fold symmetry, the extracellular domains of ionotropic glutamate receptors have bilateral symmetry.[6–8] For this reason, the assembly of the receptors is sometimes referred to as a "dimer of dimers". Although the nature of the preferred dimerization, meaning NR1/NR1 and NR2/NR2 or two NR1/NR2 dimers, is

unresolved, recent crystallography-directed experimentation points to the NR1/NR2 dimer as the functional component.[9]

2.1 Subunit Topology

The individual subunits of the NMDA receptor (as well as other ionotropic glutamate receptors) all share a similar architecture. Each subunit is a product of a single gene, and produces a single protein between 900 and 1,500 amino acids that folds into several distinct domains; two which reside external to the cell membrane, the transmembrane region, and a small internal domain (see Figure 2.2). The actual ion channel through the membrane is comprised of three transmembrane helices (M1, M3, and M4) as well as a re-entrant loop (M2 or the P-loop) and is similar in structure to potassium channels, although inverted.[10] There is a small, intracellular C-terminal domain after the M4 helix which varies in length between subunits and contains regions recognized by calmodulin. The first 350 residues fold to form the amino terminal domain, or ATD. This domain shares sequence homology with a bacterial leucine/isoleucine/valine binding protein (LIVBP) as well as the glutamate binding domain of the G-protein coupled receptor mGluR1. Both of these domains form a bi-lobed structure, indicating a similar fold is probable for the ATD. The ATD is thought to play an organizational and modulatory role and may aid in receptor assembly.[11] The receptor can still function in the complete absence of the amino

A

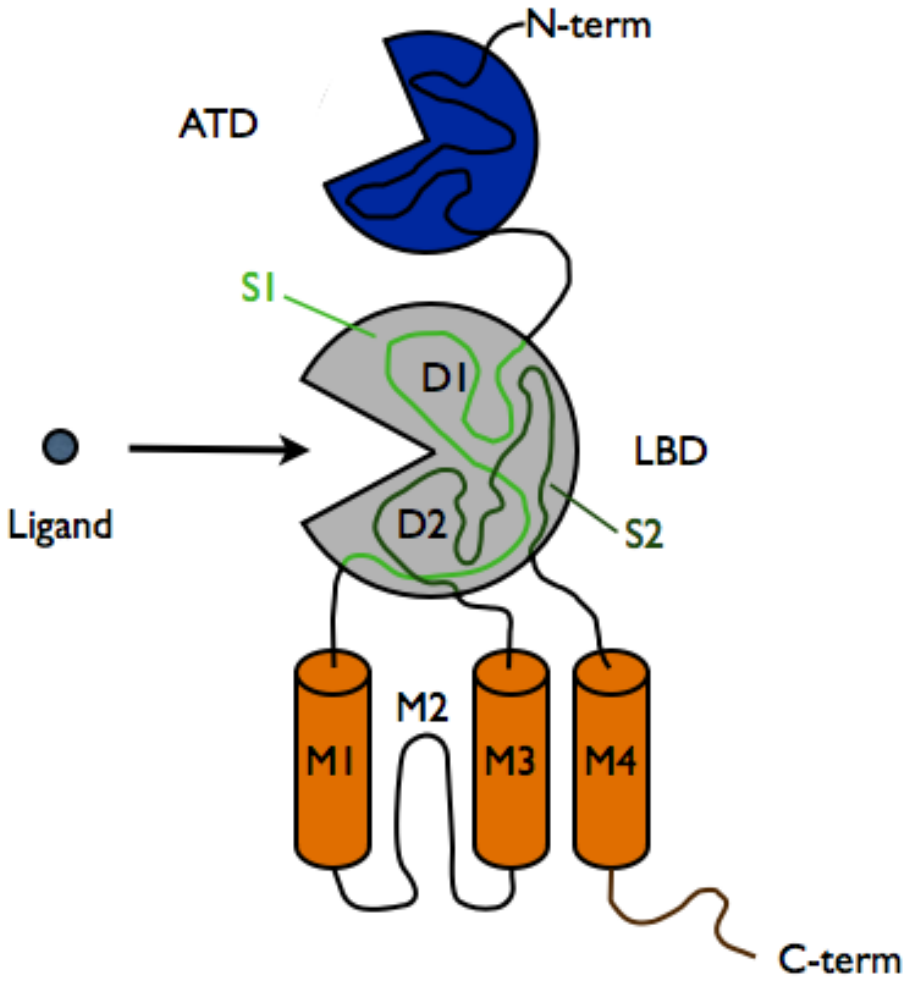

B

Figure 2.2 *Representation of the different domains in an NMDA receptor subunit as an unfolded peptide (A) and a folded protein (B)*

terminal domain. Below this domain is another bi-lobed domain, the ligand binding domain (LBD) sometimes referred to as the agonist binding domain. It is this domain, composed of about 280 amino acids, to which the agonist glutamate binds to in NR2 subunits, while the co-agonist glycine binds to in NR1. The domain is formed of two domains, the upper (D1) and lower (D2) and is assembled from two distinct sections of of the peptide.[12] Although each peptide contributes to both domains, the S1 peptide, the region between the ATD and the M1 transmembrane helix, is predominantly in the D1 domain. The second length of peptide, S2, is the extracellular loop between the M3 and M4 helices, and forms the bulk of the lower D2 domain. Linkers connect this domain to the pore region directly below it, and ligand binding is translated down from the LBD to the pore and results in opening of the channel.

2.2 Variation by Subtype

Several aspects of the function of NMDA receptors vary based on the identity of the NR2 subunits from which the receptor is composed.[2] The distinct expression patterns of the different NMDA receptor subunits change over the course of development, and study of unique pharmacological characteristics of recombinant NMDA receptors of each subtype has allowed for interpretation of the functional differences that these modifications might produce. The potential to target a pharmaceutical effect at a specific subtype has led to high demand for selective inhibitors and potentiators.

2.2.1 Regional and Temporal Distribution

The most general trend in subtype changes throughout development is a shift from predominance of NR2B- and NR2D-containing receptors to those composed of NR2A and NR2C.[5] NR2B and NR2D are expressed even in the embryonic brain, with NR2A expression beginning during the postnatal period and continuing throughout maturation. NR2B-containing receptors are replaced by those with NR2A to large extent at maturity, except in the forebrain. Levels of NR2C are increased in the cerebellum at adulthood, while NR2A is present throughout the brain.[2] There is even evidence that a single neuron is capable of expressing different NR2 subtypes at different synapses.[5] One reason for this ability may be the subtle differences in function between subtypes.

2.2.2 Functional Variation

NMDA receptors exhibit a remarkable capacity for modulation by many stimuli, much of which is subtype-dependant. While channels composed of all subtypes are subject to voltage-dependant block by Mg^{2+} cations, receptors constituted of NR2C and NR2D subtypes show decreased sensitivity and faster unblock than those with NR2A and NR2B.[13] NMDA receptors are also sensitive to extracellular pH, illustrated by the 50% inhibition of NR2A-containing channels by protons at pH 7.4. Both the identity of the NR2 subtype and the splice variant of NR1 can alter this effect,

and several residues in the linker between the ligand binding domain and the transmembrane helices have been identified as important through mutagenesis.[14] NR2A-containing receptors are also regulated by Zn^{2+} ions, and have been found to contain a high-affinity site located on the NR2A amino terminal domain.[15] In a similar manner, allosteric inhibitors of NR2B-containing receptors that likely bind to the amino terminal domain have been discovered, the first being the phenylethanolamine ifenprodil (Figure 2.3).[16] However, both Zn^{2+} and ifenprodil produce their effects by intensifying desensitization through the inherent proton sensitivity of the NMDA receptor.[17–18] This implies an allosteric effect that translates from the amino terminal domain down through the ligand binding domain.[19–20]

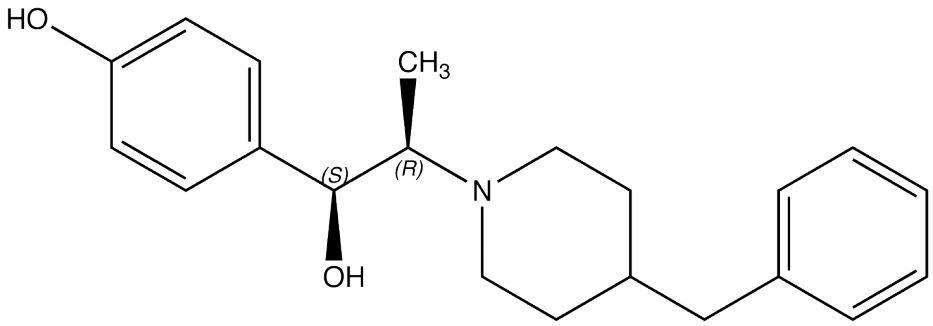

Figure 2.3 *Ifenprodil*

Studies of recombinant NMDA receptors have revealed that properties such as agonist affinity, mean channel conductance, open probability, and deactivation all differ between receptors composed of different subtypes.[21] For each of these, the greatest differences are between receptors comprised of NR2A or NR2D subtypes, as highlighted

in Table 2.1. There are at least 10-fold differences in the EC_{50} of glutamate as well as the peak open probability, or the fraction of time the channel is open while agonist and co-agonist are bound.[22–24] The difference in deactivation, the rate at ion flow ceases upon removal of agonist, is even more drastic. NR2A-containing receptors have a deactivation time course of 50 ms while the deactivation of NR1/NR2D channels in response to a pulse of glutamate and gycine takes over 1 second.[21–22]

Table 2.1 *Functional differences between receptors containing NR2A and NR2D*

Property	**NR2A**	**NR2D**
Glutamate EC_{50}	5.4 μM	0.51 μM
Conductance	40-50 pS	20-40 pS
Deactivation (τ)	50 ms	1.7 s
Open Probability	0.5	0.04

2.3 Ligand Binding Domains: Structures and Simulations

The study of the ligand binding domains of NMDA receptors through modeling and crystallography have provided more structural information about this domain of the receptor than any other region. The availability of crystal structures of the related AMPA receptor ligand binding domains provided starting points for early modeling attempts, but the release of first the NR1 ligand binding domain, and more recently the NR2A ligand binding domain and NR1/NR2A LBD dimer provided a wealth of structural data for further examination.

2.3.1 Crystal Structures

Although some homology modeling of the NMDA ligand binding domain in the literature was performed using crystal structures of the AMPA glutamate binding domain, the release of the first NMDA crystal structure highlighted important differences in the behavior of the NMDA domains. The initial crystallization of the NR1 ligand binding domain by Furukawa and Gouaux in 2003 was achieved through expression of only the S1 and S2 peptides joined by a small two-resiude linker.[12] Crystallization of this construct with glycine resulted in a closed structure for the agonist, but inclusion of an antagonist resulted in a more open conformation, similar to that observed in crystal structures of a GluR2 (an AMPA receptor) ligand binding domain.[25] However, crystallization with the partial agonist D-cycloserine did not produce the partial closure seen in structures of AMPA ligand binding domains bound with partial agonists. Instead, the full domain closure observed with agonists was also present when the partial agonists were bound, and partial agonists induced small conformational changes in the hinge region near helix F, which sits directly below the ligand binding site.[26]

While structures of the NR1 ligand binding domain provide a more acceptable template for homology models of NR2 subunits, there is only approximately 50% sequence homology between NR1 and NR2 ligand binding domains, while the homology

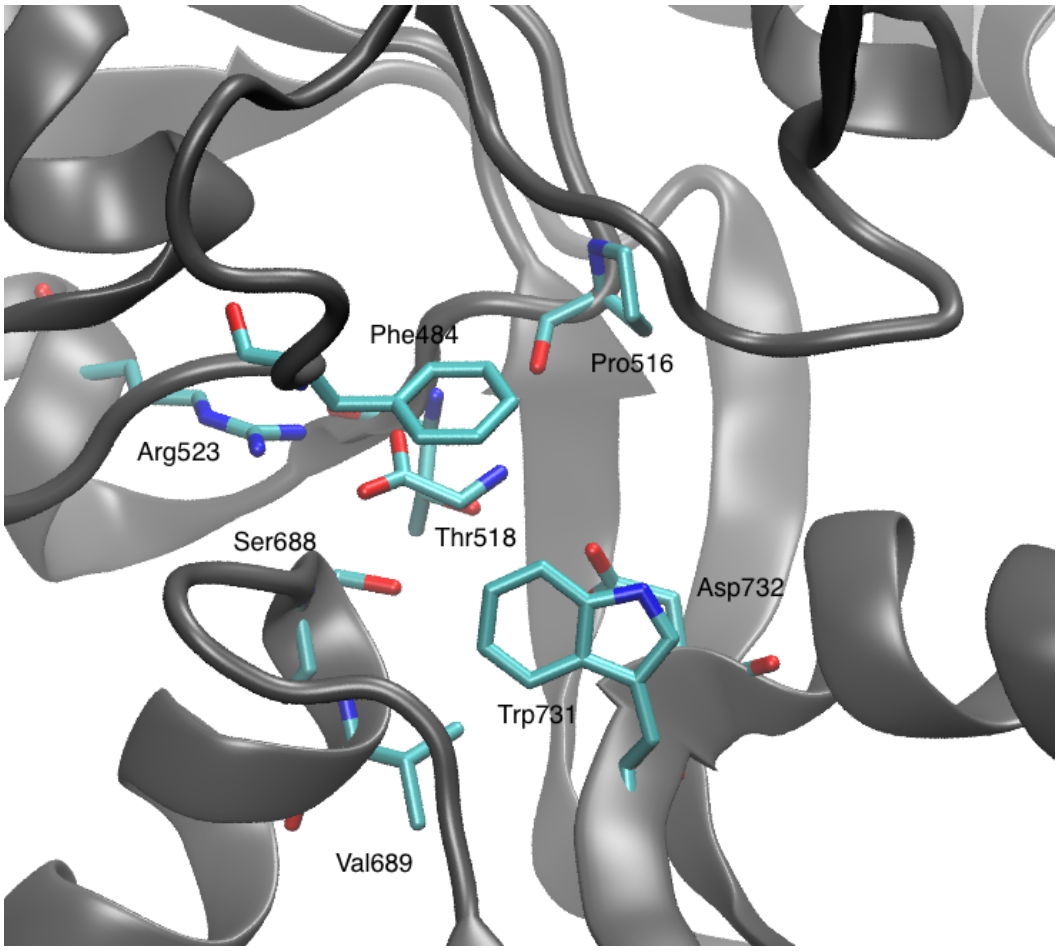

Figure 2.4 *Glycine binding site of the NR1 crystal structure with bound glycine. The ligand forms hydrogen bonds with the Arg523.*

between the LBDs of NR2 subtypes is over 80%. Therefore, the crystallization of the NR2A ligand binding domain, both alone and in complex with the NR1 ligand binding domain, provided information not only about the critical dimer interface but also revealed the first direct structural knowledge of an NR2 glutamate binding domain.[9] The NR1/NR2A dimer places the two ligand binding domains back-to-back but with a rotation of one relative to the other, as depicted in Figure 2.5. Notice D1 of NR1 on

the left (largely formed by the dark blue S1 peptide) is positioned in the foreground, while the corresponding D1 of NR2A (right, mostly the red S1) is farther away.

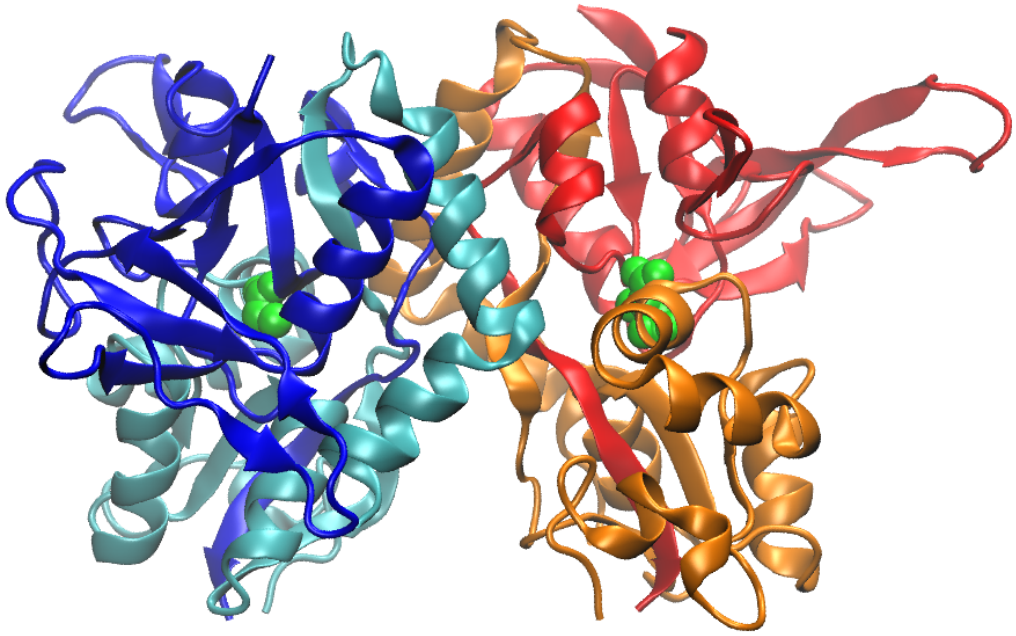

Figure 2.5 *Crystal structure of the NR1/NR2A dimer with the S1 peptide colored darker than the corresponding S2 and ligands in green*

The glutamate binding pocket, and to a lesser extent the glycine binding site, in the NR1 and NR2A crystal structure shares many of the same characteristics as previously-crystallized glutamate binding domains from other ionotropic glutamate receptors.[9] Those critical contacts, shown in Figure 2.6, include a bifurcated hydrogen bond or salt bridge between Arg499 and the α-carboxyl of glutamate, as well as hydrogen bonds between the γ-carboxyl of glutamate and Ser670 and Thr671 as well as glutamate's amino group and Ser492 and Thr494.

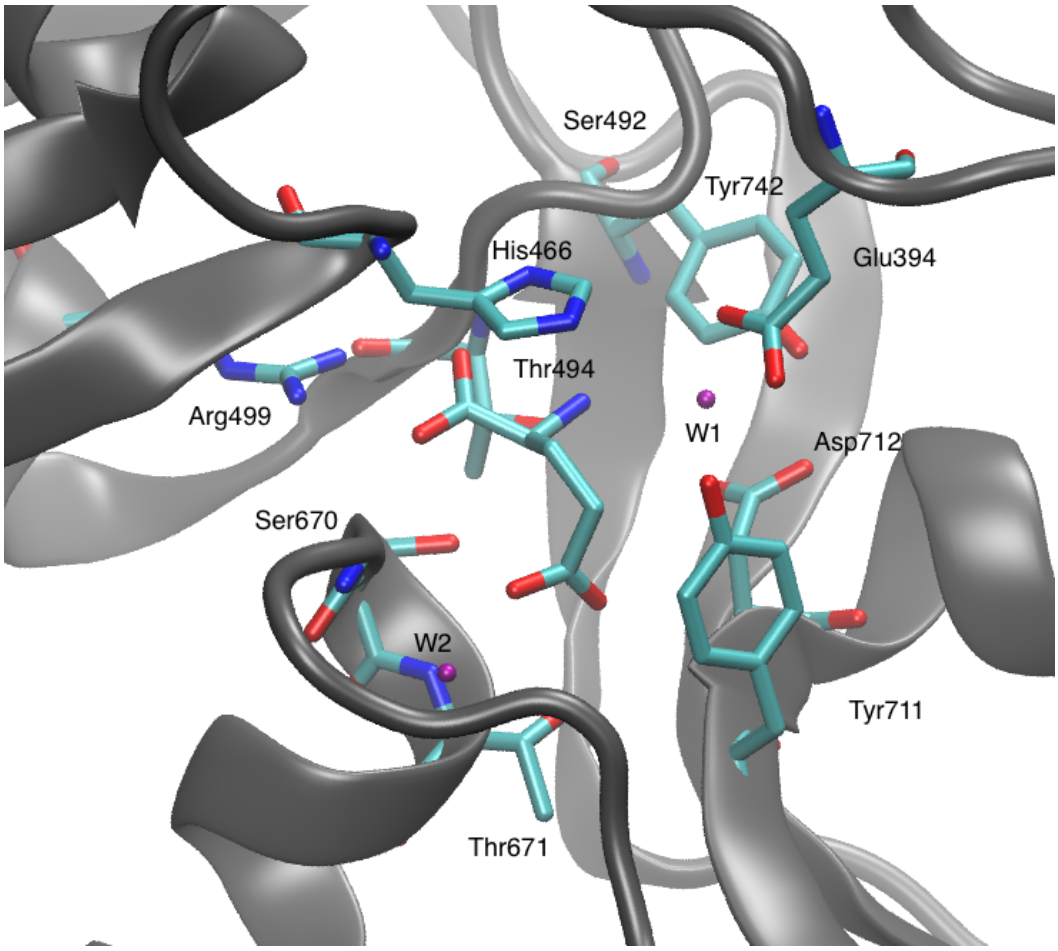

Figure 2.6 *Crystallographic binding site of glutamate in the NR1/NR2A dimer structure. Resolved waters are colored purple. The γ-carboxyl hangs down and contacts Ser670 and Thr671 on helix F.*

2.3.2 Modeling and Molecular Dynamics Simulations

Computational methods such as molecular dynamics have the potential to provide a window into the concerted motions and dynamics that proteins can undergo in solution near physiological temperatures.[27–29] However, these methods have only recently begun to be applied to domains of the NMDA receptor. Prior to release

of the crystal structure of the NR1 ligand binding domain, studies of NMDA ligand binding domains were limited to homology models based on the GluR2 ligand binding domain, which shares only around a 30% sequence homology with NR2 ligand binding domains.[30] However, molecular dynamics simulations of these GluR2 domains provided important cognizance of important issues in simulations of ionotropic glutamate receptor domains.[31] Arinaminpathy *et al.* conducted explicit solvent MD simulations of various structures of the GluR2 ligand binding domain for 2 ns to 5 ns, and found a correlation between increased mobility between domains and partial agonism. The subsequent release of several NR1 crystal structures with different bound ligands allowed a similar analysis of NR1 by the same group, where they found no evidence for partial domain opening induced by partial agonists.[32–33] Blaise *et al.* modeled NR2 ligand binding domains from the NR1 structure, however their homology models were used primarily for docking, with short, post-docking MD performed for optimization.[34–35] Furthermore, several of their proposed models failed to reproduce critical binding interactions such as the salt bridge between Arg499 and the α-carboxyl.

2.3.3 Obstacles to Molecular Dynamics Approach

Although the identity of the NR2 subtype influences many aspects of the function of a NMDA receptor, there has been no attempt to use molecular dynamics purely

to examine the NR2 ligand binding domains for structural differences that may characterize aspects of the functional variance. Any molecular dynamics simulation is susceptible to sources of potential error including but not limited to force field quality, electrostatics treatment and cutoffs, and solvent representation. While every method has its limitations, several potential impediments specific to the application of this technique to the NMDA ligand binding domain must be understood. First, limitation of the study to the ligand binding domain ignores much of the surrounding protein machinery of the receptor that surely influences the conformation and dynamics of the domains. Simulation of the NR1/NR2 LBD dimer only slightly mitigates this issue, but lack of additional structure at the atomic level as well as computational limitations make expansion of the system impractical. Second, the high level of sequence similarity between the NR2 ligand binding domains (over 80% sequence homology) raises questions of the existence of significant differences in this domain. Figure 2.7, which displays the structure of the NR2A ligand binding domain, compares the NR2A and NR2D LBD sequences by coloring the backbone blue where the sequences are identical and red where they diverge. Note that the region around the glutamate binding site is completely uniform in sequence. Third, the timescale of channel activation must be contrasted to the length of simulation. As discussed previously, NMDA receptors open and close on a millisecond timescale, a prohibitive simulation period given the

size of these systems. Additionally, previous simulations of both GluR2 and NR1 ligand binding domains did not observe opening of a "closed" structure with the ligand removed throughout 5 ns and 20 ns of simulation respectively, although a structure starting in an "open" conformation was observed to close temporarily.[31–32] The observation of dynamic domain opening and closing events are improbable in simulations of the duration currently computationally accessible for systems of this size. Therefore, simulations can be expected to reflect local conformational changes and equilibrium structures rather than demonstrating large transitions between stable structures.

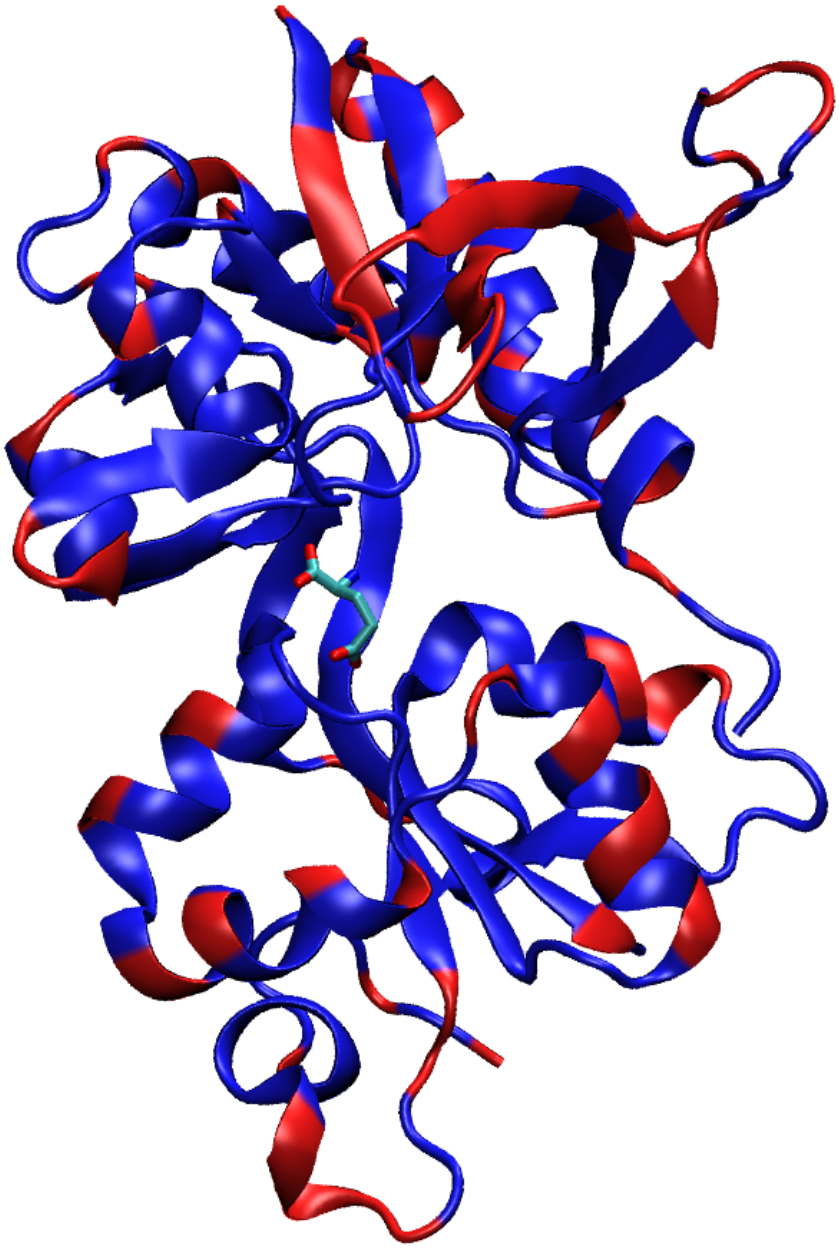

Figure 2.7 *NR2A LBD colored by sequence identity between NR2A and NR2D*

Chapter 3

Ligand Binding Domain Simulations

> "Essentially, all models are wrong, but some are useful."
>
> — George E. P. Box

NMDA receptors comprised of different NR2 subtypes vary in pharmacology and function. As more structural information about the ligand binding domain (LBD) of these receptors becomes available, modeling methods can be applied to investigate questions regarding structure and motion. Despite the high homology between subtypes, the ability of simulation to address structural and functional differences between different subtypes or due to different ligands must be evaluated.

3.1 Homology-based Partial Agonist Simulations

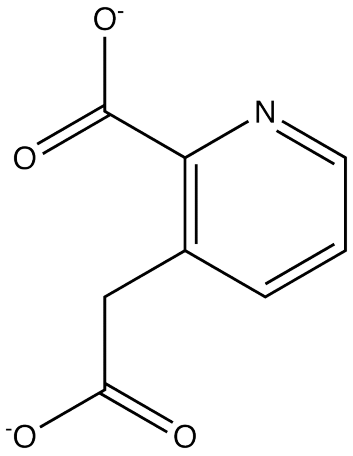

Figure 3.1 *Homoquinolinic acid, an NMDA receptor partial agonist*

Prior to the release in 2005 of the first experimental structures for the ligand binding domain of NR2 subunits, the nearest homolog structure was the NR1 ligand binding domain solved in 2003.[12] A homology model of the LBD of the NR2A subunit, previously built by collaborators in the Emory lab of Dr. Traynelis from the NR1 crystal structure, was compared to structures of related AMPA receptors.[36] This model provided the basis for our initial exploration comparing the effects of bound homoquinolinate, a partial agonist, to both the glutamate-bound and unliganded form of the NR2A ligand binding domain.

3.1.1 Structure Preparation and Simulation Parameters

The initial homology model of the NR2A ligand binding domain (LBD) with bound glutamate ligand was based on the NR1-glycine crystal complex (pdb code 1PB7).[12, 36] The glutamate ligand was removed to form the unliganded protein, while the homoquinolinate was built in place of the glutamate to form the third starting structure. Ligands and protein were parameterized in GROMOS96, a united-atom forcefield.[37] The topology for homoquinolinate was built manually through comparison to the standard amino acid paramterization with the pyridinal nitrogen unprotonated. In preparation for simulations with GROMACS 3.2.1 each structure was placed in a periodic box sized to insure a minimum of 8 Å between any protein atom and the nearest periodic boundary.[38–39] These periodic boxes, approximately 345 nm^3, were filled with around 11,000 SPC water molecules and 1 to 3 chloride ions.[40]

These solvated structures were first subjected to a simple energy minimization to remove any gross steric clashes. Harmonic restraints were placed on every protein and ligand atom, leaving only the water and ions unrestrained. Each of the three systems then underwent a position-restrained MD simulation for 20 ps at 300K which allowed the water and ions to adjust to the protein and ligand. Next, the restraints were removed and each system was simulated for at least 3 ps at 20K. This initial low temperature simulation provides an opportunity for small adjustments in conformation

with a small amount of thermal energy without the high atom velocities that occur at higher temperature simulations. Structures from the end of the 20K simulations were then simulated at 200K for 500 ps. The temperature of 200K rather than a more physiologically-relevant 300K was employed due to concerns over the stability of the homology model with increased thermal energy. All simulations were performed using a Berendsen thermostat[41] under NPT conditions and using a particle-mesh Ewald electrostatic treatment[42] with a cutoff of 9 Å. All simulations used at 2 fs timestep except for the initial simulations at 20K, which used a timestep of 1 fs. Average structures were derived from a two stage fitting and position averaging of the final 150 ps of simulation, and then energy minimized.

3.1.2 Results

An important issue to address first is the stability of the NR2A LBD structure over the course of the MD simulation to determine whether the systems have reached an equilibrium structure under the simulation conditions. One way to measure this is to observe the root mean square displacement (RMSD) to a starting structure evolve over the time course of the simulation. When performed on the three simulations, a trend emerges of initial adjustment over the first 50 ps, followed by more mild structural change, and finally settling around a stable value over the final 150 ps of the simulation (Figure 3.2).

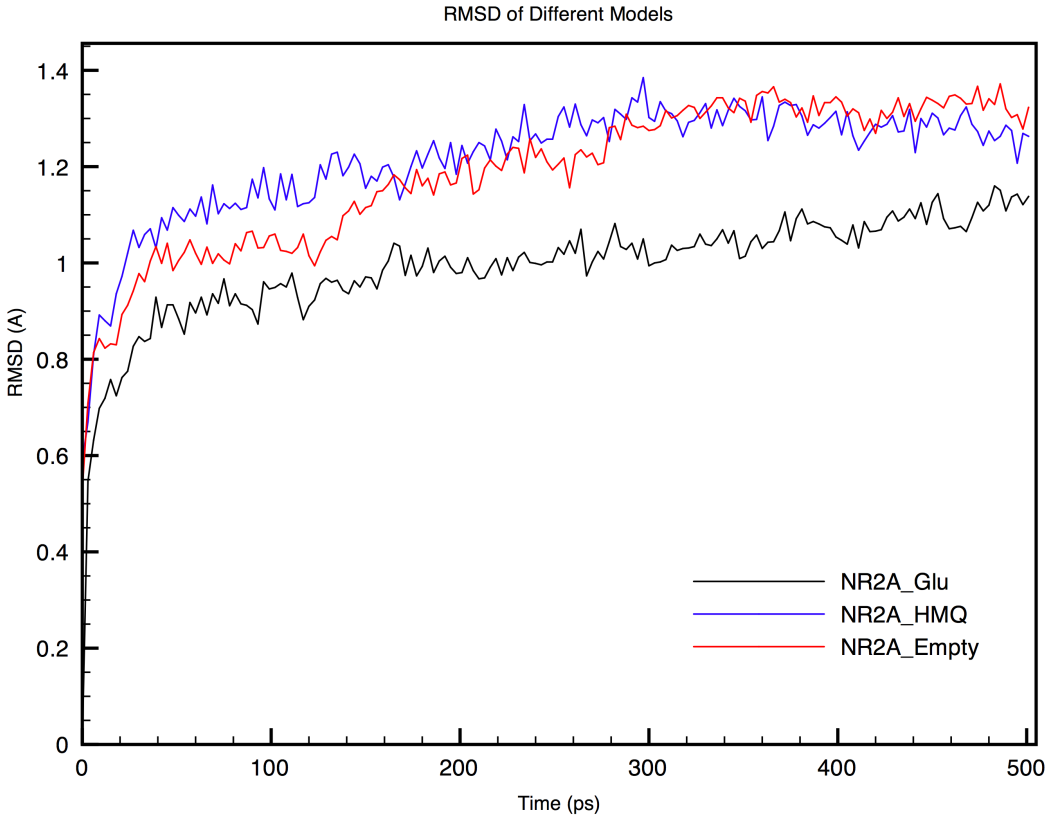

Figure 3.2 *The RMSD of each structure from the starting homology model over the course of the simulations.*

Unsurprisingly the glutamate-bound structure shows a lower RMSD over the course of the simulation than the other two systems. Comparison of the average structures derived from the equilibrium over the final 150 ps reveals a shift in helix F on the lower domain of the LBD when homoquinolinate is bound that is not seen in either the glutamate-bound or empty structure (Figure 3.3). Rather than a lateral displacement, this shift is an angular displacement of the lower end of helix F and to a lesser extent the neighboring helix G. The backbone of the upper end of helix F, which forms part

of the lower extend of the ligand binding pocket, remains in the same position. Also, a slight enlargement of the binding pocket can be seen when homoquinolinate is bound, evidenced by a slight shift of the backbone in the regions around the binding site.

When focus is turned to the ligand binding site clear differences are present in the interactions between the pocket and the two ligands. The glutamate ligand retains a similar hydrogen-bond network from the starting structure, most importantly retaining a hydrogen bonding interaction between the α-carboxyl and the sidechain of Arg499, a critical residue in every similar glutamate-binding domains.[11] The amino group of the ligand forms a hydrogen bond with the phenolic hydroxyl of Tyr742, and the γ-carboxyl hydrogen bonds with the sidechain and backbone of Ser670 as well as the sidechain of Thr671: two residues at the top of the first turn of helix F.(Figure 3.4) The γ-carboxyl group also forms an intermittent hydrogen bond across the lower portion of the binding pocket with the backbone amide of Asp712.

Despite the overall similarity in the average position of homoquinolinate when compared to glutamate, the binding site has adjusted to the subtle differences the partial agonist presents. Along with increased size of the aromatic ring, homoquinolinate has lost both the positive charge and hydrogen bond donating capability of glutamate's amino group. Although the number of carbons between the two carboxyl groups is the same for the two ligands, the aromatic ring of homoquinolinate severely restricts the

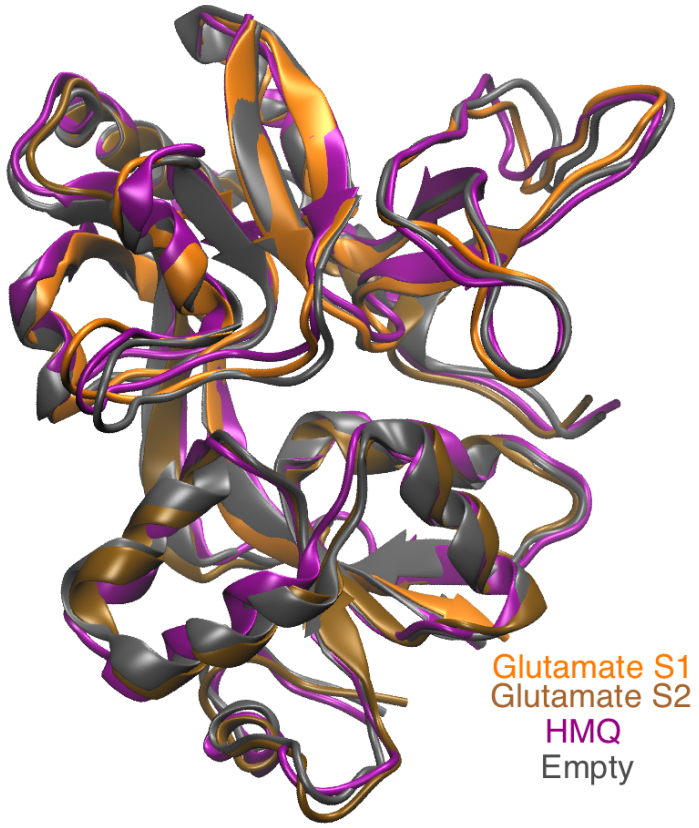

A

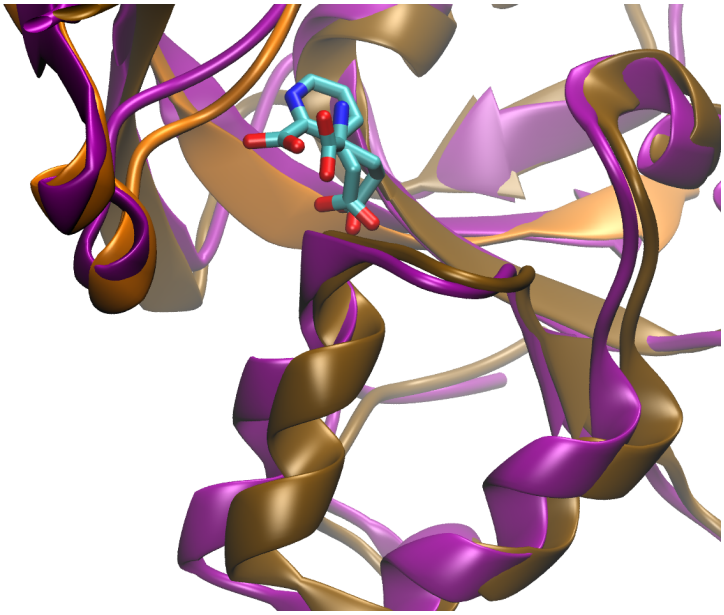

B

Figure 3.3 *Three average protein structures are shown (A) while a close-up highlights different positioning of helix F (B)*

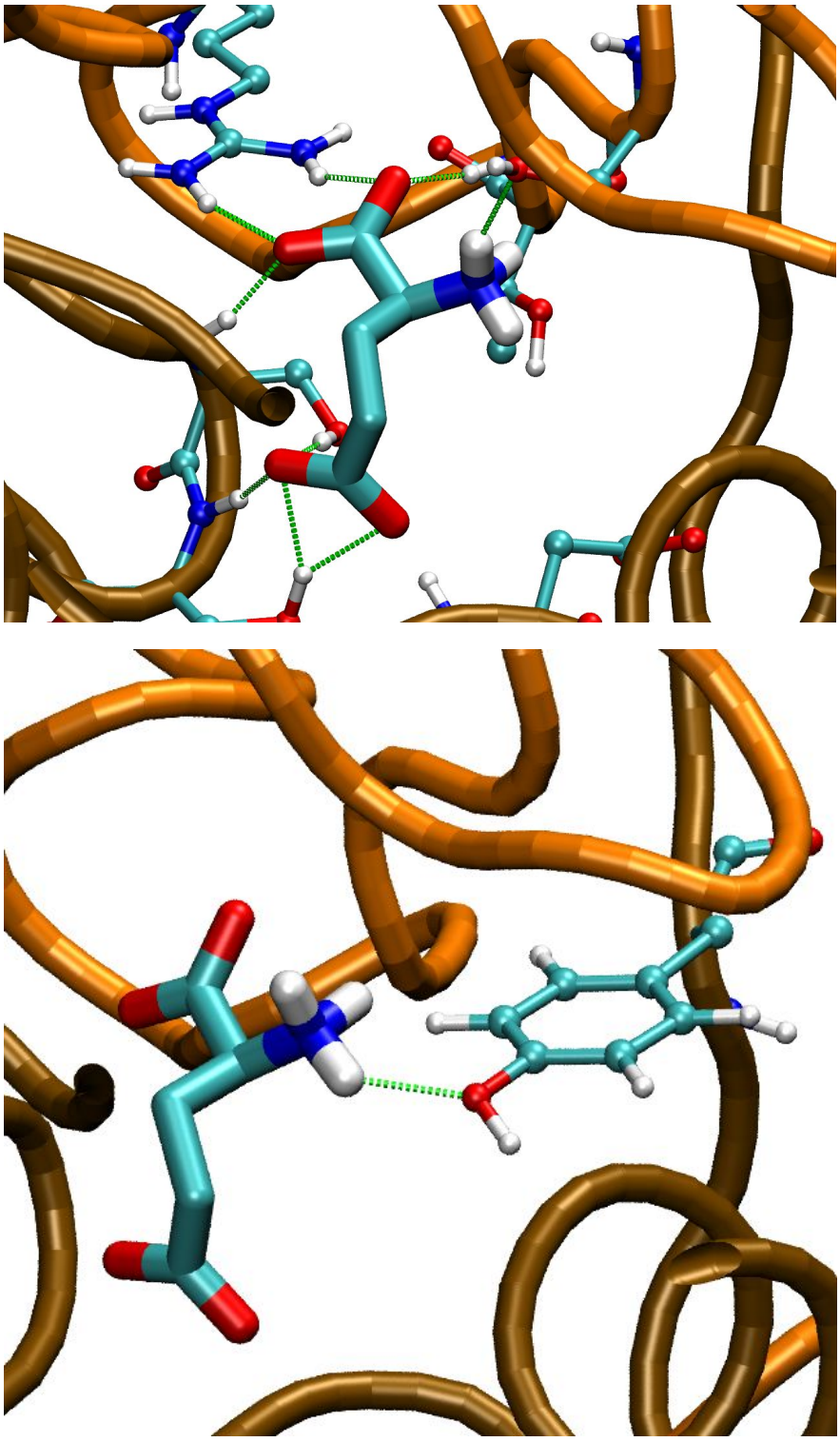

Figure 3.4 *Interactions between glutamate and NR2A binding pocket*

conformational flexibility of this portion of the molecule. Despite this reduction in conformational freedom, homoquinolinate shares some similarity with glutamate in their interactions with the binding pocket, such as hydrogen bonds between the α-carboxyl and Arg499 as well as between the γ-carboxyl and Thr671. However, the aromatic ring of homoquinolinate displaces the sidechain of Tyr742 relative to its position with bound glutamate, pushing it back from the pocket and disrupting a hydrogen bonding network with neighboring residues. (Figure 3.5)

The sidechain of Ser670 also changes from a hydrogen bonding interaction with the γ-carboxyl of glutamate to an interaction with the α-carboxyl of homoquinolinate. This observation is supported by the experimental result of a much greater sensitivity of glutamate to the S670G mutant than homoquinolinate (92-fold shift for glutamate, 6-fold for homoquinolinate).[43] The changes in interactions in the γ-carboxyl region likely stem from the additional steric bulk and rigidity of the aromatic ring placing the γ-carboxyl of homoquinolinate in a position angled away from the right wall of the pocket. This also results in the absence of an analogue to the cross-pocket hydrogen bond between the γ-carboxyl of glutamate and the backbone of Asp712. The larger size of the homoquinolinate pocket also results in the loss of a stable hydrogen bond between the backbone amide of Gly467 and carbonyl of Asn668, which is present in both the empty and glutamate-bound structures. Thus, the homoquinolinate-bound complex has lost two anchor points at the top of helix F. (Figure 3.6)

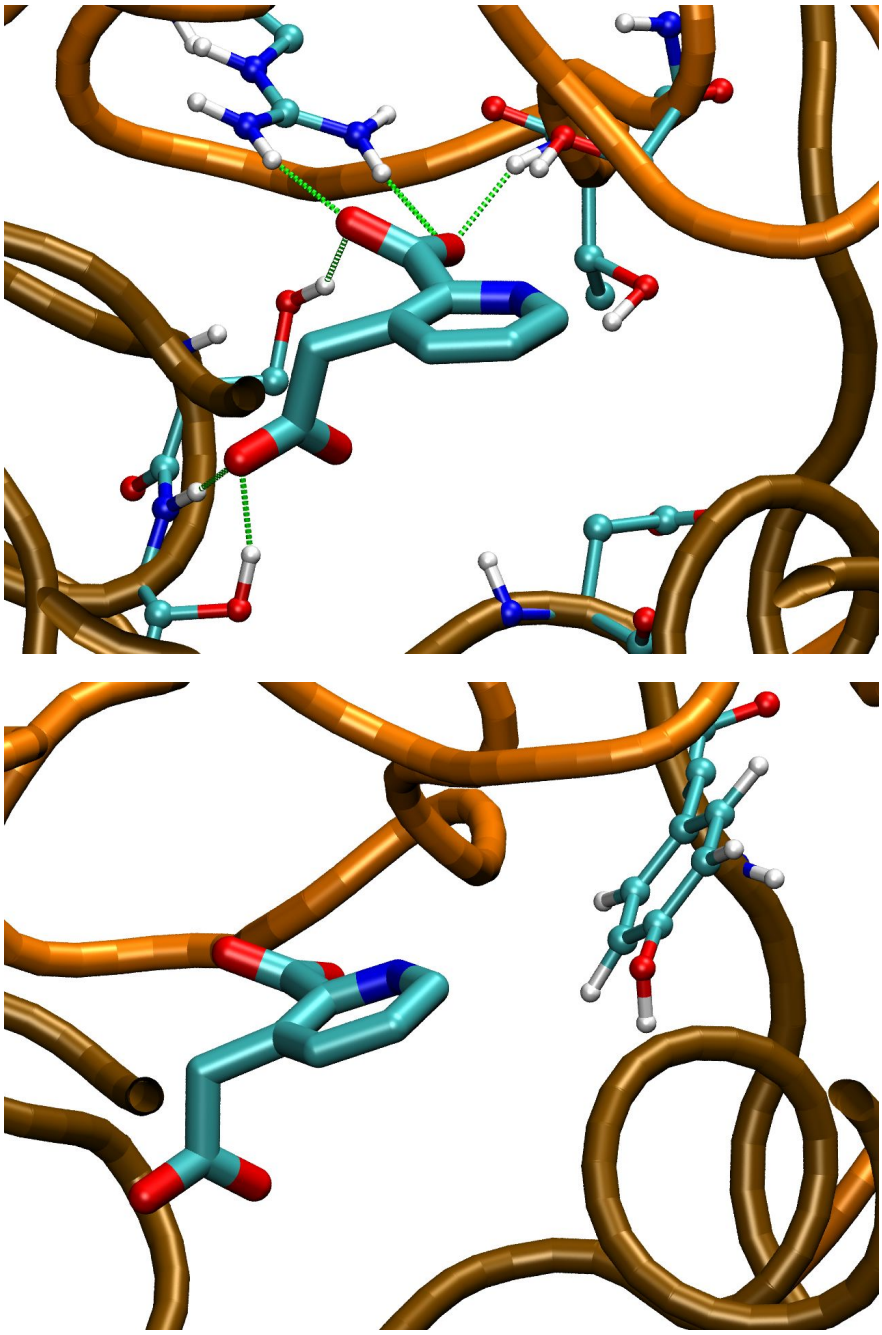

Figure 3.5 *Interactions between homoquinolinate and NR2A binding pocket*

Molecular dynamics simulations afford the opportunity to examine the motion of

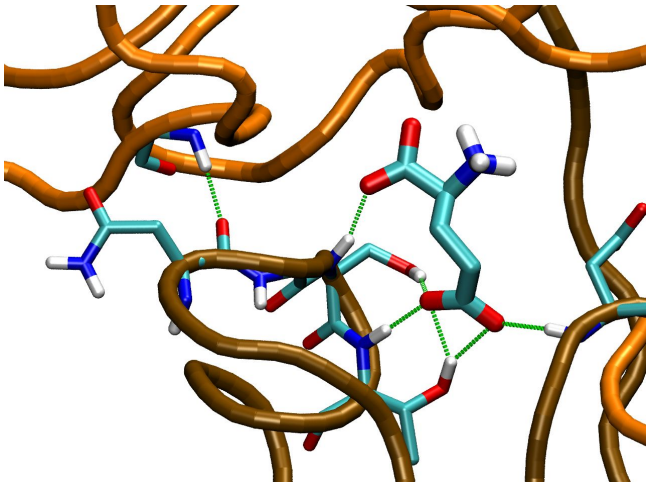

A

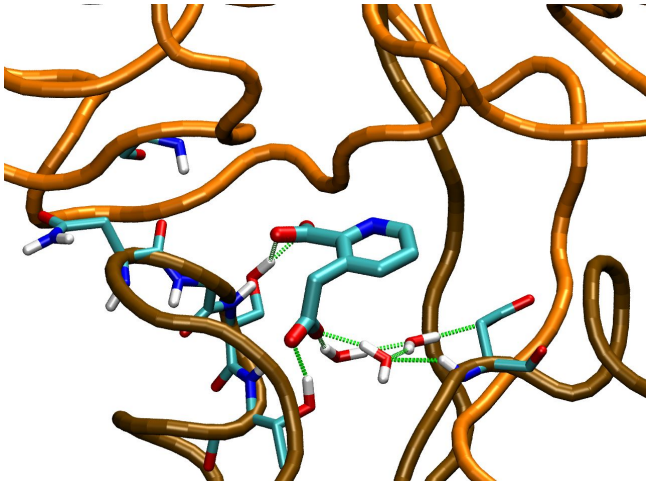

B

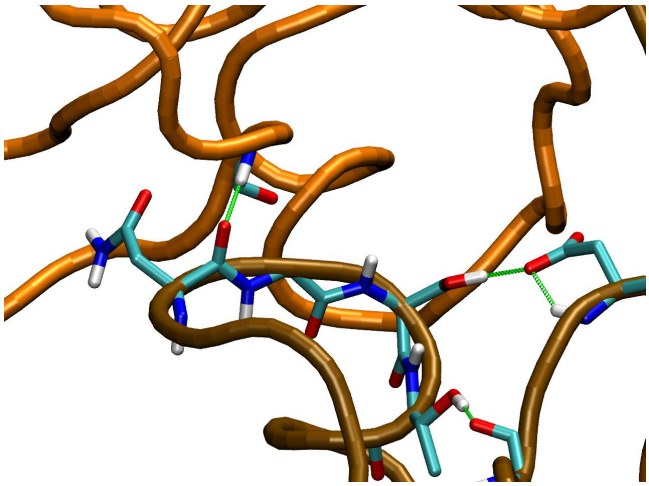

C

Figure 3.6 *Comparison of bridging interaction in simulation of NR2A with bound glutamate (A), homoquinolinate (B), and the empty protein (C)*

the system in addition to the equilibrium structure. In order to probe differences in the motion of the binding pocket, the room mean square fluctuation (RMSF) of 22 residues in the binding pocket was calculated over the final 150 ps of the simulations. With the exception of Tyr742, which oscillates in and out of hydrogen bonding with the charged amino group of glutamate but has no such interaction with homoquinolinate, each of the residues examined showed increased motion with homoquinolinate bound (Figure 3.7). The average increase in fluctuation (excluding Tyr742) was over 30 percent between the homoquinolinate-bound and glutamate-bound complexes.

3.2 Crystal-Based Simulations of NR2A and NR2D

Release of the crystal structure of NR2A in 2005 provided an opportunity to compare MD simulations based on an actual crystal structure of an NR2 ligand binding domain to simulations based on a homology model, as well as supplying a close homolog for modeling other NR2 subtypes. Also, since the location and orientation of glutamate within the binding pocket was now confirmed, docking simulations could be employed with greater confidence to model the binding modes of other ligands.

3.2.1 Structure Preparation and Simulation Parameters

The crystal structure of the NR2A LBD with bound glutamate was utilized directly for the NR2A simulations and provided the template for the NR2D homology model.[9]

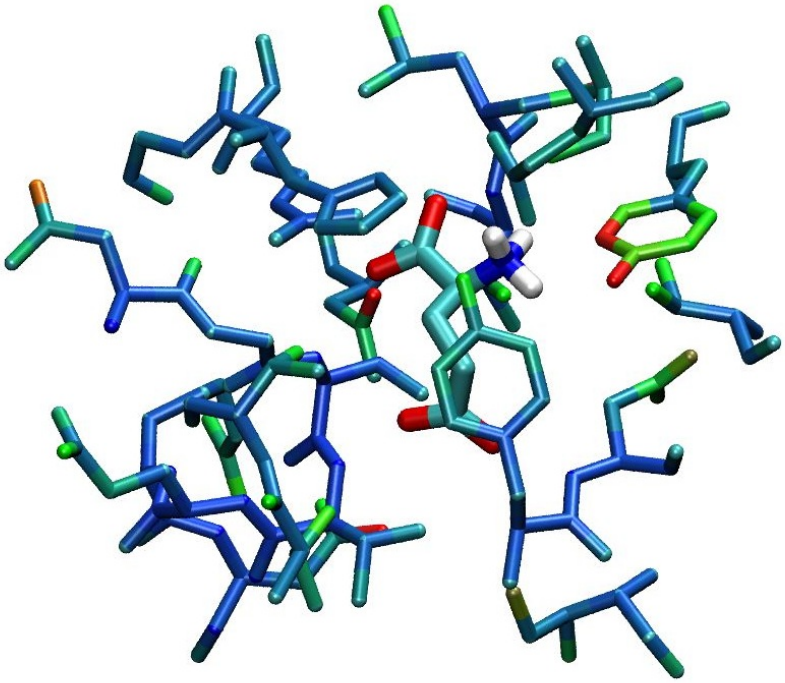

A

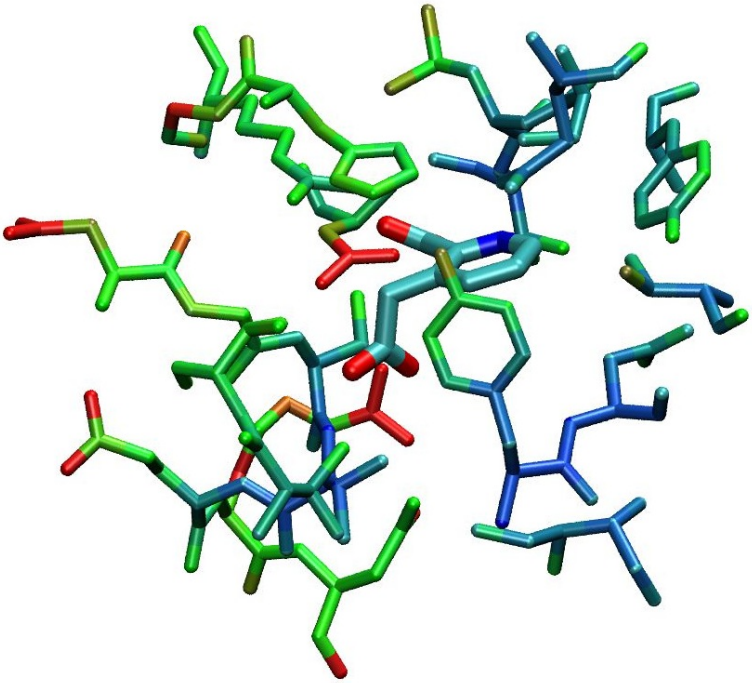

B

Figure 3.7 *Comparison of the the glutamate binding site (A) and the homoquinolinate binding site(B) with atoms colored by RMSF on a scale from little fluctuation (blue) to high fluctuation (red).*

All water molecules were removed from the crystal structure. The two residue linker found in 2A5S, used to connect the S1 and S2 chains which combine to form the LBD, was removed and two additional residues added to recreate the wild-type human NR2A sequence. This was then used as a template for the NR2D LBD homology model. The sequence of the S1 and S2 portions of NR2D have an 82% homology to the corresponding regions in NR2A, indicating a favorable degree of similarity for constructing homology models. The sequences were aligned and the homology model of the NR2D LBD was built using Prime.[44] The glutamate ligand was left in the same location as in the NR2A crystal structure.

These crystal-based structures were prepared for MD simulation in an identical way as the homology-based simulations described above. After parameterization, setup of the periodic conditions, and solvation, the systems were energy minimized, which was followed by a 20 ps simulation at 300K with position restraints on all protein atoms. Similarly to the previous simulations, the systems were next run unrestrained at 50K for 5 ps, allowing them to undergo small initial adjustments while provided only a small amount of thermal energy. The temperature of the system was then increased from 50K to 300K over the course of 25 ps of simulation, permitting a gentle transition to a room temperature environment. Once at 300K, the simulations were extended to 5 ns, a full order of magnitude longer than the previous simulations. All other aspects

of the simulation setup remained consistent to the previous work. Average structures were derived from the final 2 ns of simulation.

3.2.2 Results

Again, we begin the analysis of the simulation trajectories by examining the stability of the structures over the course of the simulation.(Figure 3.8)

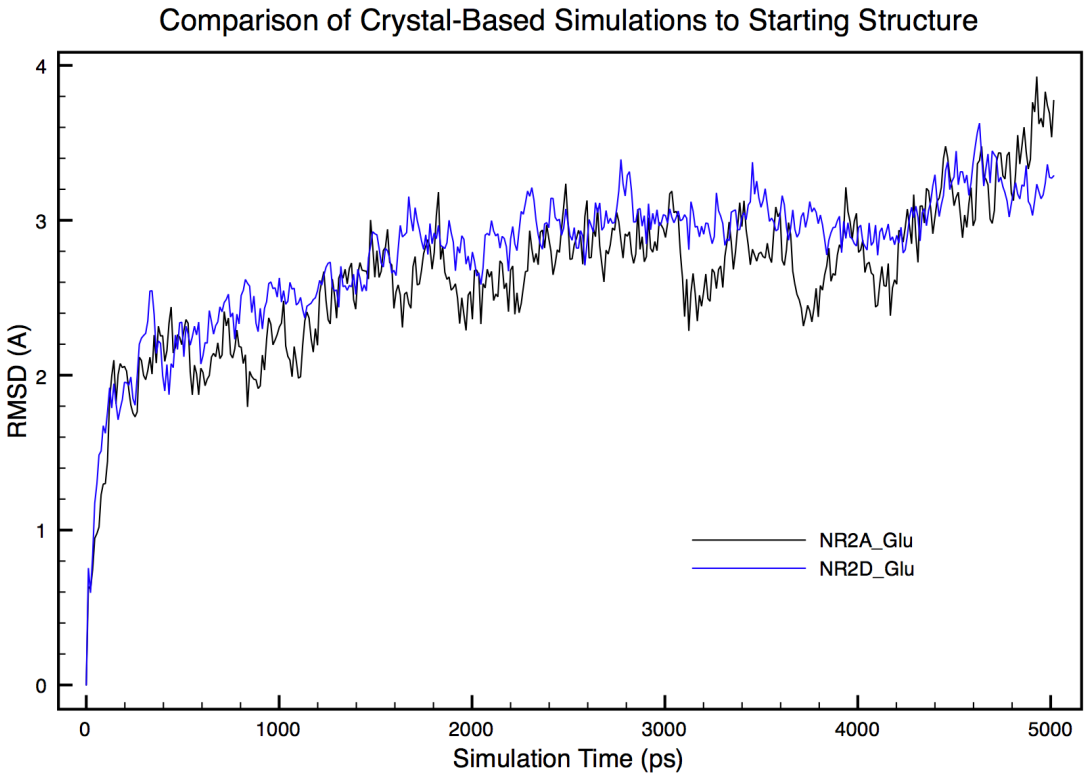

Figure 3.8 *The RMSD of both the NR2A crystal structure and the NR2D crystal-based homology model to their respective starting structures over the course of the simulations.*

Upon examination of the RMSD of the trajectory to the starting (crystal) structure, both the NR2A and NR2D simulations show an initial equilibration period over the first 1.5 ns, with RMSD gradually increasing. This is followed by a period of stability that lasts for several nanoseconds, although the RMSD of both simulations seems to be trending upward in the last 500 ps of each simulation. Whether this is a sign of decreasing structural integrity in the model or a natural fluctuation is unclear. However, average structures derived from the final 2 ns of simulation retain remarkable backbone similarity to the crystal structure of NR2A.

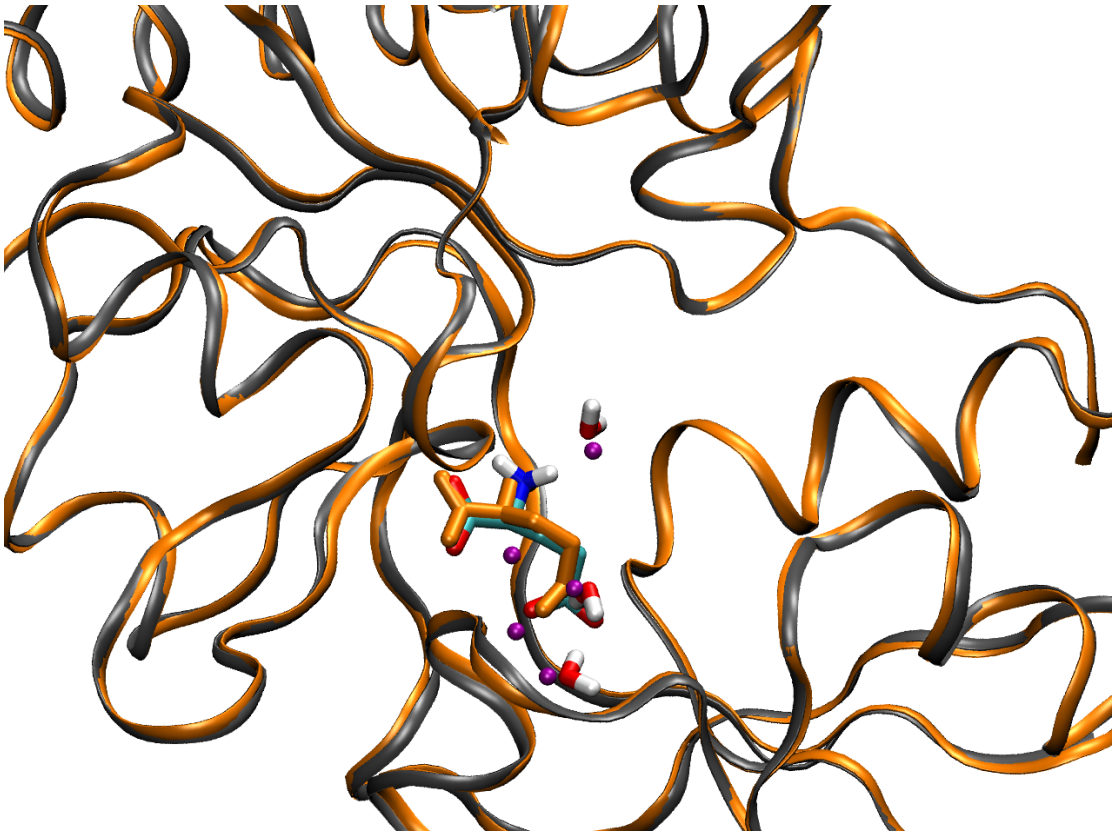

Figure 3.9 *Comparison of crystal and simulation structures and water*

As shown in Figure 3.9, there is remarkable alignment between the backbones of the crystal structure and a structure from the final 1 ns of NR2A simulation that is representative of the average structure. The simulation also retains the binding mode of glutamate, and several long lived water molecules are identifiable in positions equivalent to crystallographic waters.

Comparison of the average NR2A structure and the average NR2D structures reveals larger changes than seen between the NR2A crystal and the NR2A model. The difference between the two structures is best described as a horizontal rotation of one domain relative to the other. Visual evidence is provided by aligning the backbones of either the top domain (D1) of each structure, or the bottom domain (D2) of each structure, as shown in Figure 3.10. Alignment by either the top or bottom domain results in close agreement between the aligned domains, but a relative

rotation of the other. This effect can also be quantified through use of the hingefind algorithm, which quantifies both the effective axis of rotation as well as the extent of rotation for specified rigid domains.[45] The difference in these two structures defines a 23 - 28 degree rotation around an axis that runs vertically through the upper domain (D1), shown below in Figure 3.11. This large-scale change in the

relative positioning of the two domains accompanies more specific changes in and around the agonist binding pocket.

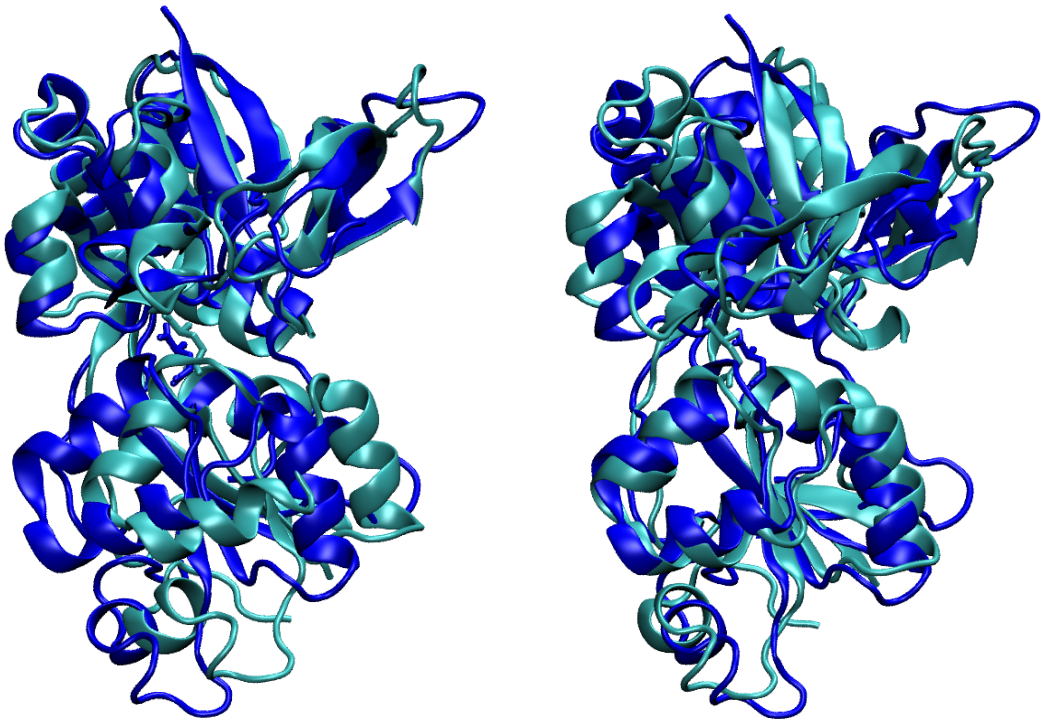

Aligned by D1 Aligned by D2

Figure 3.10 *Alignment of average structures of NR2A (dark blue) and NR2D (light blue).*

As seen in Figure 3.9, the simulation of glutamate bound to the NR2A LBD reproduces the positioning of the ligand and the surrounding protein, and retains many of the interactions within the small, polar binding pocket. The glutamate in the MD simulation of the NR2A LBD maintains hydrogen bonding between the α-carboxyl and the sidechain of Arg499, a residue known to be important to glutamate binding both through mutagenesis and from comparison to other related receptors.(Figure 3.12)

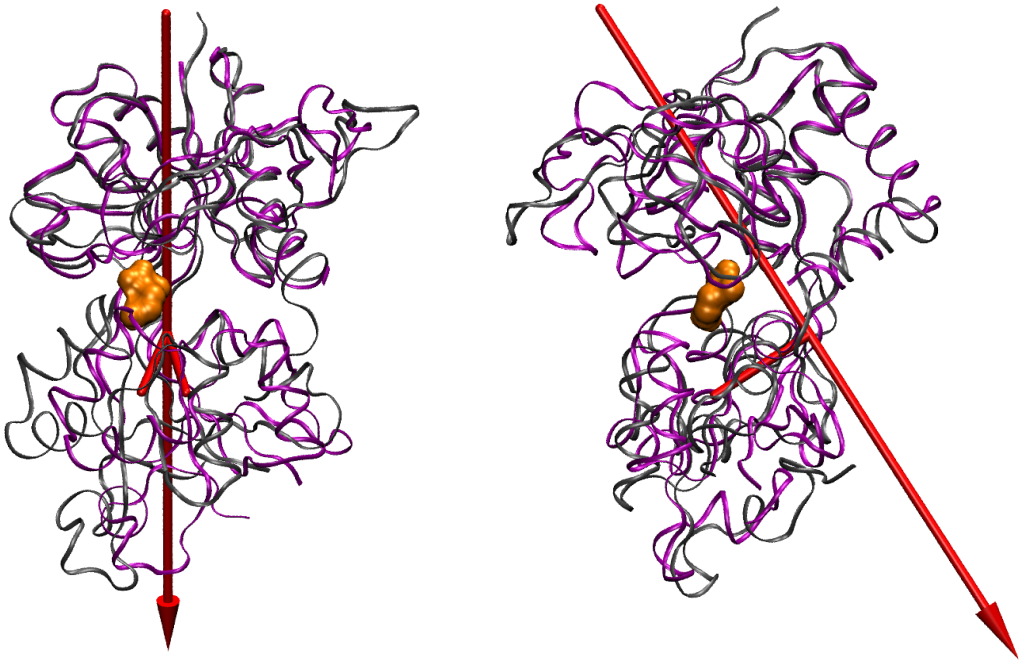

front view rotated 90°

Figure 3.11 *Predicted effective rotation of D1 to D2 between NR2A (grey) and NR2D (purple) structures*

The α-carboxyl of the glutamate ligand also sustains persistent hydrogen bonds with the sidechain of Ser670 and the backbone amide of Thr494. The hydroxyl sidechain of Thr494 interacts with the charged amino of the glutamate ligand, which also interacts with the Asp712 sidechain. The γ-carboxyl of the glutamate ligand forms hydrogen bonds with several groups at the top of helix F, namely the amide protons of Ser670 and Thr671, as well as the sidechain of Thr671. As seen in the previous homology model-based simulations, there is a bridging hydrogen bond between the γ-carboxyl of glutamate and the amide backbone of Asp712.

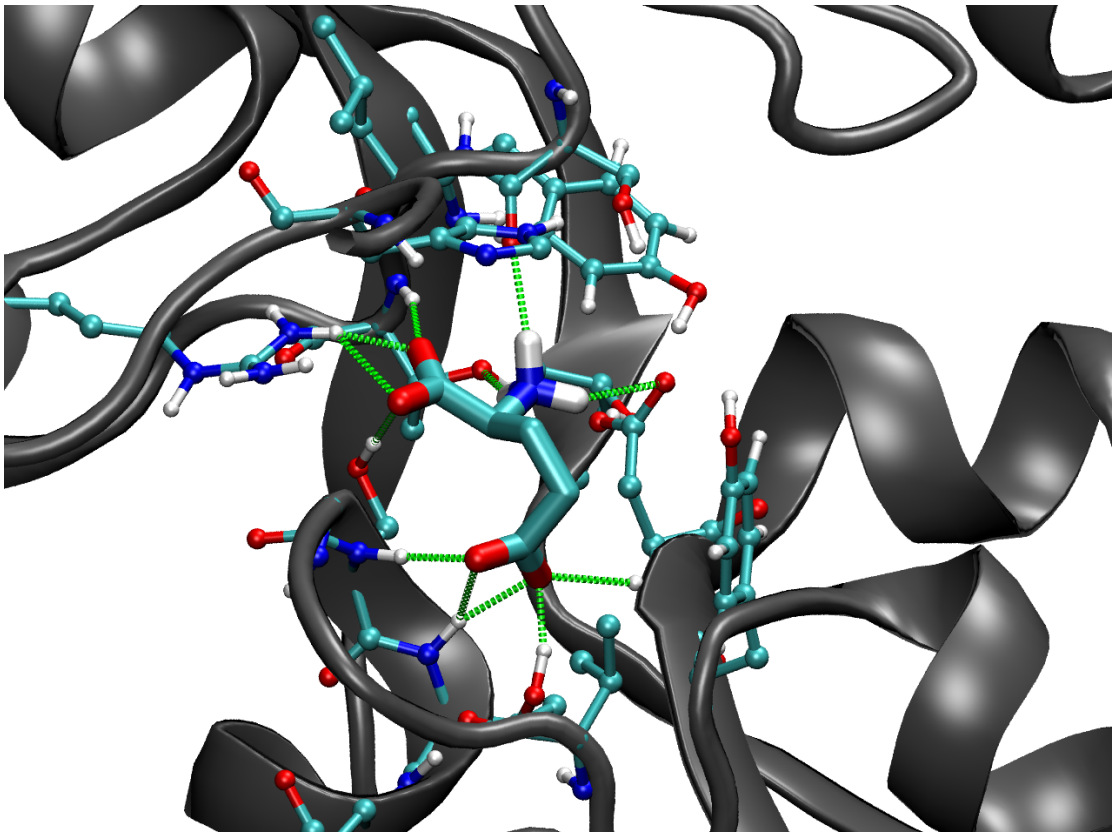

Figure 3.12 *Predicted contacts between NR2A LBD and glutamate ligand.*

The binding pocket of the NR2D LBD model changes over the course of the simulation in concert with the larger structural changes identified earlier. Near the end of the simulations, several differences in the ligand positioning relative to the NR2A crystal structure are apparent.(Figure 3.13)

The most significant difference is the lack of hydrogen bonding between the α-carboxyl and the sidechain of Arg520 (equivalent to Arg499 in NR2A), which has now swung down and away from the ligand binding pocket. Instead, a different positioning of a loop near the top of the pocket has brought the protein backbone closer to the

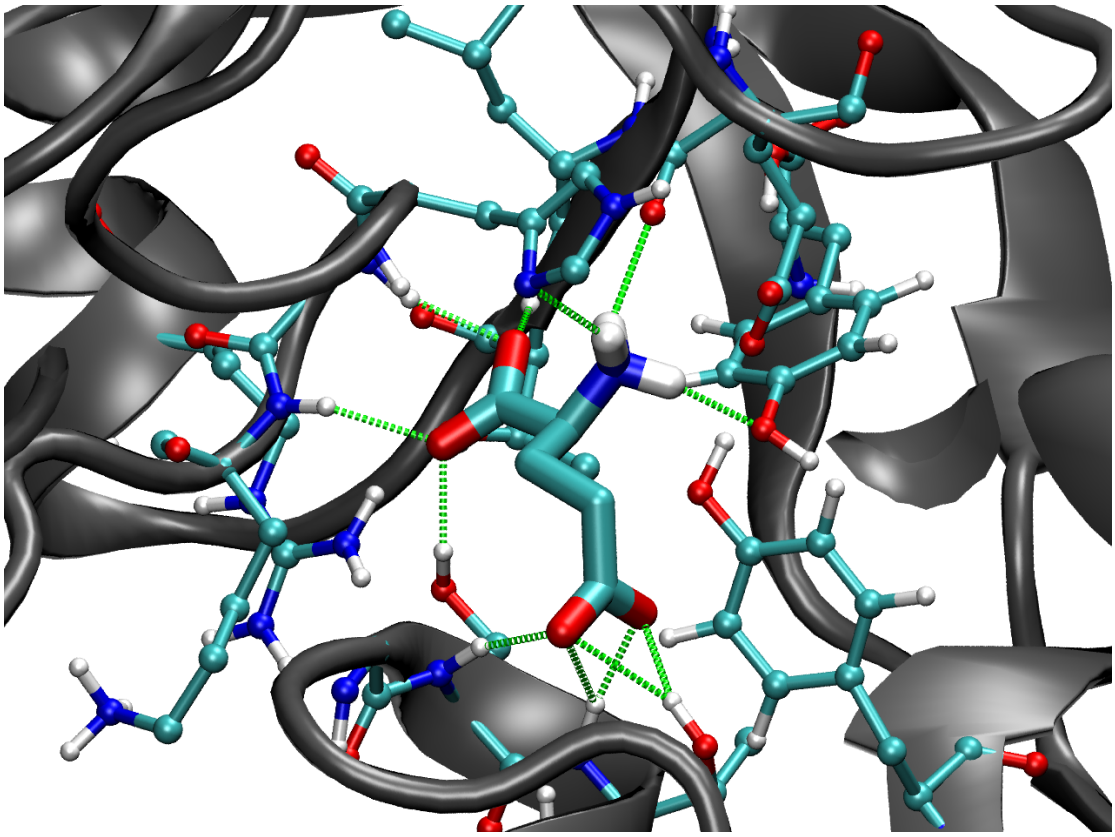

Figure 3.13 *Predicted contacts between NR2D LBD and glutamate ligand.*

glutamate ligand, resulting in hydrogen bonding to the amide hydrogens of Gly467 and Lys468. Also, the amino group of glutamate now hydrogen bonds directly to Tyr763, rather than Asp733 (Asp712 in NR2A).

By pulling back from a view focused only on the ligand binding site, it becomes apparent that the relative rotation of the upper and lower domains in NR2D has modified the points of contact between them.(Figure 3.14)

The simulation of NR2A reveals four persistent hydrogen bonding interactions between the upper and lower domains. A salt-bridge interaction between Glu498 (ad-

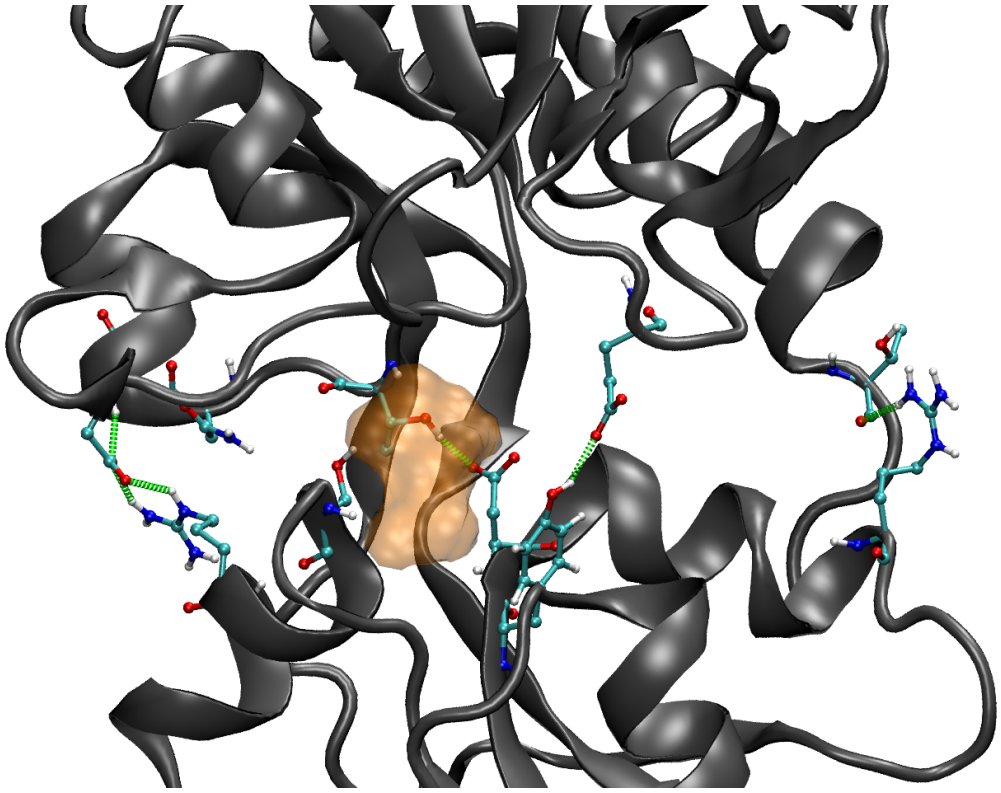

Figure 3.14 *Predicted contacts between the upper and lower domains of the NR2A LBD. The volume of the glutamate ligand is shown in orange.*

jacent to critical residue Arg499) and Arg673, which is located midway down helix F, may provide a tethering point between the binding site and the helix. Hydrogen bonds between Thr494 and Asp712 sidechains and Tyr711 and Glu394 sidechains provide stable inter-domain contacts that bound the ligand binding site on two sides. On the far side of the domain interface there is a contact between Arg722 and Thr778, near the C-terminal end of the LBD. In contrast, the simulation of NR2D has many more points of interaction between the upper and lower domains, as demonstrated

in Figure 3.15. These contacts surround the ligand binding site and there is more fluctuation in these interactions than is seen in the NR2A simulation.

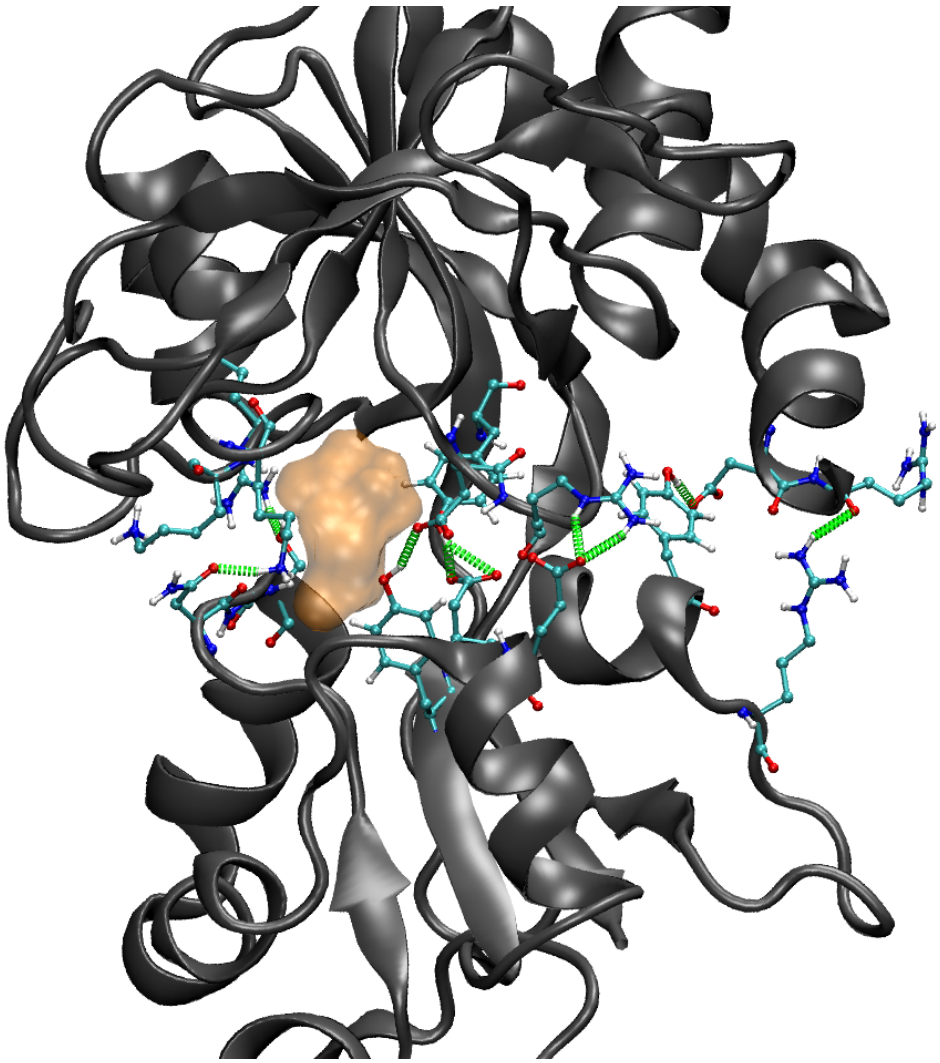

Figure 3.15 *Predicted contacts between the upper and lower domains of the NR2D LBD. The volume of the glutamate ligand is shown in orange.*

3.3 Synopsis

Two sets of two molecular dynamics simulations were performed on models of NR2 ligand binding domains. The first set of simulations utilized a homology model of the NR2A LBD built from the structure of the NR1 LBD. Glutamate and a partial agonist homoquinolinate were placed in the binding site. The second set both contained a glutamate ligand, and compared a crystal structure of the NR2A LBD to a homology model of NR2D built from the NR2A crystal. Both sets of simulations seemed to reach a stable structure after several hundred ps of simulations, although the crystal-based simulations took longer to reach an equilibrium, an understandable effect of their higher simulation temperature. Both the shorter, homology-based simulations at 200K and the longer, crystal-based simulations at 300K predicted contacts between a glutamate ligand and the NR2A LBD that were very similar to those seen in the published crystal structure (Figures 3.4 and 3.12).

The homology-based simulation of the partial agonist homoquinolinate and the homology model of NR2D derived from the crystal structure of NR2A showed similar levels of RMSD over the course of their simulation to the equivalent simulations of NR2A with glutamate. Comparison of the homology-based simulations reveals structural differences that develop over 500 ps between the structure with bound agonist

and bound partial agonist, especially the displacement of helix F, a short α-helix directly below the ligand binding site. Dynamic differences are also evident, with almost all sidechains that comprise the binding pocket exhibiting higher levels of fluctuation with bound homoquinolinaterelative to bound glutamate, possible due to the partial agonists increased size and rigidity.

These simulations demonstrate that structural differences do develop between structures on an accessible molecular dynamics timescale, and suggest that despite shortcomings, the MD method can provide insight into the structural variation between different subtypes and ligand effects. Expansion of the length of simulations as well as inclusion of additional structural information could prove valuable to increasing understanding of the NMDA receptor function.

Chapter 4

NR1/NR2 Ligand Binding Domain Dimer Simulations

> "We choose to go to the moon ... not because [it is] easy, but because [it is] hard."
>
> — John F. Kennedy

The previous chapter dealt with molecular dynamics simulations of one ligand binding domain (LBD) of the NMDA receptor. Although atomic-resolution structural information is scarce, it is clear that the ligand binding domain functions in the context of a large receptor, and is surrounded by LBDs from other subunits as well as other domains of the receptor. Although the addition of surrounding protein will increase the computational cost of simulations, the inclusion of neighboring domains may provide beneficial stabilization and result in more realistic behavior.

4.1 Structure Preparation and Simulation Parameters

4.1.1 Model Construction

Models for the NR1/NR2 dimer simulations were constructed directly from the crystal structure of NR1/NR2A (pdb code 2A5T) published in 2005 by Furukawa *et al.* using Prime.[9, 44] This structure was altered in several ways in order to match the wild-type protein. Two flexible loops, one of 9 residues and the other of 4, were unresolved in the crystal structure. These residues, both in large loops in the S1 length or the NR1 LBD, were rebuilt into the gap in the structure. Another small, two-residue gap in a loop on the NR2A S2 peptide was similarly rebuilt. Lastly, the crystal construct connected the S1 and S2 peptides of both NR1 and NR2A with two-residue linkers, which were removed from the structure prior to simulation. All these modifications were distant from the ligand binding sites on both domains.(Figure 4.1)

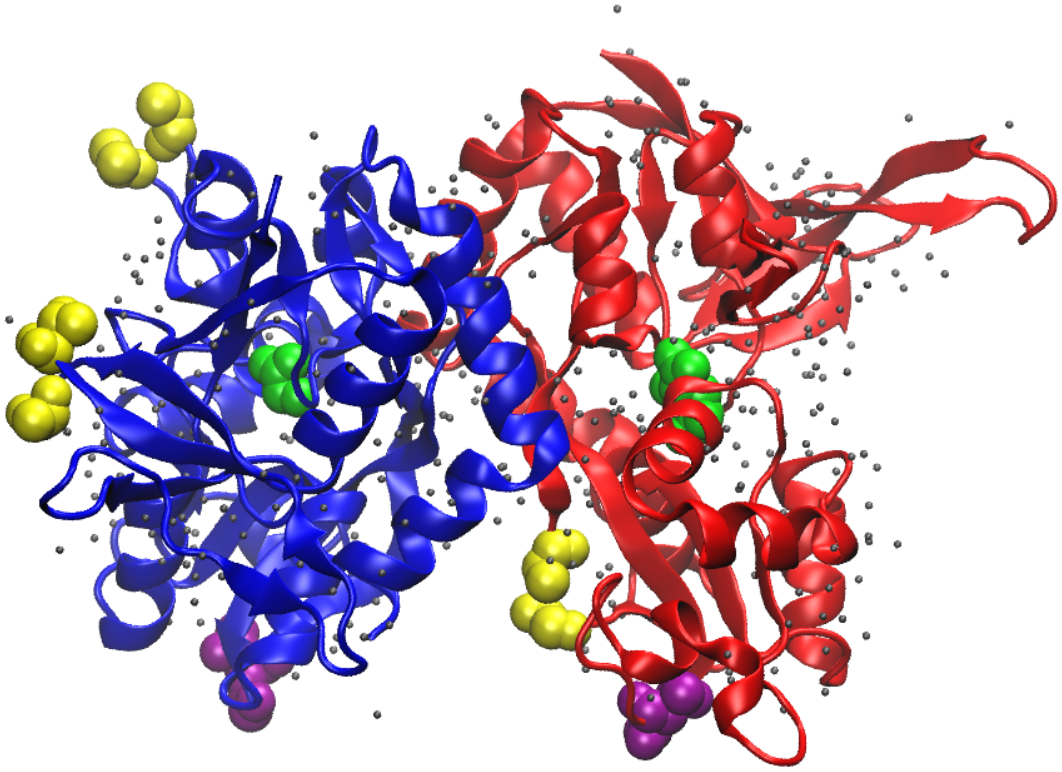

Figure 4.1 *The crystal of the NR1/NR2A dimer is displayed with NR1 colored in blue and NR2A colored in red. Ligands are colored in green while water is grey. Linker regions removed from the model are colored purple, while the ends of missing regions are colored yellow.*

Sequences of the LBDs of NR2B, NR2C, and NR2D were obtained from GenBank and aligned against the sequence of the NR2A LBD from the crystal structure using BLAST. Due to the approximately 80% homology among the LBDs, an initial homology model could be built with little difficulty, with only one gap of one or two residues per model occurring in a flexible loop region far from the binding pocket. Each homology model was combined with the NR1 structure from 2A5T to form a dimer. Residues within 4 Å from the dimer interface were treated with multiple iterations of energy minimization and sidechain optimization to relieve any steric clashes caused by the homology modeling. The positioning of the crystallized glutamate and glycine ligands was left unchanged. Alternative ligands, such as (2S,4R)-4-methylglutamate and D-cycloserine (also known as SYM2081 and DCS respectively, see Figure 4.2), represent clear analogs of glutamate and glycine respectively, and were placed into the binding site to match up common moieties with the crystallized ligands.

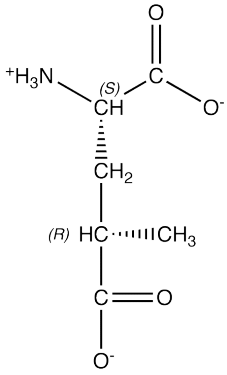

SYM2081

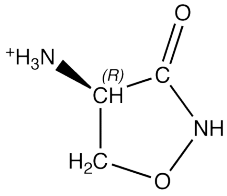

DCS

Figure 4.2 *Glutamate and glycine analogs*

4.1.2 Simulation Conditions

These complexes were simulated using the same conditions as the work described in the previous chapter. Protein and ligand were parameterized in the GROMOS96.1

force field[37] and placed in a periodic box with a minimum of 8 Å between all protein atoms and a periodic boundary. The system was then solvated with between 26,000 and 27,000 water molecules using the SPC water model.[40] Sufficient chloride atoms were added to result in a net charge of zero for the entire system. The systems were first energy-minimized using a simple steepest descent method. Next, a 50 ps simulation was run at 300K with harmonic restraints placed on ligands and protein, enabling solvent relaxation to the protein. This was followed by an unrestrained simulation at 50K for 10 ps, again to allow for small adjustments and alleviation of any remaining steric clashes under low-temperature conditions. This simulation was then extended for an additional 250 ps, with the temperature increasing to 300K over the course of the simulation. From this stage, simulations were continued at 300K for 10 ns. All simulations were performed using GROMACS v3.2.1 with NPT conditions and a Berendsen thermostat.[38–39, 41] Electrostatics were treated with the PME method utilizing a cutoff of 9 Å.[42] Again all simulations except for the initial 50K simulation were performed with a timestep of 2 fs, while the low-temperature run used a 1 fs timestep. Average structures were obtained by fitting and averaging structures from the final 2 ns of simulation.

4.2 Comparing NR2A and NR2D

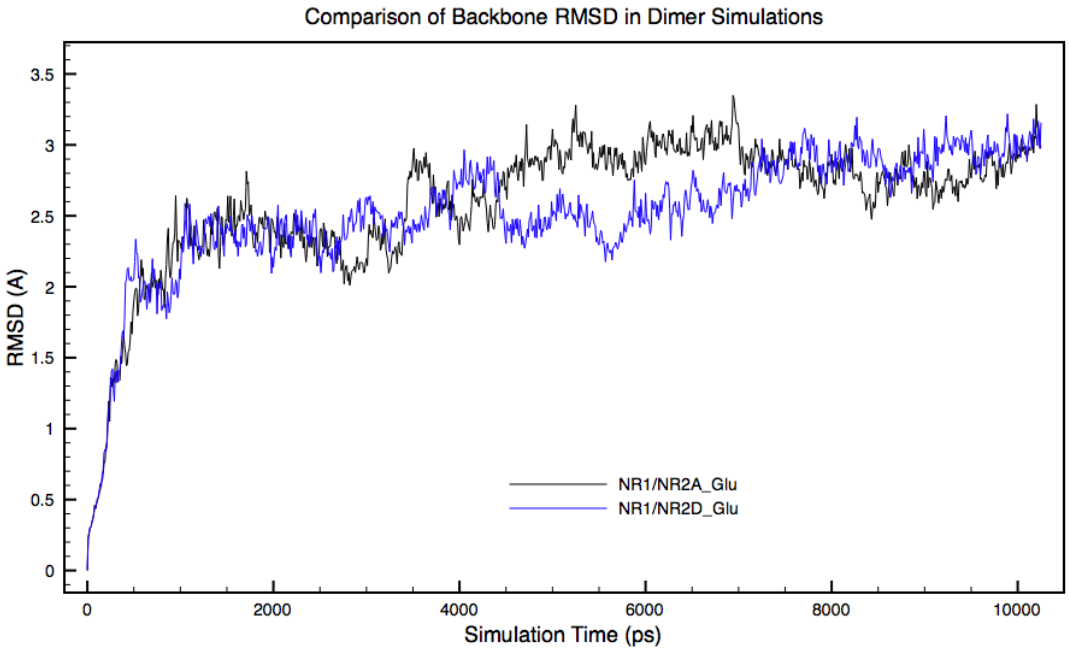

Figure 4.3 *The RMSD of both the NR1/NR2A and the NR1/NR2D dimers to the crystal structure over the course of simulation at 300*K*.*

Initial analyses of the backbone-to-backbone RMSD of both the NR1/NR2A dimer and the NR1/NR2D dimer reveal largely stable structures over the course of 10 ns of simulation at 300K.(Figure 4.3) It is clear that although the size of protein simulated is effectively doubled when compared with prior simulations (due to the inclusion of the NR1 LBD), the total RMSD from the starting structure is about equal to previous simulations of the NR2 LBD only at 300K (see Figure 3.8). This implies a closer agreement in the dimer simulations than the previous simulations since RMSD can scale with the number of atoms compared.

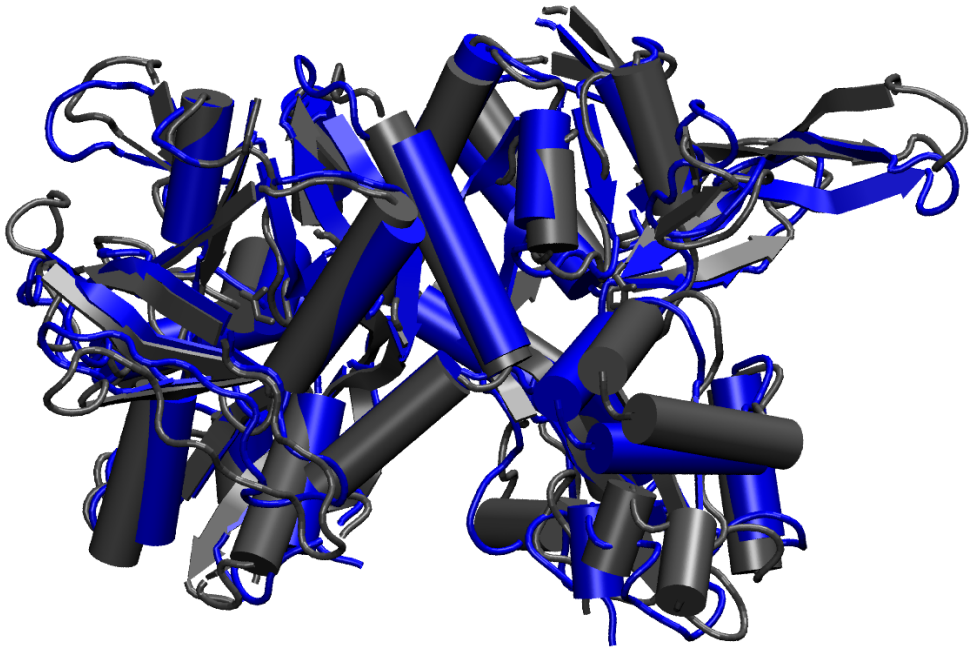

Figure 4.4 *Alignment between crystal structure in grey and average simulation structure in blue of the NR1/NR2A LBD complex*

An alignment of the crystal structure of NR1/NR2A and the average structure from the final 2 ns of the NR1/NR2A simulation reveals good backbone comparison in most regions of the dimer complex.(Figure 4.4) Secondary structure elements in NR1 and the upper (D1) domain of NR2A align well despite over 10 ns of simulation, although some highly flexible loops are displaced. The lower domain (D2) of NR2A demonstrates a somewhat different positioning between the crystal and simulation structure, especially in the region of helix F and G just below the glutamate binding site.

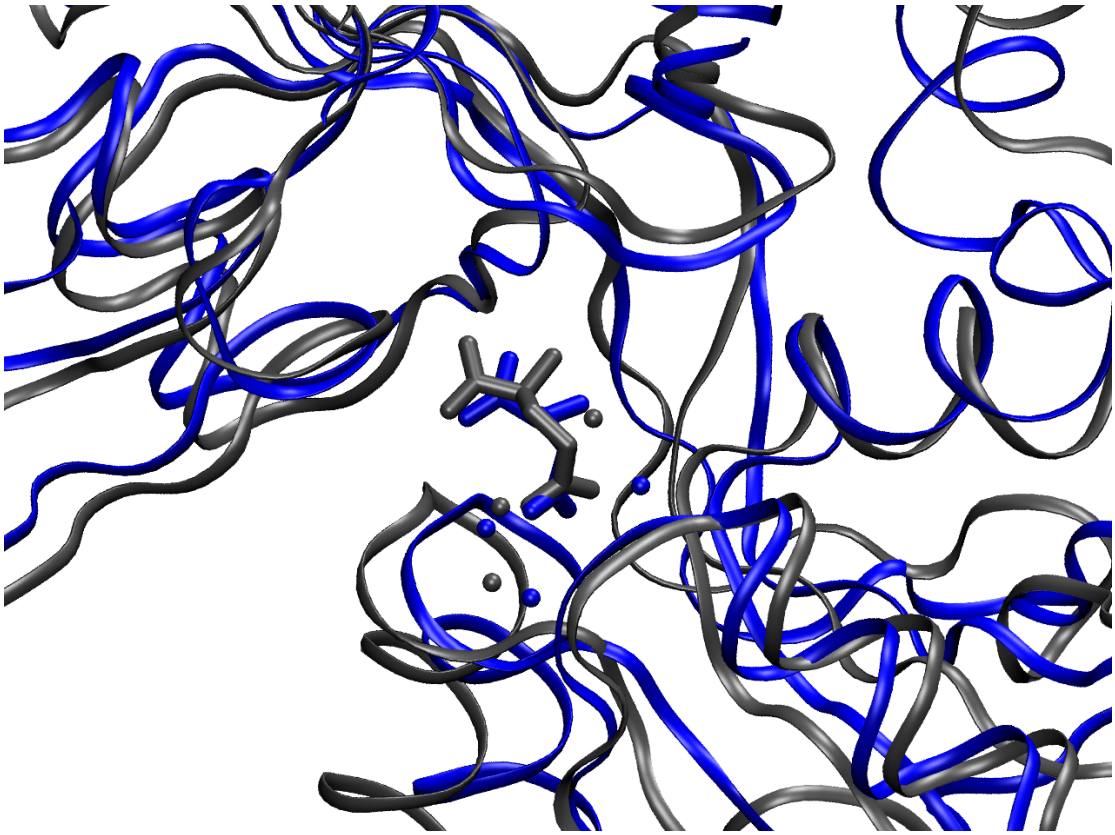

Figure 4.5 *Close-up of the NR2A ligand binding site displaying correlation between placement of the crystal (grey) and average simulation (blue) backbone, ligand, and water molecules.*

Focusing in on the glutamate binding site unveils good alignment between the backbones of the crystal and average simulation structures.(Figure 4.5) Although there is some deviation between the backbones, especially in the helix F region below the binding site, differences between the placement of the glutamates are minor. The ligands maintain very similar orientations relative to their respective binding sites, and persistent water molecules can be found in the simulation that correlate

to crystallographically-resolved waters. This suggests that the simulation represents the internal hydrogen bonding of the binding site in a fashion similar to the crystal structure.

4.2.1 Average Structure Comparison

Before a thorough examination of differences between the average structures, it is important to verify that the averages are in fact representative of a large portion of the simulation. By computing the RMSD of the trajectory to the average structure one can ascertain whether the simulation does stabilize around the average, or whether the average represents a midpoint along some trajectory. As shown in Figure 4.6, at approximately 3 ns into each simulation both trajectories had reached structures within 1.4 Å backbone RMSD to the average structure. Both simulations fluctuated within this range for the remainder of the simulation.

Superposition of the NR1/NR2A and NR1/NR2D dimer average structures allows for identification of regions where the structures differ after 10 ns of MD simulation. It is clear in Figure 4.7 that the NR1 LBDs of the two average structures align very well, with only subtle differences in positioning of secondary structure elements. This is not surprising, as the NR1 sequences are identical between these simulations. The alignment of the NR2 region is not as good, especially in a flexible loop in the upper (D1) domain as well as helix F and G in the lower (D2) domain. An analysis by the

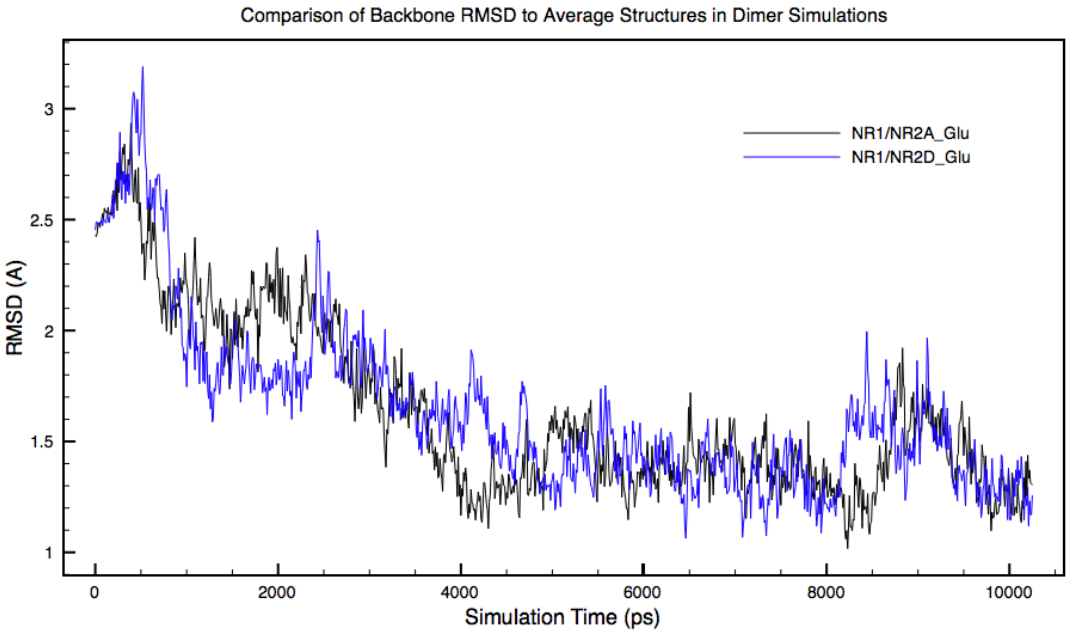

Figure 4.6 *The RMSD of both the NR1/NR2A and the NR1/NR2D dimers to the average structure over the course of simulation at 300*K.

hingefind analysis used previously reveals a rotation of 15°, however the rotation is only present in a portion of the lower domain, unlike in the previous simulations of NR2 only (shown in Figure 3.11).[45] Another way of visualizing the same comparison is shown in Figure 4.8, which shows the average NR1/NR2A structure colored by the displacement between itself and the NR1/NR2D average structure. Excepting some flexible loops, it is clear that the lower region of the NR2 domain shows more displacement between the structures than other regions.

Given the differences observed in the position of helices F and G in the simulations of NR1/NR2A and NR1/NR2D, further care should be taken to characterize

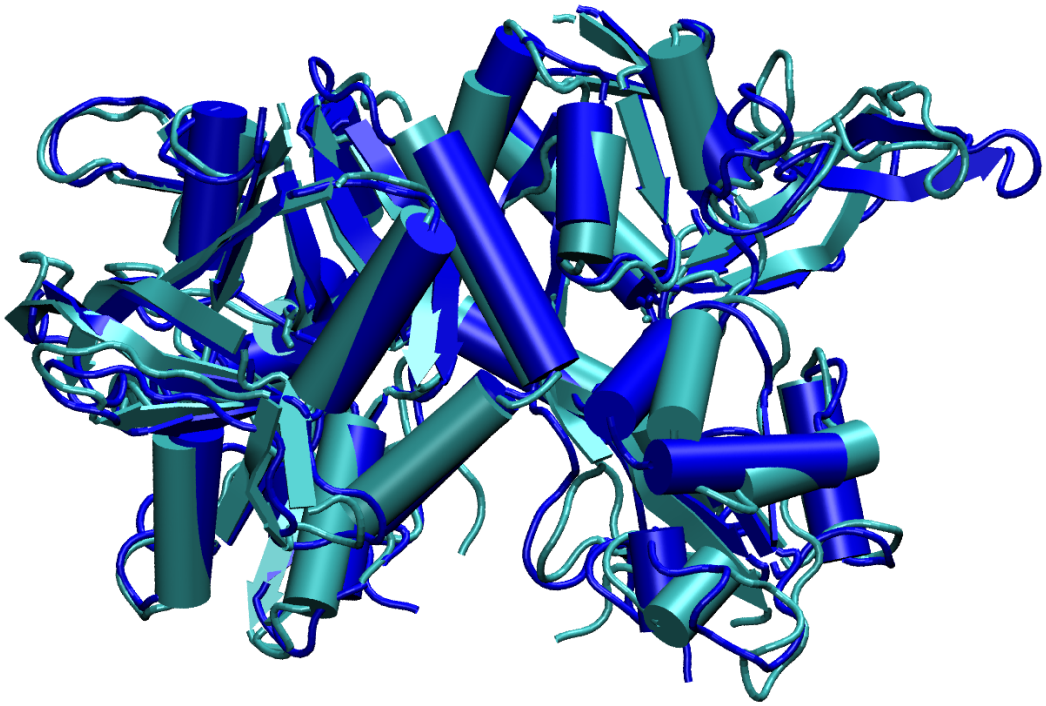

Figure 4.7 *Alignment of the average structures of the NR1/NR2A and the NR1/NR2D dimers reveals considerable superposition over most of the complex.*

the behavior of this region over the course of the simulation. While Figure 4.6 provides a measure of confidence that the average structures are indicative of the overall structure of the protein during much of the simulation, it is feasible that this portion of the complex may undergo more variation than other portions, and that the averages have captured different positions of these flucuations. The backbone RMSF of both the NR1/NR2A and NR1/NR2D structures were calculated over the course of the simulation, and the structure of NR1/NR2D is shown in Figure 4.9 colored by its

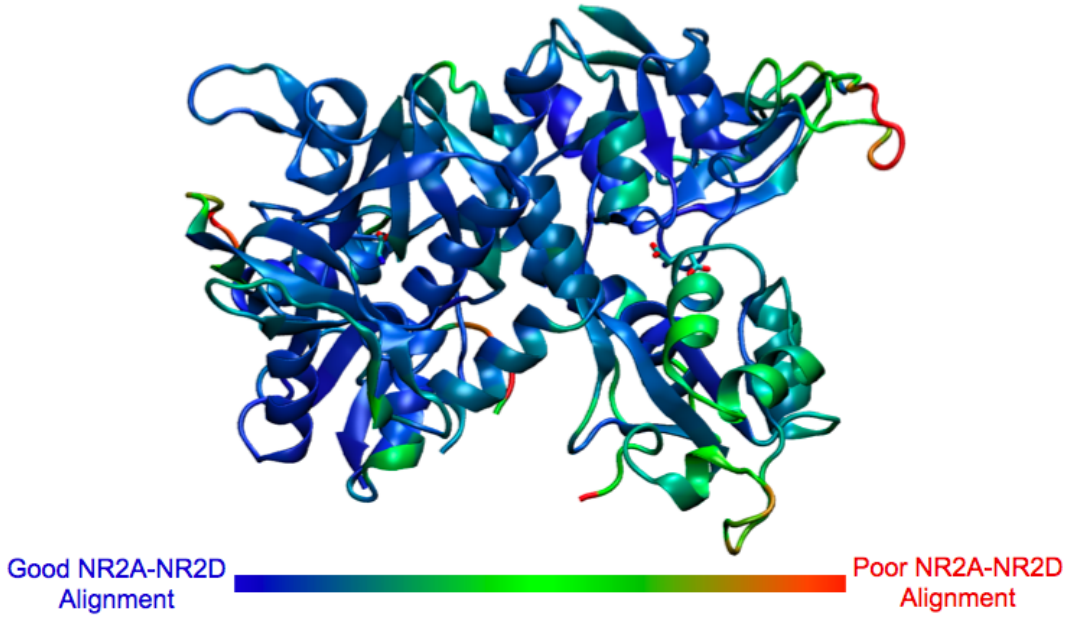

Figure 4.8 *The average structures of the NR1/NR2A dimer colored by displacement between the NR1/NR2A and NR1/NR2D average structures.*

RMSF. It is clear that the lower domain of NR2 does not undergo more fluctuation than other regions at equivalent positions within the dimer complex, implying that the positioning of the helices in question is stable, and not an arbitrary position due to higher degrees of variation.

4.2.2 Ligand Binding Site

Despite the identical sequences of the the glutamte binding sites in NR2A and NR2D (see Figure 2.7), the simulations of these systems reveal subtle differences in the positioning of both ligand and important binding site residues. Examination of an alignment of the agonist binding sites of the NR1/NR2A_Glu and NR1/NR2D_Glu

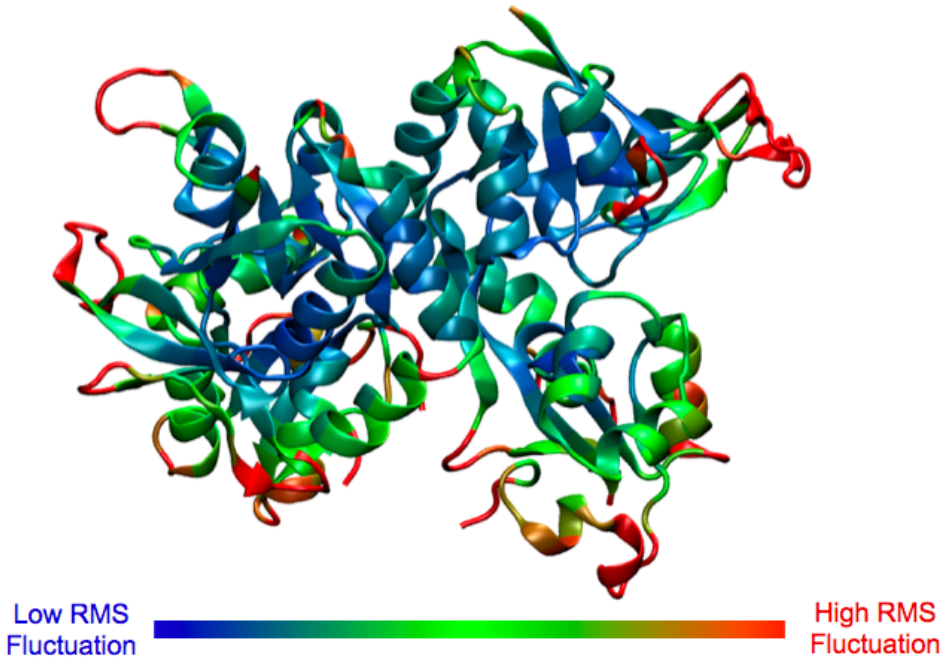

Figure 4.9 *The NR1/NR2D dimer is colored by backbone RMSF, demonstrating that helix F does not fluctuate more than other regions of similar placement within the complex*

simulations reveals a subtle difference in posture of the sidechain of the glutamate ligand, as shown in Figure 4.10. Note that although the relative positions of the γ-carbon and to some extent the β-carbon are different, the placement of the amino and carboxyl functionality is very stable and similar over the course of the two simulations.

Both simulations show similar contacts between the glutamate ligands and critical residues on the left side of the binding pocket. Hydrogen bonds between the α-carboxyl both Arg499 and Thr494, and the γ-carboxyl and residues at the top of helix F such as Ser670 and Thr671 are stable and persist throughout the simulations.

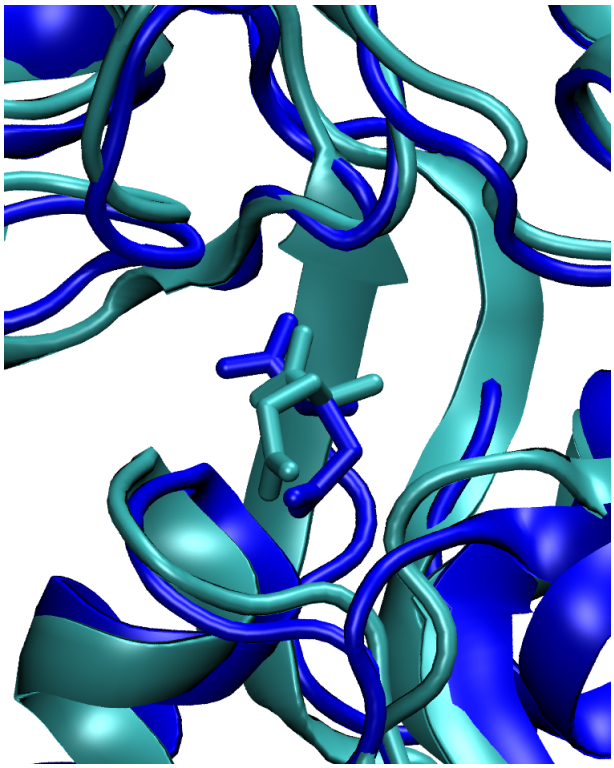

Figure 4.10 *Comparison between the ligand positioning of NR1/NR2A_Glu (dark blue) and NR1/NR2D_Glu (light blue)*

Corresponding interactions occur between the ligand and the equivalent residues in NR2D (Thr515, Arg520, Ser691 and Thr692), as shown below in frames from the final ns of simulation and are representative of stable interactions found throughout the trajectories.(Figure 4.11)

Examination of interactions on the right side of the binding pocket reveals more variation between the simulations than was seen on the left. In the NR1/NR2A_Glu simulation, the glutamate ligand forms hydrogen bonds between the charged amine

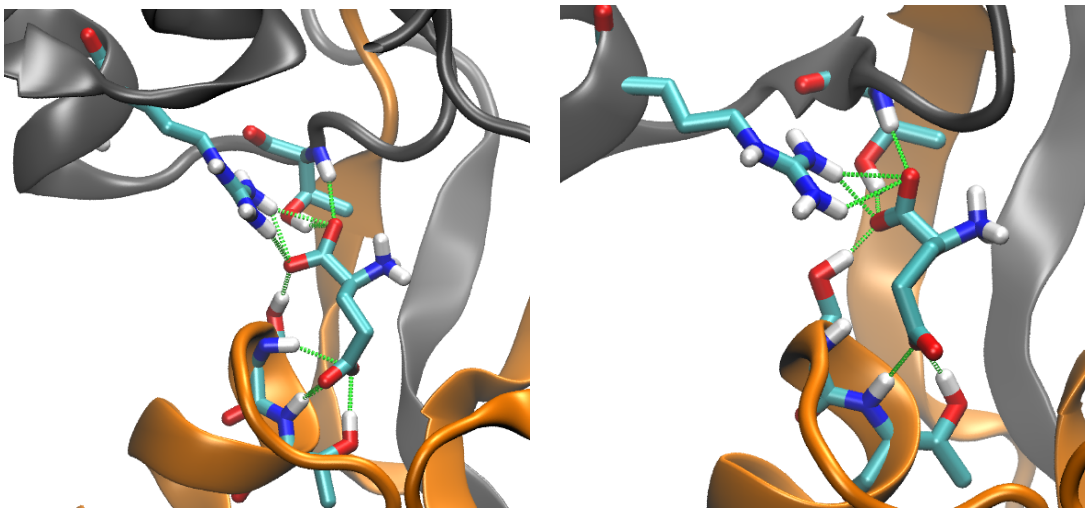

NR1/NR2A_Glu NR1/NR2D_Glu

Figure 4.11 *Similar contacts on the left side of the binding site for both NR1/NR2A_Glu and NR1/NR2D_Glu*

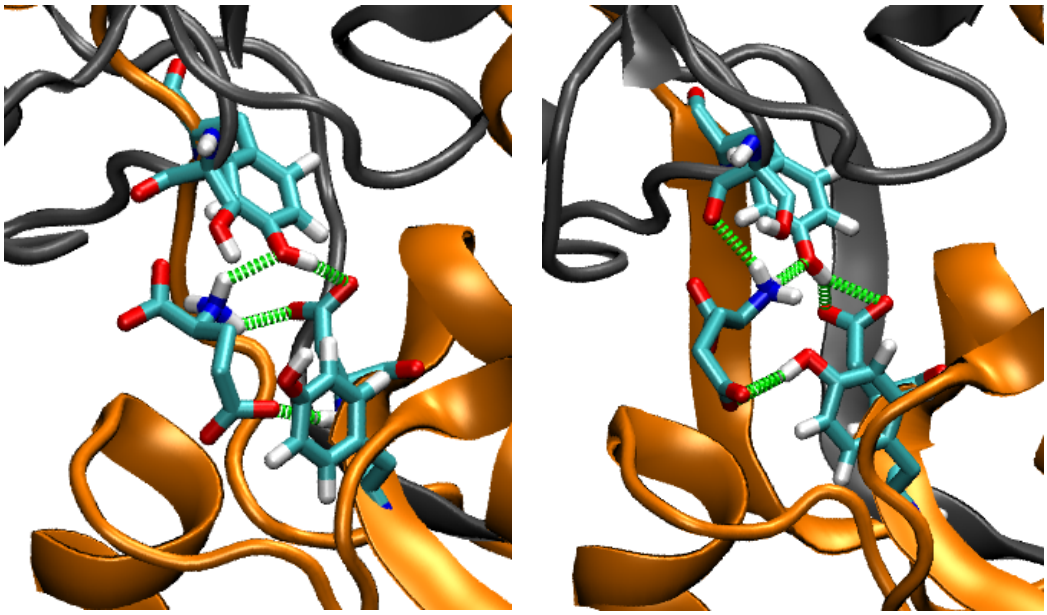

NR1/NR2A_Glu NR1/NR2D_Glu

Figure 4.12 *Contacts for the glutamate ligand differ slightly on the right side of the binding pocket*

and the sidechains of Tyr742 and Asp712, and the backbone of Asp712 forms a hy-

drogen bond with the γ-carboxyl, the same "cross-pocket" hydrogen bond observed in previous simulations (see Figures 3.6 and 3.12). However, in the simulation of the NR1/NR2D_Glu complex, the slight difference in positioning of the γ-carboxyl eliminates the interaction with the backbone of Asp733 (equivalent to Asp712 in NR2A). This is countered by a hydrogen bond with the sidechain of Tyr732, which rotates down and interacts directly with the γ-carboxyl of glutamate (see Figure 4.12), an interaction not found in the simulation of NR1/NR2A_Glu. The equivalent residue, Tyr711 in NR2A, forms a stable hydrogen bond with Glu394 throughout the entire simulation of NR1/NR2A_Glu.

4.2.3 Interdomain Interactions

Given the differences seen in previous simulations of the NR2 LBD only, an examination was conducted of the inter-domain contacts present in these two simulations. Both the NR1/NR2A_Glu and NR1/NR2D_Glu simulations exhibit two similar, stable interdomain contacts shown in Figure 4.13. In NR2A there is a salt bridge between Glu498 and Arg673, with the arginine position in the middle turn of helix F. This is mirrored by a salt bridge in the equivalent position in NR2D between Glu519 and Lys694. Additionally, there is an identical hydrogen bond proximal to the binding pocket between Thr512 and the critical Asp712 (Thr533 and Asp733 in NR2D).

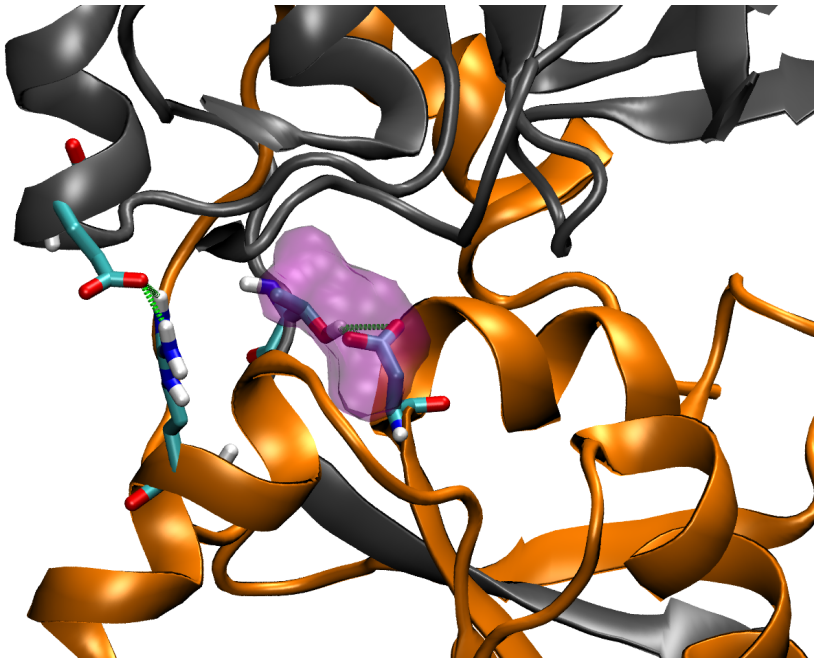

NR1/NR2A_Glu

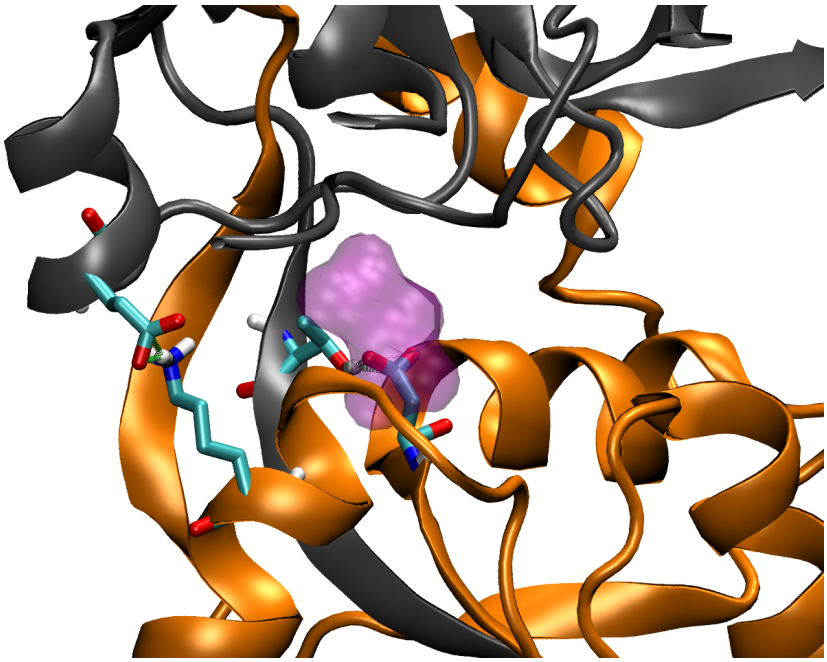

NR1/NR2D_Glu

Figure 4.13 *Similar inter-domain contacts formed by NR1/NR2A and NR1/NR2D*

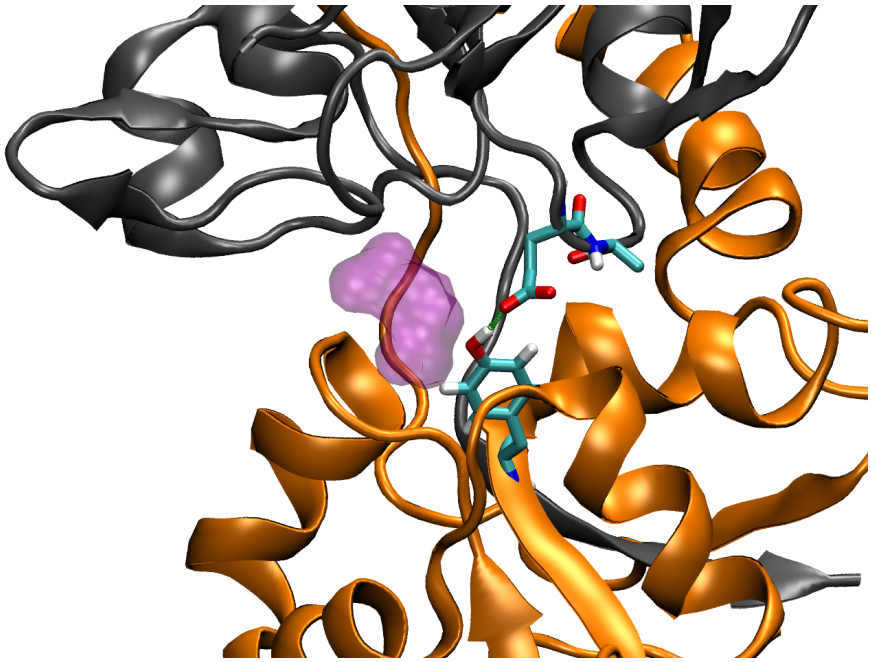

NR1/NR2A_Glu

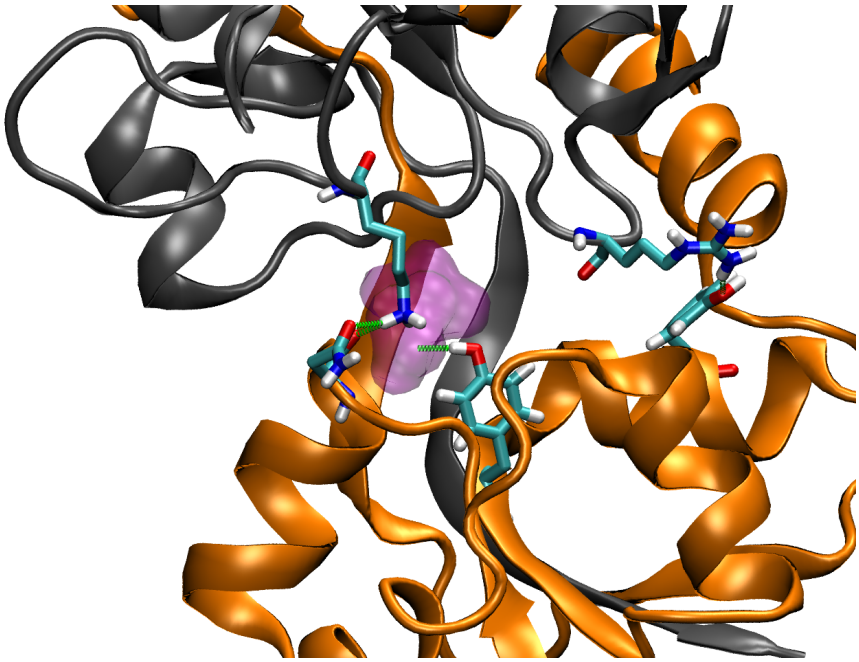

NR1/NR2D_Glu

Figure 4.14 *Differing inter-domain contacts between NR1/NR2A and NR1/NR2D*

Differences in the inter-domain contacts between the upper and lower domains of the LBD also reinforce the distinctions in the binding sites that was highlighted above, and are represented in Figure 4.14. As previously noted, the simulation of NR1/NR2A_Glu predicts a stable, persistent hydrogen bonding interaction between two residues that define the front right boundary of the ligand binding site, Glu394 and Tyr711. This interaction is present in the NR1/NR2A crystal structure, and so the NR1/NR2D homology model replicates this interaction. However, just before 5 ns of simulation, the equivalent tyrosine, Tyr732, rotates down and interacts with the γ-carboxyl of the glutamate ligand, while the Glu413 swivels up slightly to interact with His487 and Ser513 at the top of the pocket. In the same region is Lys486, which in NR2D is predicted to form a hydrogen bond with both the sidechain and backbone of Asn689, a residue just adjacent to the first turn of helix F. This lysine is also situated near the γ-carboxyl of the glutamate ligand in the NR1/NR2D_Glu simulation, and forms an intermittent salt bridge several times over the 10 ns of simulation. In contrast, the equivalent residue in NR2A, Lys465, forms only brief interactions with the equivalent asparagine, but spends more time forming intermittent hydrogen bonds with both residues of the stable Glu394-Tyr711 contact. Lastly, the residue adjacent to the important Glu394 is Ala395 in NR2A, but in NR2D the alanine is replaced by Arg414, a significant change. This arginine stretches away from the binding site and

forms a persistent hydrogen bond with Tyr739. Thus, the NR1/NR2D dimer simulation predicts altered interaction between the D1 and D2 domains of the NR2D LBD compared to the simulation of NR1/NR2A which arise both from altered positioning of identical residues and differences in sequence.

4.3 SYM2081

The ligand (2S,4R)-4-methylglutamate (SYM2081, Figure 4.15) provides a discriminating probe of the NR2 glutamate binding site despite its similarity to glutamate. Although nearly all NR2 agonists show increased potency at NR2D compared to NR2A, SYM2081 has an enhanced ratio of 46 when comparing EC_{50} values at NR2D-containing receptors to those composed of NR2A, compared to an approximately 10-fold difference for glutamate. Despite the sequence similarity between the binding sites of NR2A and NR2D, as detailed previously, structural differences arose during the molecular dynamics simulation of glutamate-bound NR1/NR2A and NR1/NR2D. Several of these differences in both ligand, as well as binding site sidechain, positioning occurred in the region around the β and γ carbons of the glutamate ligand, precisely the region where SYM2081 differs from glutamate. This implies that simulation may shed

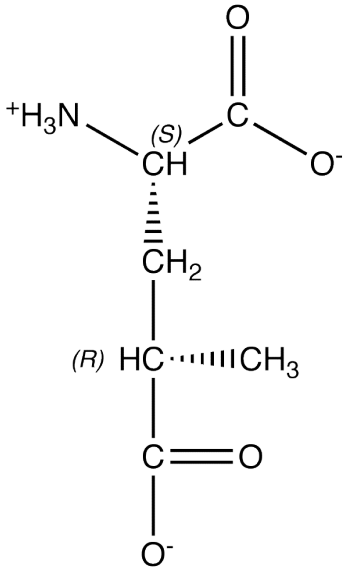

Figure 4.15 *SYM2081*

light on the structural roots of the functional difference in the response of these subtypes. In order to test the sensitivity of the simulations to this ligand, the glutamate in the starting structures of NR1/NR2A and NR1/NR2D was replaced with SYM2081, and molecular dynamics simulations were then performed as described above for 5 ns of simulation.

The behavior of the ligand in the simulation of NR1/NR2D_SYM2081 was very similar to the behavior of the same protein with glutamate seen in the simulations described above, with SYM2081 remaining in the binding pocket with the same stable interactions as seen in the simulation of NR1/NR2D with glutamate. All three charged functionalities of the SYM2081 ligand are in similar positions and have similar contacts to those predicted in the simulations with glutamate. Furthermore, the same repositioning of the Tyr732 sidechain as described above in the NR1/NR2D_Glu simulation is seen in the simulation with SYM2081. A stable hydrogen bond with the γ-carboxyl of SYM2081 is formed after the sidechain swings down from its initial position of interaction with Glu413.

Alternatively, the simulation of NR1/NR2A_SYM2081 predicts an unstable binding pose between the ligand and the binding pocket in NR2A. The source of the instability seems to be a steric clash of the 4-methyl group of SYM2081 with the sidechain of Tyr711, which as seen in the previous simulation of NR1/NR2A_Glu, forms a stable interaction with Glu394. Figure 4.16 depicts the contrast in the stability of the two

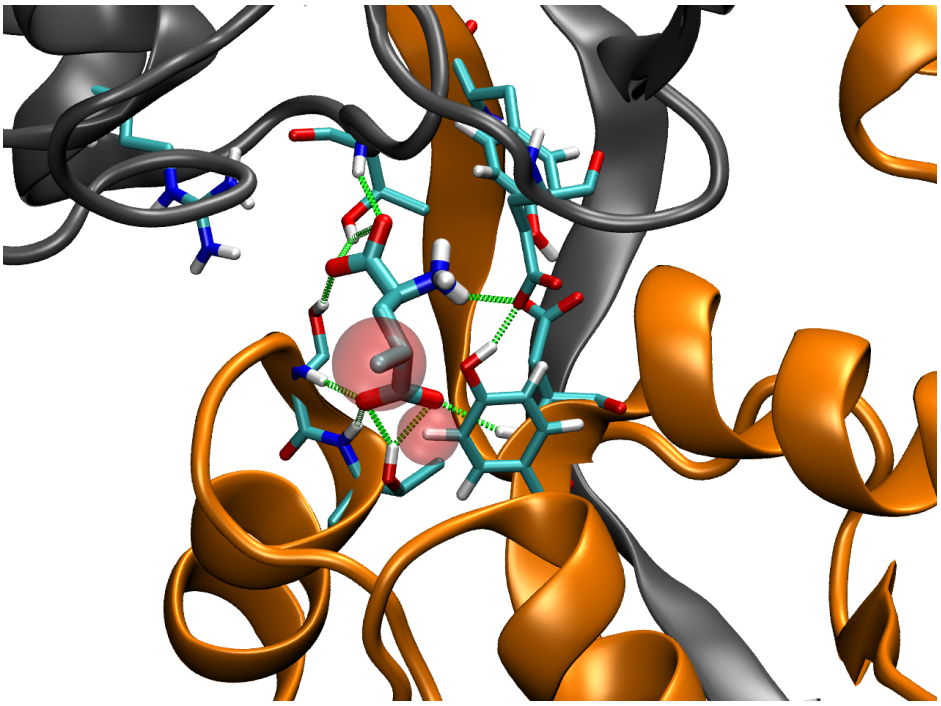

NR1/NR2A_Sym2081

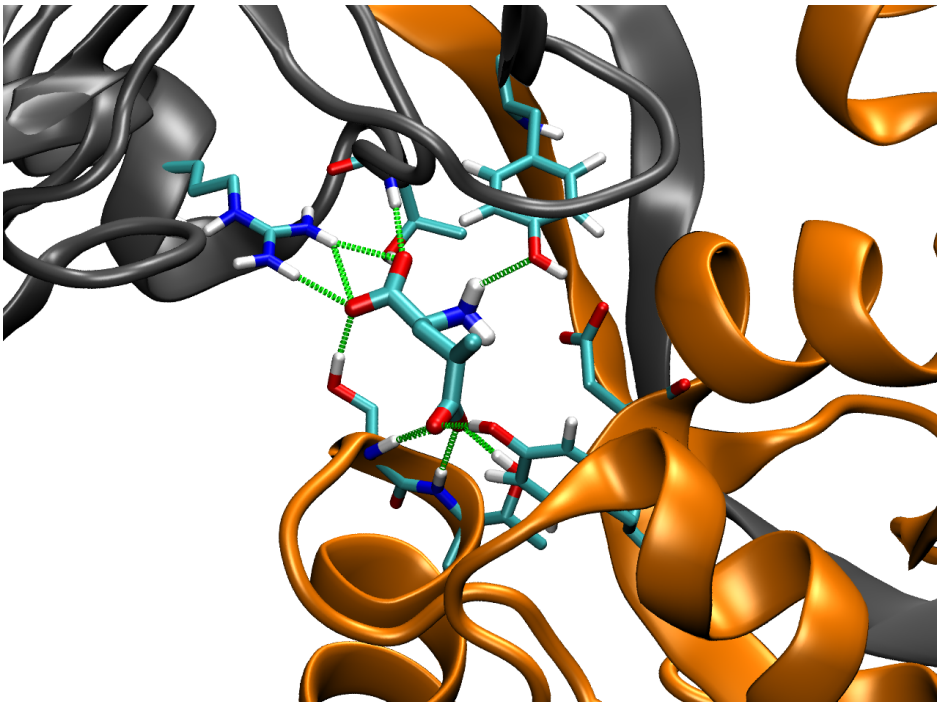

NR1/NR2D_Sym2081

Figure 4.16 *Comparison of the steric conflict in the NR1/NR2A binding pocket with bound SYM2081 to the stably bound complex in NR1/NR2D*

complexes, and highlights the location of the steric conflict. This persistent interaction appears to induce a rotational force on the ligand, which quickly results in displacement of the α-carboxyl away from the critical Arg499 sidechain. As illustrated in the filmstrip of snapshots shown in Figure 4.17, the continued steric collisions between the 4-methyl group of SYM2081 and Tyr711 result in the disengagement of the γ-carboxyl from the top of helix F, and eventually the SYM2081 rotates the 4-methyl group down while the γ-carboxyl swings up, effectively disengaging the ligand from the lower domain of the protein. The combination of the slight adjustment to the "sidechain" of the glutamate ligand and the alteration

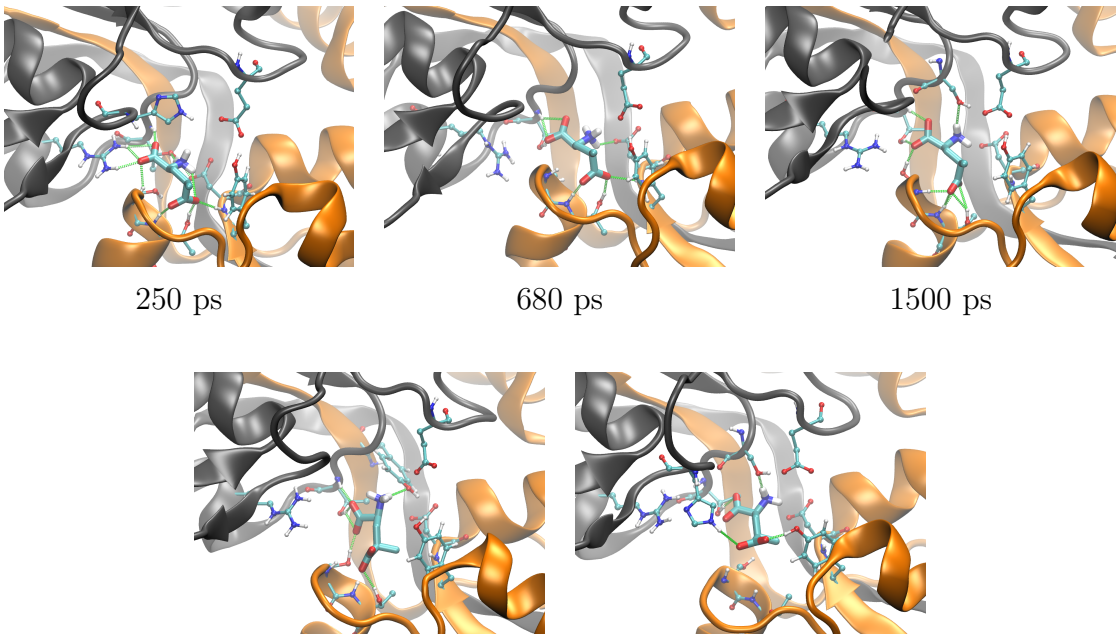

Figure 4.17 *Snapshots detailing the progression away from the starting binding pose of SYM2081 in NR1/NR2A*

of the tyrosine position predicted in the NR1/NR2D dimer relative to the NR1/NR2A dimer seems to create a small pocket that is exploited by the positioning of the 4-methyl of SYM2081. The alleviation of the steric crowding seen in NR1/NR2A is consistent with the enhanced differential potency of this particular ligand.

4.4 NR2C and D-cycloserine

D-cycloserine (DCS, Figure 4.18) is a partial agonist of NMDA receptors that interacts only at the glycine binding site in the NR1 LBD.[46–48] However, DCS is determined to have greatly increased efficacy at receptors containing NR2C while efficacies at NR2A- or NR2B-containing receptors are decreased relative to glycine.[49] Despite binding to a different domain (the NR1 LBD) which is the same between receptors, the identity of the NR2 subtype determines whether DCS results in 35% of the efficacy of glycine or 193% the response of glycine, over a 5-fold difference.

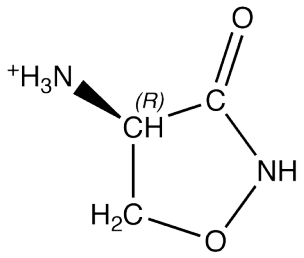

Figure 4.18 *DCS: D-cycloserine*

A homology model of the NR1/NR2C LBD dimer was created in the same manner described above for NR1/NR2D. Two forms of this model were subjected to the same treatment and molecular dynamics simulation: one with glutamate in NR2C and glycine in NR1, and the other with glutamate in NR2C and DCS in NR1. D-cycloserine was placed in the same

orientation and position as glycine.[12] As in the case of SYM2081, these complexes were run for 5 ns.

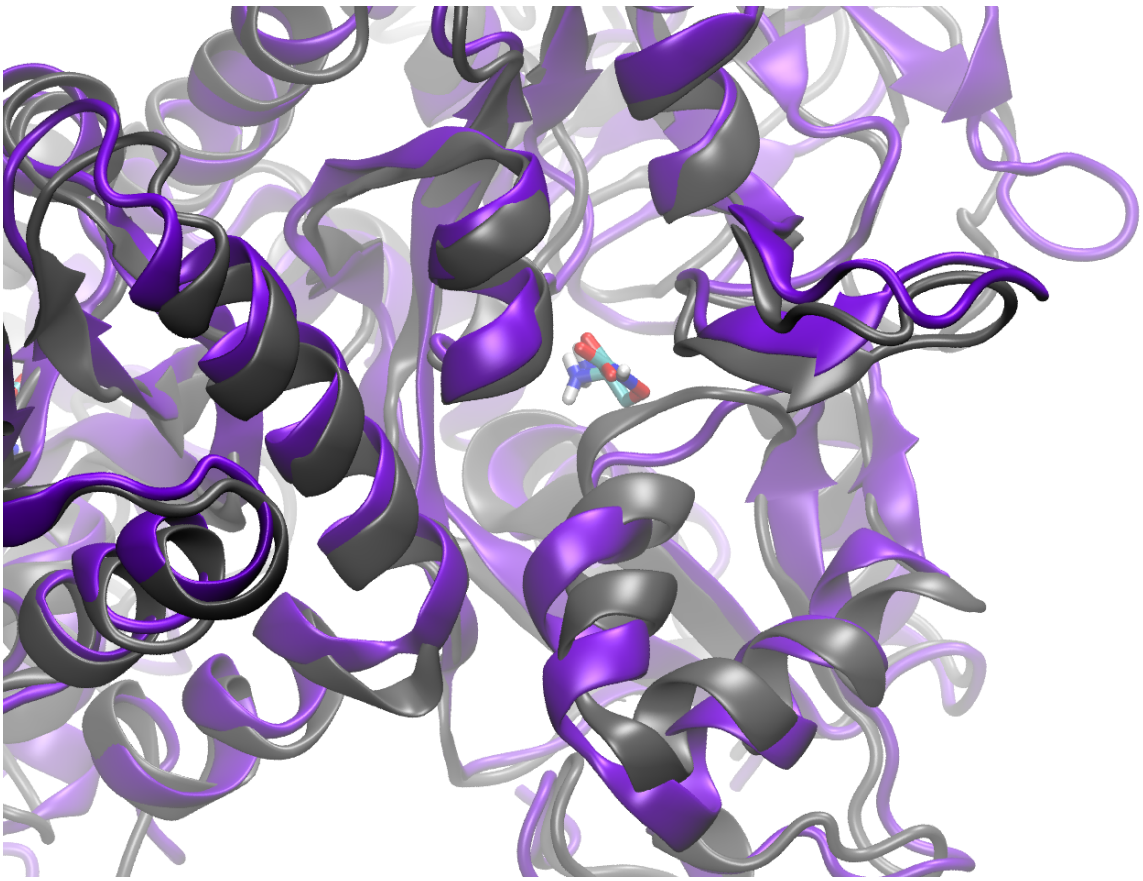

Figure 4.19 *Overlay of the glycine binding sites of the NR1_Gly/NR2C (grey) and NR1_DCS/NR2C (purple) complexes.*

While the two ligands in the NR1 co-agonist binding site remain stable within the binding site, the larger, cyclic structure of DCS has a clear effect on the arrangement of the neighboring protein region. As illustrated in Figure 4.19, the DCS displaces

a portion of the loop that forms a lower boundary to the binding site, and this perturbation is transferred down into the helix below, the analogous helix F in the NR1 domain. The NR1/NR2C complex with bound DCS pushes the central turn of helix F much closer to the neighboring NR2C domain. There is also some reorganization evident in the bend of the NR2C helix J (the angular helix left of the NR1 helix F in Figure 4.19) between the two structures.

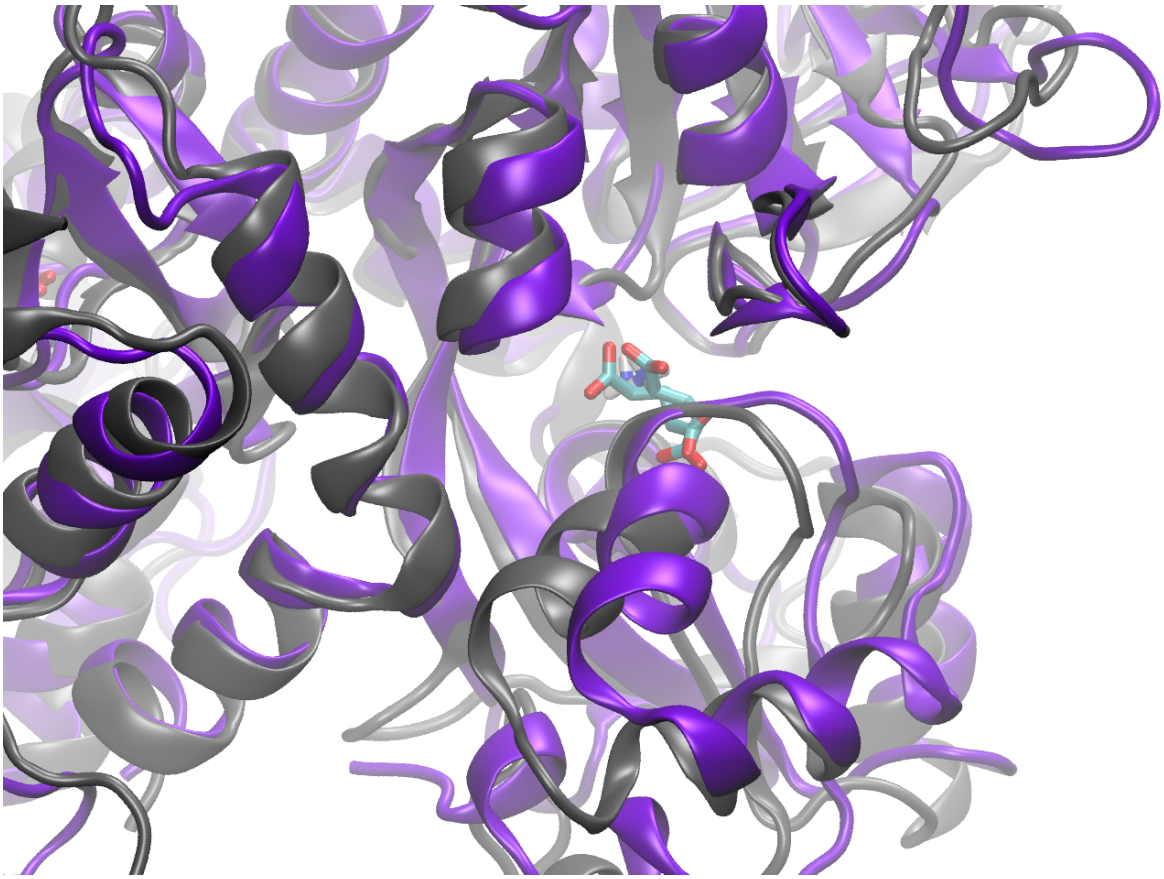

Figure 4.20 *Overlay of the glutamate binding sites of the NR1_Gly/NR2C (grey) and NR1_DCS/NR2C (purple) complexes.*

Surprisingly, there are large structural differences in the helix F region of NR2C, just below the glutamate binding site. These differences develop despite that the only initial difference in the simulations was the presence of either glycine or DCS in the binding pocket of NR1, almost 30 Å from the glutamate ligand. Both helix F and to a lesser extent the following helix, helix G, are rotated out and away from the neighboring bent helix of NR1 (see Figure 4.20). This displacement is reminiscent of the difference between NR1/NR2A and NR1/NR2D predicted previously.

Lastly, sequence comparison between the four NR2 LBDs highlights a specific residue, Gln800, that is a conserved glutamic acid in the other three NR2 subtypes. Gln800 is positioned just below the bend in the helix J of NR2C, which places it adjacent to helix F of NR1. In the NR1_Gly/NR2C simulation, a stable hydrogen bond exists between the carbonyl of the amide sidechain of Gln800 and the sidechain of Tyr692, a residue on the NR1 helix F that stretches out to form this persistent interaction. As shown in Figure 4.21, this contact does not occur in the NR1_DCS/NR2C simulation. When DCS is in the binding site, the displacement in helix F of NR1 alters the position of the Tyr692 backbone, which in turn shifts the sidechain out of position to form the hydrogen bond with Gln800.

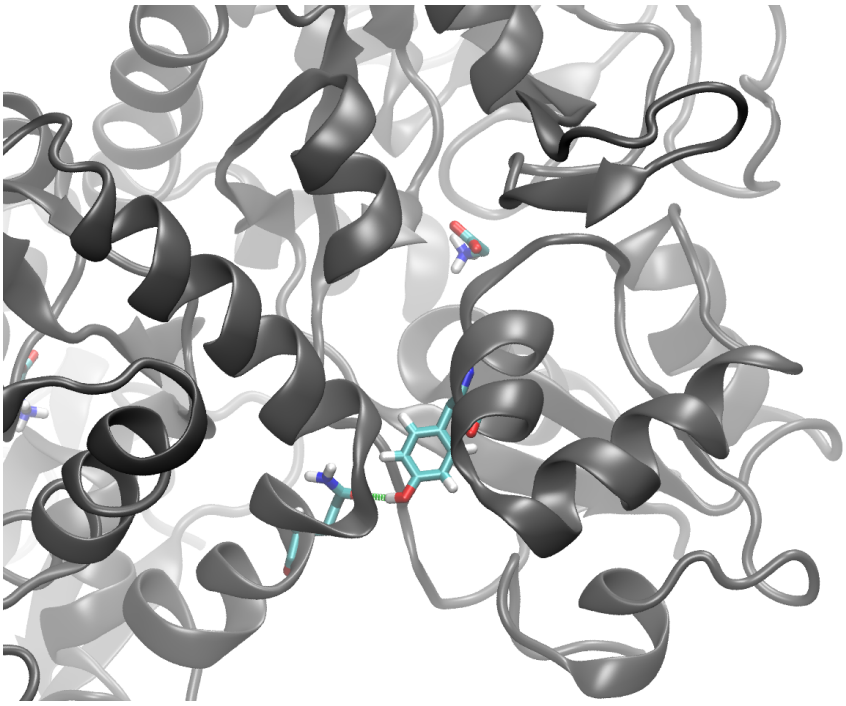

NR1_Gly/NR2C

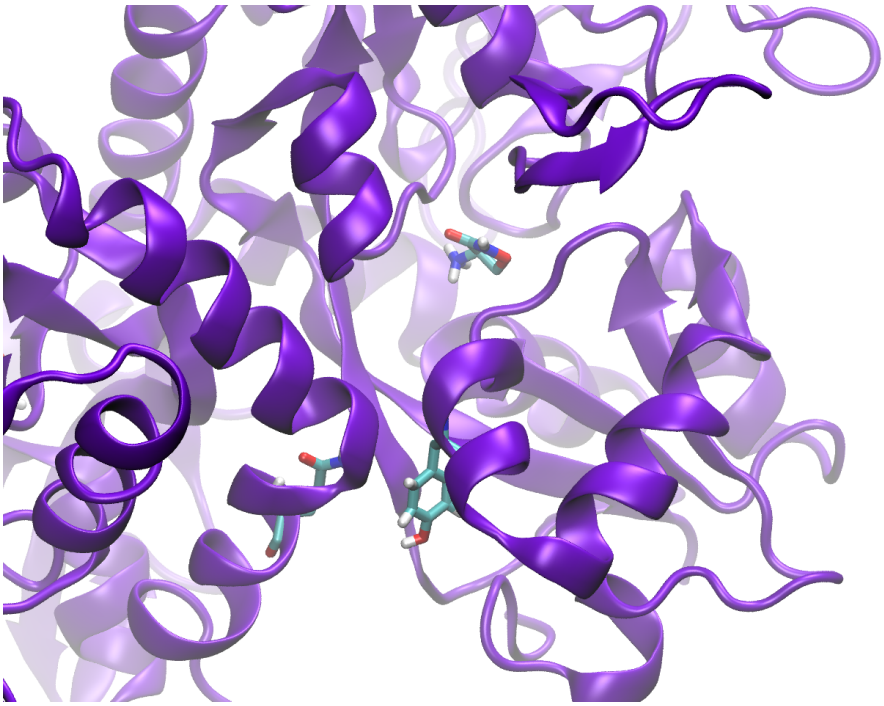

NR1_DCS/NR2C

Figure 4.21 *Comparison of the hydrogen bond found between NR1:Tyr692 and NR2C:Gln800 found in NR1_Gly/NR2C but not in NR1_DCS/NR2C*

4.5 Synopsis

Multiple simulations were performed for the NR1/NR2 ligand binding domain dimers, some with different ligands bound. Beginning with the NR1/NR2A crystal structure, homology modeling was employed to prepare dimers of NR1 with the different NR2 subtypes.[9] Most of the simulations focused on examining structural and functional differences between the NR1/NR2A and NR1/NR2D LBD dimers. These included 10 ns simulations of the receptors with the endogenous ligands, glycine and glutamate, as well as shorter 5 ns simulations where the glutamate analog SYM2081 was placed in the NR2 domain. A pair of simulations also explored the effect of the glycine analog D-cycloserine (DCS) on the NR1/NR2C dimer in contrast to the standard glycine co-agonist. All dimer simulations were prepared and performed in an identical manner, with longer initial equilibration runs than the simulations of just the NR2 domains described in the previous chapter.

The NR1/NR2A and NR1/NR2D dimers with bound glutamate were stable over the course of the long simulations. Analysis of average structures derived from the final 2 ns of simulation determined these to be stable protein structures representative of a larger portion of the molecular dynamics trajectory. A comparison of these structures revealed that most of the dimers align well to each other, with the exception of the lower domain of NR2, specifically in the region of helices F and G. Closer examination

of the agonist binding site showed a slight difference in the placement of the β and γ carbons of the glutamate ligand, yet almost all of the interactions between ligand and protein binding site were conserved. A cross-pocket interaction between the γ-carboxyl of glutamate and an adjacent backbone amide, present in NR2A, was eliminated in NR2D. Additionally, a tyrosine involved in an inter-domain contact in NR2A rotated down and formed a direct hydrogen bond with the γ-carboxyl of glutamate in NR2D. The NR1/NR2D dimer also maintained a few modified inter-domain contacts relative to the NR1/NR2A dimer. When SYM2081, a ligand with enhanced selectivity for NR2D over NR2A, was placed in the same protein structure for simulation, it proved unstable in NR1/NR2A due to a steric clash with the same tyrosine identified earlier. That tyrosine again altered its position in the NR1/NR2D simulation, alleviating any steric conflict and resulting in a stable simulation.

The simulation of NR1/NR2C containing glutamate as well as glycine or D-cycloserine examined the curious effect of the greatly increased efficacy of DCS at NR2C-containing receptors. Comparison of simulations reveal that the replacement of glycine with DCS in the NR1 ligand binding domain not only alters the position of the NR1 helices F and G, but there is an even larger displacement of helices F and G in NR2C relative to the NR1_Gly/NR2C simulation. This change in the NR1 ligand results in repositioning of regions that are over 30 Å away.

These simulations of NR1/NR2 LBD dimers predict subtle structural differences with changes in both ligand and subunit identity. Further understanding of structural differences and their functional effect on the larger receptor could facilitate the discovery of additional means of specific modulation of receptor function.

Chapter 5

Discussion

> "However beautiful the strategy, you should occasionally look at the results."
>
> — Winston Churchill

The previous chapters have described our simulations of the NR2 ligand binding domains and identified regions of the protein which vary in positioning when comparing two different NR2 subtypes as well as when comparing full and partial agonists. However, any model should be tested for validity and correlation with experimental data. Comparison of NR2 ligand binding domains revealed consistent differences over several sets of simulations. These ranged from a different positioning of a single residue in the ligand binding site to changes in the placement of portions of the lower domain. Each of these distinctions will each be examined for compatibility with other data.

5.1 Agonist Binding Site

Initial simulations of NR2A and NR2D structures derived from the NR2A LBD crystal structure were described in Chapter 3. However, analysis of the binding pocket revealed a loss of interaction between Arg520 and the α-carboxyl of glutamate (see Figure 3.13), an interaction present in every structure of an ionotropic glutamate receptor ligand binding domain and found to be critical through mutagenesis (see R520A and R520K in Table 5.1, below). This raised doubts about the validity of the simulations, and was one of the factors that prompted the transition to simulations of the NR1/NR2 ligand binding domain dimer, despite the doubling of protein size.

Comparisons of simulations of the NR1/NR2A and NR1/NR2D dimers with bound glutamate revealed some similar large-scale changes to the previous simulations of NR2

only, but glutamate kept many of the same interactions in NR2D as in the simulation of NR2A, especially on the left side of the binding pocket. The only difference observed was the repositioning of Tyr732 in NR2D, which swung down from the position of the equivalent Tyr711 in NR2A, and formed a hydrogen bond to the γ-carboxyl of glutamate (see Figure 4.12). In order to probe the differences observed in simulations and in potencies of many compounds, collaborators in the Emory lab of Traynelis as well as labs in Scotland and Denmark assembled mutagenesis data on equivalent binding site residues for the NR2A and NR2D ligand binding domains.[24] This is summarized in Table 5.1 below.

Table 5.1 *Results from Parallel Mutagenesis of Binding Site Residues in NR2A and NR2D[24, 36, 50–51]*

NR2A Mut.	$\mathbf{EC_{50}}^{\mathbf{Mut}}/_{\mathbf{WT}}$	**NR2D Mut.**	$\mathbf{EC_{50}}^{\mathbf{Mut}}/_{\mathbf{WT}}$	$^{\mathbf{shift2A}}/_{\mathbf{shift2D}}$
H466A	140	H487A	150	0.9
H466F	14	H487F	4.7	3.0
G467V	>1000	G488V	>1000	
R499A	>1000	R520A	>1000	
R499K	>1000	R520K	>1000	
S670A	0.5	S691A	0.4	1.3
S670G	120	S691G	94	1.3
T671A	900	T692A	1400	0.6
Y711F	**45**	**Y732F**	**0.4**	**113**
D712A	>1000	D733A	N.R.	
Y742F	12	Y763F	12	1.0

It is important to realize that changes in EC_{50} values do not necessarily reflect effects on ligand affinity for agonists, as they would for antagonists. There are many steps

between ligand binding and channel opening, and altered EC_{50} values may reflect modulation at any step along that pathway. Nevertheless, it is clear that among the binding site residues, the tyrosine identified through simulation is the only one with a differential effect upon mutation in NR2A versus the same mutation in NR2D. In this case, the Tyr711F mutant in NR2A decreases potency 45-fold, while the equivalent Y732F mutant in NR2D actually increases potency by a factor of two. While individual mutants may have larger effects on the EC_{50} their equivalent mutant in the other subtype has a similar effect in all cases except Tyr711/Tyr732. We hypothesize that the conservative tyrosine-to-phenylalanine mutation eliminates the inter-domain hydrogen bond between Tyr711 and Glu394, and without that interaction a phenylalanine might rotate its sidechain down into the pocket, partially occluding an open pocket or providing a steric clash with an occupied binding site. This result also corroborates the importance of including the NR1/NR2 LBD dimer in simulations. Previous simulations of just the NR2 ligand binding domain discussed in Chapter 3 predict a difference in the contact between the ligand and Arg499/Arg520, an interaction confirmed to be critical in NR2 subunits and unlikely to differ between subtypes. A distinction in the behavior of Tyr711/Ty732 only arises in simulations involving the NR1/NR2 dimer, and that difference is also singled out through mutagenesis.

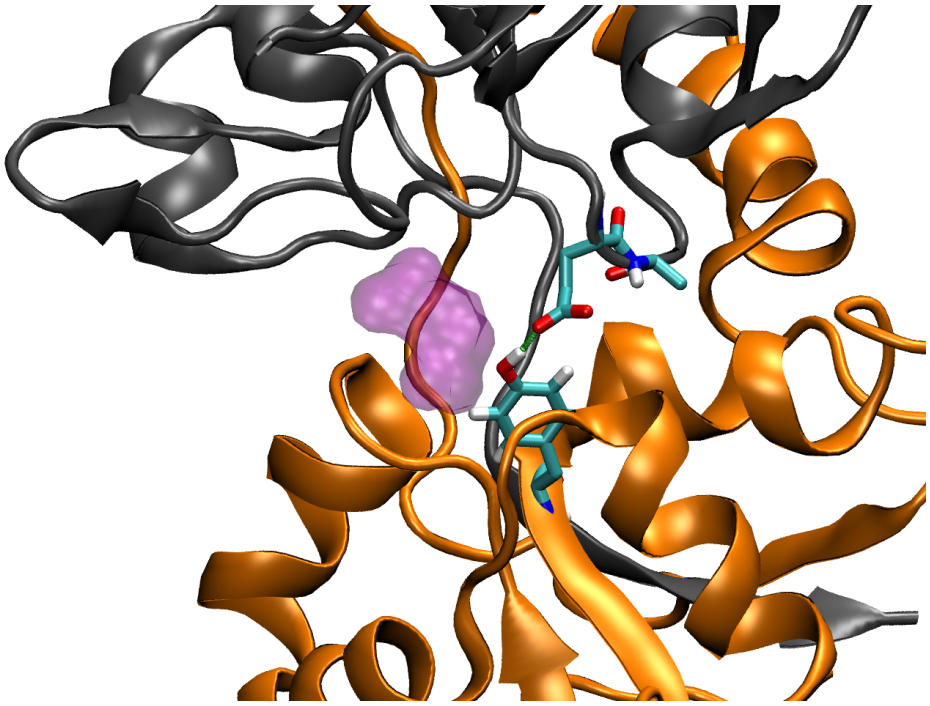

Figure 5.1 *Contact between Tyr711 and Glu394 in NR2A*

The glutamate analog SYM2081 (see Figure 4.15) was tested against the same tyrosine mutants. The Y711F mutation in NR2A decreased the potency of SYM2081 by a factor of 7, while in NR2D the Y732F mutant decreased potency 29-fold. While it may be surprising that this mutant has a larger effect on SYM2081 EC_{50} in NR2D over NR2A, several factors must be considered. First, the simulation of SYM2081 in NR1/NR2A already predicted a steric conflict between Tyr711 and the 4-methyl of SYM2081 (see Figure 4.16), therefore the effect of increased clash by the replacement of tyrosine with phenylalanine may already be a component of the increased EC_{50} of SYM2081 in NR2A. The 7-fold increase in EC_{50} may in fact be a more accurate

measure of solely the loss of the Glu394-Tyr711 interaction. The disparity between the 2-fold increase in potency for the Y732F mutation on glutamate versus a 29-fold decrease in potency for SYM2081 is harder to reconcile with the models, as both simulations place Tyr732 in a hydrogen bond with the γ-carboxyl of the ligand. However, the position of the SYM2081 ligand in NR2D is more similar to the position of glutamate in NR2A than in NR2D, implying their may be more opportunity for steric conflict (see Figure 4.10). Secondly, this mutant may influence processes prior to opening of the channel other than ligand binding. Lastly, there may be an upper limit to EC_{50} for a poor-fitting glutamate analog resulting in a smaller effect in NR2A, as the EC_{50} of SYM2081 in NR2A-containing receptors is above 1 mM.

5.2 Inter-domain Contacts

Contacts between the upper and lower domains of the ligand binding domain were noted as important factors in the complete domain closure observed with partial agonists during crystallization of the NR1 domains.[12, 26] In our simulations of NR2A and NR2D, changes occurred in the inter-domain contacts between the upper and lower domain of the LBD. This was first observed in the simulations of just the NR2 ligand binding domain, and is demonstrated in Figures 3.14 and 3.15. However, the degree of rotation between the upper and lower domains (Figure 3.11) as well as the loss of a critical interaction in the NR2D binding site raise concerns over the changes

seen in those simulations. Subsequent simulations of NR1/NR2 ligand binding domain dimers showed similar increases in the number of inter-domain contacts in the NR1/NR2D model. Consequently, our collaborators at Emory and abroad measured the effects of multiple mutations for three of the inter-domain interactions identified in the NR1/NR2D model. The results of this mutagenesis is shown below in Table 5.2.

Table 5.2 *Results from Mutagenesis of Interdomain Contacts in NR2D[24]*

NR2D Mutant	**H-bond Partner**	**EC_{50} (μM)**	**EC_{50} $^{Mut}/_{WT}$**
E519A	K694	2.5	5.0
K694A	E519	0.29	0.6
K694R	E519	0.36	0.7
K486A	N689	0.48	1.0
N689A	K486	3.1	6.4
R414A	Y739	1.9	3.8
R414K	Y739	0.82	1.7
Y739A	R414	0.06	0.1
Y739F	R414	0.6	1.3

The effects of mutation do not reveal a clear-cut case for removal of either of the residues in an inter-domain interaction resulting in similar effects on EC_{50}. However, at least one mutant at each interaction shifts EC_{50} by at least a factor of 5, with the 10-fold decrease in EC_{50} for the Y739A mutant of particular interest given the high initial potency of glutamate in NR2D. In that case in particular, the effect may be

due more to the switch of a large residue for a small one, as the Y739F mutant has little effect, and Tyr739 is in a region of hydrophobic packing between the domains. Each of these interdomain contacts is distant from the binding site, and so the shift in EC_{50} is unlikely to be the result of a direct effect on ligand binding. Multiple studies provide a precedent for the coupling of agonist affinity and efficacy in NMDA receptors, and indicates that modification of inter-domain interactions can change EC_{50} values through altering efficacy and the kinetics of receptor activation.[52–53] Thus, this increased number inter-domain contacts may modulate efficacy and contribute to the lower EC_{50} of most ligands in NR2D-containing channels compared to those with NR2A.

5.3 Displacement of Helix F and Efficacy

The rotation of the lower D2 domain of NR2D relative to NR2A was observed in both the simulations of the NR2 ligand binding domain and the later simulations of NR1/NR2 LBD dimers. Although the rotation observed in the earlier simulation is probably unrealistic, the reproduction of a 15° difference between the NR1/NR2A and NR1/NR2D dimers in portions of the D2 domain (Figure 5.2) even with the stabilizing presence of the NR1 ligand binding domain as well as correlation of binding site changes with mutagenesis lends credence to this distinction between the structures. The implications of this change in position are difficult to interpret, as NR2A-

and NR2D-containing receptors differ in many functional aspects, as highlighted in Table 2.1.

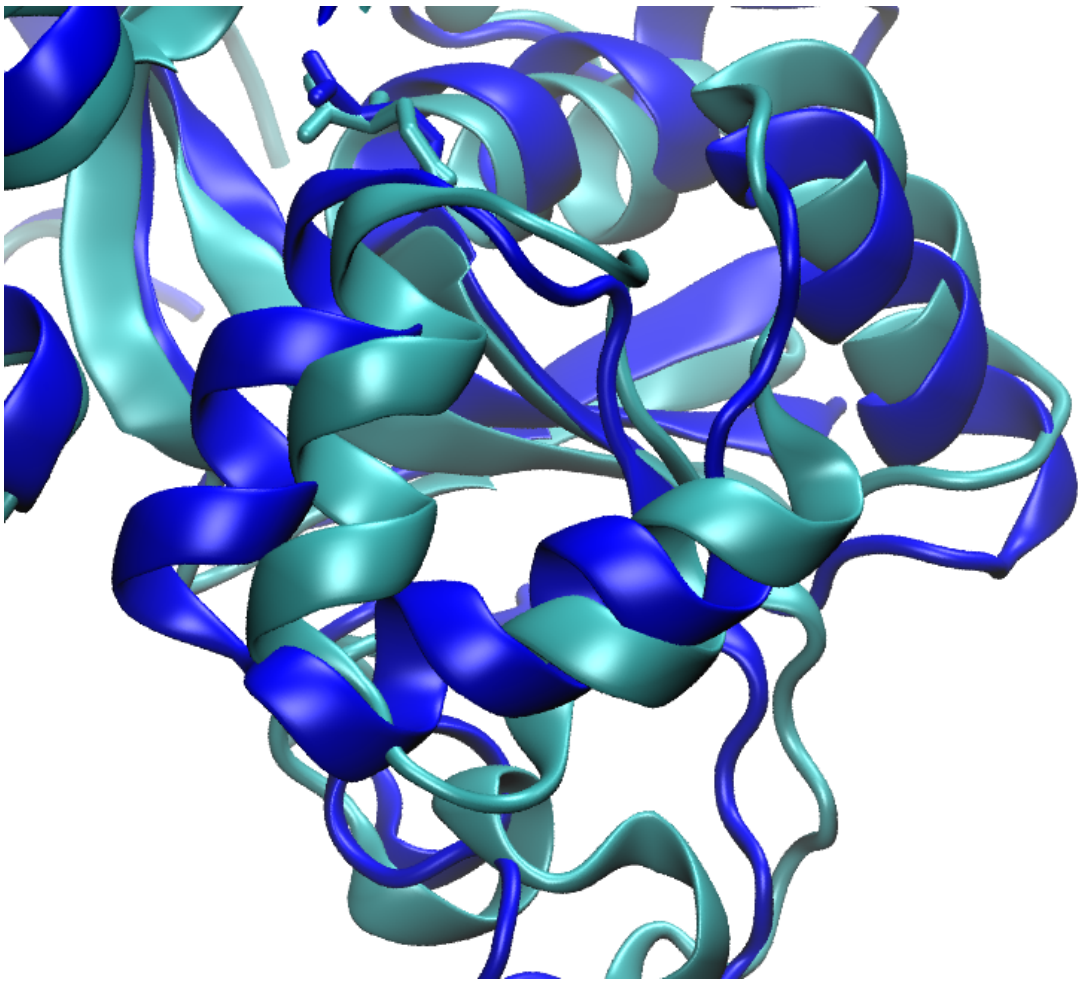

Figure 5.2 *Close up of helices F and G in average structures of NR1/NR2A_Glu (dark blue) and NR1/NR2D_Glu (light blue)*

Altered sidechain packing of residues on helix F with neighboring protein was identified as characteristic of partial agonism in crystal structures of NR1.[26] The various systems simulated over the course of this work provide three opportunities to compare

ligands with different efficacies within the same protein: the NR2A ligand binding domain with glutamate and homoquinolinate (75% efficacy), the NR1/NR2D dimer with glutamate and SYM2081 (75% efficacy), and the NR1/NR2C dimer with glycine and D-cycloserine (193% efficacy) in the NR1 binding site.[24, 49]

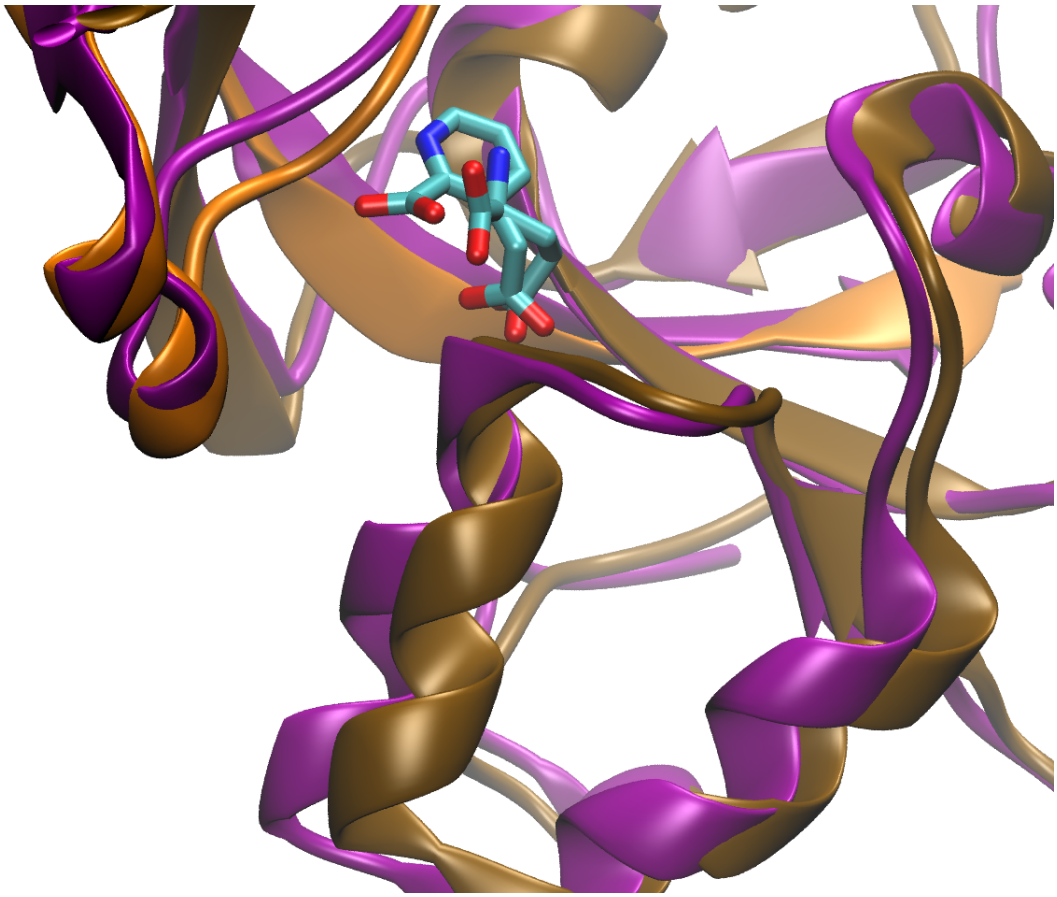

Figure 5.3 *NR2A and with glutamate (brown) and homoquinolinate (purple)*

Figures 5.3, 5.4, and 5.5 highlight the difference in positioning of helix F in each of these cases. The repositioning of the NR2 helix F is particularly interesting in the

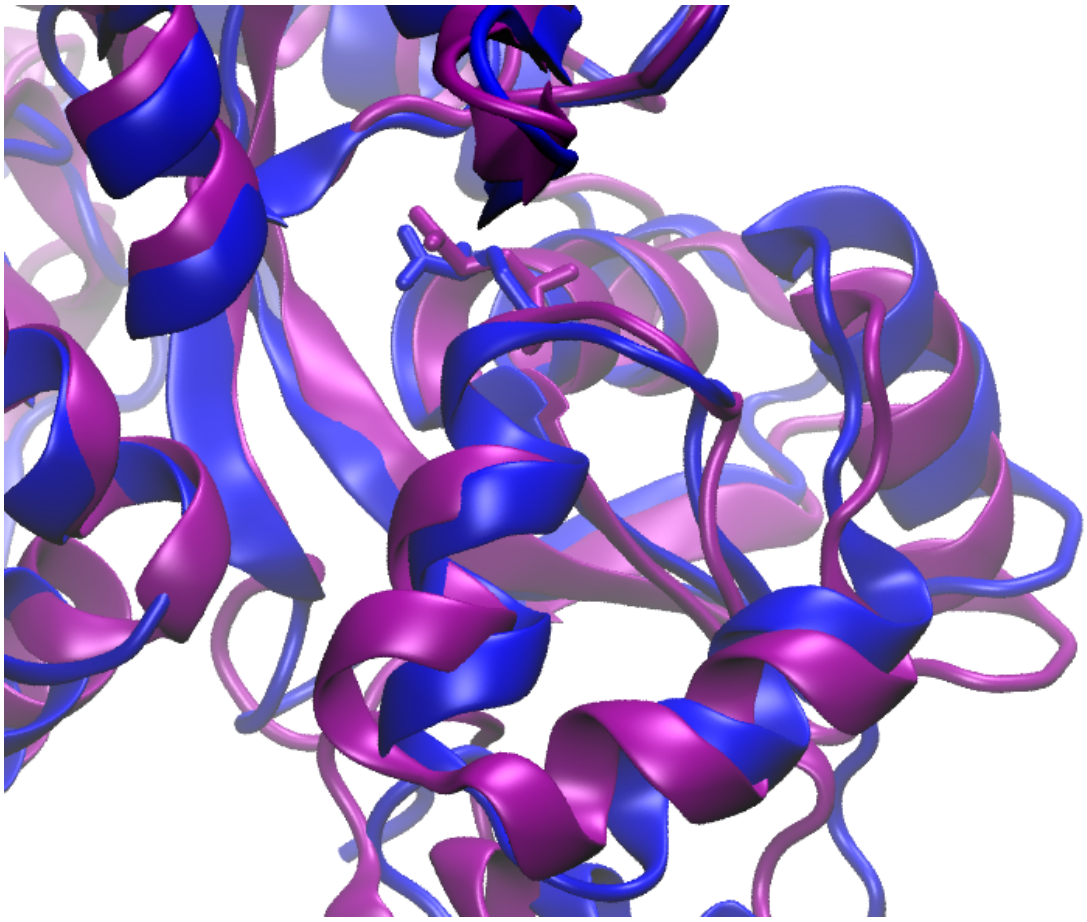

Figure 5.4 *NR2D helix F displacement with NR1/NR2D_Glu (blue) and NR1/NR2D_SYM (purple)*

case of NR1/NR2C, as the only difference between the systems simulated was the ligand (glycine or DCS) in the NR1 binding site, yet the displacement of the NR2C helix F was larger than the alteration of the NR1 helix F (see Figure 4.19) despite its proximity to the NR1 ligands. While the displacement is smaller in the cases of homoquinolinate and SYM2081 than with DCS, in each complex with lower efficacy helix F is shifted to the left, located closer to the neighboring helices of the NR1 ligand

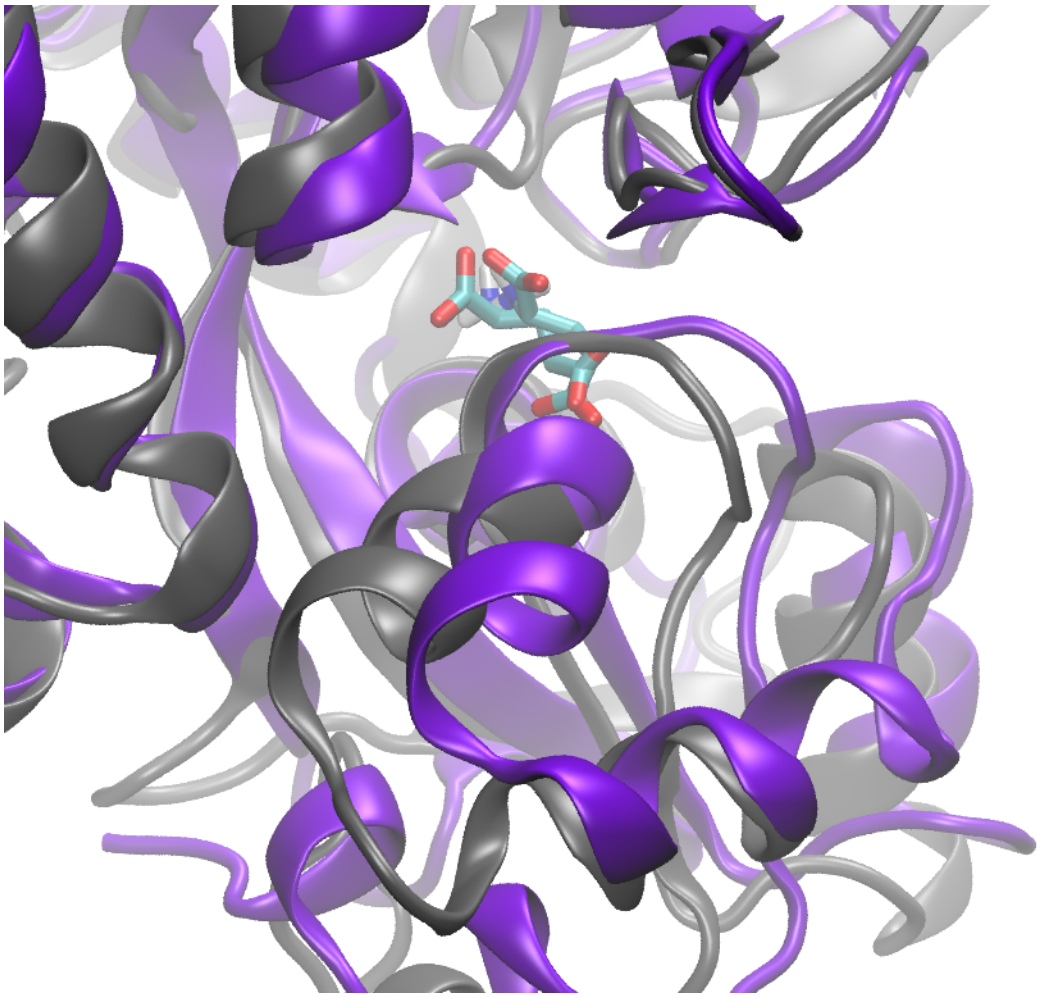

Figure 5.5 *NR2C helix F positions of NR1_Gly/NR2C (grey) and NR1_DCS/NR2C (purple)*

binding domain (although NR1 is not present in the earliest simulation with homo-quinolinate, the same shift occurs). This trend is also present in the NR1/NR2A and NR1/NR2D dimers with glutamate as shown in Figure 5.2, although it is difficult to compare efficacy between subtypes. Many functional characteristics of these subtypes

differ, but in the aspect directly connected to the ligand binding domain, ligand potency, ligands demonstrate increased potency at NR2D-containing receptors over those comprised of NR2A. Crystallographic evidence for "open" and "closed" structures of ligand binding domain dimers from other ionotropic glutamate receptors reveals that separation between the D2 domains occurs during ligand binding and is hypothesized to be a critical step in translating agonist binding to opening of the channel.[11, 54] Shifting helix F towards the neighboring NR1 LBD may subtly modulate interactions between the lower regions of the two ligand binding domains.

5.4 Conclusions

The first steps of activation of the NMDA receptor take place in the ligand binding domains. These structures bind glycine and the neurotransmitter glutamate, and change conformation from an "open clamshell" to a "closed" conformation. This conformational change is then transmitted down into the transmembrane channel situated just below the ligand binding domains, but the pathway through which agonist binding is transmitted to the pore region is unclear. The identity of the NR2 subtypes which compose the NMDA receptor clearly modulate this procedure, but the structural origins of the functional modulation are unknown.

The recent release of structural data for ligand binding domains of the NMDA receptor has brought atomic-level simulation into the realm of possibility. Stable molecular dynamics simulations of NMDA ligand binding domains in explicit solvent described in the previous chapters have enabled evaluation of predicted structural differences between subtypes as well as alterations in protein structure induced by different ligands. This modeling of the NMDA ligand binding domains has predicted variation in positioning of a sidechain within two sequentially identical binding sites that was borne out experimentally by disparate effects to equivalent mutations. Beyond individual residues, general variations in the relative positions of helix F that correlate with ligand efficacy facilitate a hypothesis for the structural determinants of partial agonism, and provide a potential rationale for the lack of partial domain closure in crystal structures of partial agonists bound to NR1. While further experiments are necessary validate and challenge these models, these simulations have predicted features of and distinctions between NR2 ligand binding domains. Advanced simulation methods with increased sampling such as replica exchange molecular dynamics as well as analysis techniques like principal component analysis will enable future simulations to address the dynamic processes of systems like the NMDA receptor. These could foster new understanding of the movements that characterize the function of this module of the NMDA receptor, as well as larger questions pertaining to the reasons behind the evolution of the NR2 subtypes.

References

[1] R. Dingledine, K. Borges, D. Bowie, and S. F. Traynelis, *The glutamate receptor ion channels*, Pharmacol Rev **51** (1999), no. 1, 7–61

[2] S. Cull-Candy, S. Brickley, and M. Farrant, *NMDA receptor subunits: diversity, development and disease.*, Curr. Opin. Neurobiol. **11** (2001), no. 3, 327–35

[3] B. Laube, J. Kuhse, and H. Betz, *Evidence for a tetrameric structure of recombinant NMDA receptors*, J Neurosci **18** (1998), no. 8, 2954–61

[4] J. E. Chatterton *et al.*, *Excitatory glycine receptors containing the NR3 family of NMDA receptor subunits*, Nature **415** (2002), no. 6873, 793–8

[5] G. Köhr, *NMDA receptor function: subunit composition versus spatial distribution*, Cell Tissue Res **326** (2006), no. 2, 439–46

[6] W. Tichelaar *et al.*, *The three-dimensional structure of an ionotropic glutamate receptor reveals a dimer-of-dimers assembly*, J. Mol. Biol. **344** (2004), no. 2, 435–42

[7] T. Nakagawa *et al.*, *Structure and different conformational states of native AMPA receptor complexes*, Nature **433** (2005), no. 7025, 545–549

[8] M. L. Mayer, *Glutamate receptor ion channels*, Curr. Opin. Neurobiol. **15** (2005), no. 3, 282–8

[9] H. Furukawa, S. K. Singh, R. Mancusso, and E. Gouaux, *Subunit arrangement and function in NMDA receptors.*, Nature **438** (2005), no. 7065, 185–92

[10] T. Kuner, P. H. Seeburg, and H. R. Guy, *A common architecture for K+ channels and ionotropic glutamate receptors?*, Trends Neurosci **26** (2003), no. 1, 27–32

[11] M. L. Mayer, *Glutamate receptors at atomic resolution*, Nature **440** (2006), no. 7083, 456–62

[12] H. Furukawa and E. Gouaux, *Mechanisms of activation, inhibition and specificity: crystal structures of the NMDA receptor NR1 ligand-binding core.*, EMBO J. **22** (2003), no. 12, 2873–85

[13] R. J. Clarke and J. W. Johnson, *NMDA receptor NR2 subunit dependence of the slow component of magnesium unblock*, J. Neurosci. **26** (2006), no. 21, 5825–34

[14] S. F. Traynelis, M. Hartley, and S. F. Heinemann, *Control of proton sensitivity of the NMDA receptor by RNA splicing and polyamines*, Science **268** (1995), no. 5212, 873–6

[15] A. Fayyazuddin *et al.*, *Four residues of the extracellular N-terminal domain of the NR2A subunit control high-affinity Zn^{2+} binding to NMDA receptors*, Neuron **25** (2000), no. 3, 683–94

[16] K. Williams, *Ifenprodil discriminates subtypes of the N-methyl-D-aspartate receptor: selectivity and mechanisms at recombinant heteromeric receptors*, Mol. Pharmacol. **44** (1993), no. 4, 851–9

[17] D. D. Mott *et al.*, *Phenylethanolamines inhibit NMDA receptors by enhancing proton inhibition*, Nat. Neurosci. **1** (1998), no. 8, 659–67

[18] Y. B. Choi and S. A. Lipton, *Identification and mechanism of action of two histidine residues underlying high-affinity Zn^{2+} inhibition of the NMDA receptor*, Neuron **23** (1999), no. 1, 171–80

[19] C. M. Low, F. Zheng, P. Lyuboslavsky, and S. F. Traynelis, *Molecular determinants of coordinated proton and zinc inhibition of N-methyl-D-aspartate NR1/NR2A receptors*, Proc. Natl. Acad. Sci. USA **97** (2000), no. 20, 11062–7

[20] C. Low *et al.*, *Allosteric interaction between the amino terminal domain and the ligand binding domain of NR2A*, Nat. Neurosci. (2001)

[21] S. Vicini *et al.*, *Functional and pharmacological differences between recombinant N-methyl-D-aspartate receptors.*, J. Neurophysiol. **79** (1998), no. 2, 555–66

[22] D. J. Wyllie, P. Béhé, and D. Colquhoun, *Single-channel activations and concentration jumps: comparison of recombinant NR1a/NR2A and NR1a/NR2D NMDA receptors*, J. Physiol. (London) **510** (1998), no. 1, 1–18

[23] N. Chen, T. Luo, and L. A. Raymond, *Subtype-dependence of NMDA receptor channel open probability*, J. Neurosci. **19** (1999), no. 16, 6844–54

[24] K. Erreger *et al.*, *Subunit-specific agonist activity at NR2A-, NR2B-, NR2C-, and NR2D-containing N-methyl-D-aspartate glutamate receptors*, Mol. Pharmacol. **72** (2007), no. 4, 907–20

[25] R. Jin *et al.*, *Structural basis for partial agonist action at ionotropic glutamate receptors*, Nat. Neurosci. **6** (2003), no. 8, 803–10

[26] A. Inanobe, H. Furukawa, and E. Gouaux, *Mechanism of partial agonist action at the NR1 subunit of NMDA receptors*, Neuron **47** (2005), no. 1, 71–84

[27] M. Karplus and G. A. Petsko, *Molecular dynamics simulations in biology*, Nature **347** (1990), no. 6294, 631–9

[28] M. Karplus and J. A. McCammon, *Molecular dynamics simulations of biomolecules*, Nat. Struct. Biol. **9** (2002), no. 9, 646–52

[29] M. Karplus and J. Kuriyan, *Molecular dynamics and protein function*, Proc. Natl. Acad. Sci. USA **102** (2005), no. 19, 6679–85

[30] I. G. Tikhonova *et al.*, *Structural basis for understanding structure-activity relationships for the glutamate binding site of the NMDA receptor*, J. Med. Chem. **45** (2002), no. 18, 3836–43

[31] Y. Arinaminpathy, M. Sansom, and P. Biggin, *Molecular dynamics simulations of the ligand-binding domain of the ionotropic glutamate receptor GluR2*, Biophysical Journal **82** (2002), no. 2, 676–683

[32] S. L. Kaye, M. S. P. Sansom, and P. C. Biggin, *Molecular dynamics simulations of the ligand-binding domain of an N-methyl-D-aspartate receptor*, J. Biol. Chem. **281** (2006), no. 18, 12736–42

[33] S. L. Kaye, M. S. P. Sansom, and P. C. Biggin, *In silico mutation of cysteine residues in the ligand-binding domain of an N-methyl-D-aspartate receptor*, Biochemistry **46** (2007), no. 8, 2136–45

[34] M.-C. Blaise, R. Sowdhamini, and N. Pradhan, *Comparative analysis of different competitive antagonists interaction with NR2A and NR2B subunits of N-methyl-D-aspartate (NMDA) ionotropic glutamate receptor*, Journal of Molecular Modeling **11** (2005), no. 6, 489–502

[35] M.-C. Blaise, R. Sowdhamini, M. R. P. Rao, and N. Pradhan, *Evolutionary trace analysis of ionotropic glutamate receptor sequences and modeling the interactions of agonists with different NMDA receptor subunits*, Journal of Molecular Modeling **10** (2004), no. 5-6, 305–16

[36] P. E. Chen *et al.*, *Structural features of the glutamate binding site in recombinant NR1/NR2A N-methyl-D-aspartate receptors determined by site-directed mutagenesis and molecular modeling.*, Mol. Pharmacol. **67** (2005), no. 5, 1470–84

[37] W. F. van Gunsteren *et al.*, *Biomolecular Simulations: The GROMOS96 manual and user guide*. (Vdf Hochshulverlag, ETH Zurich, Switzerland, 1996).

[38] H. Berendsen, D. van der Spoel, and R. van Drunen, *GROMACS: A message-passing parallel molecular dynamics implementation*, Computer Physics Communications (1995)

[39] D. van der Spoel *et al.*, *GROMACS: fast, flexible, and free*, J. Chem. Phys. **26** (2005), no. 16, 1701–18

[40] J. Hermans, H. Berendsen, and W. van Gunsteren, *A Consistent Empirical Potential for Water-Protein Interactions*, Biopolymers **23** (1984), no. 8, 1513-1518

[41] H. Berendsen, J. Postma, and W. van Gunsteren, *Molecular dynamics with coupling to an external bath*, The Journal of Chemical Physics (1984)

[42] U. Essmann *et al.*, *A smooth particle mesh Ewald method*, The Journal of Chemical Physics **103** (1995), no. 19, 8577-8593

[43] K. Erreger *et al.*, *Mechanism of partial agonism at NMDA receptors for a conformationally restricted glutamate analog*, J. Neurosci. **25** (2005), no. 34, 7858–66

[44] Prime, *version 1.5*, Schrödinger, LLC, New York, NY (2006)

[45] W. Wriggers and K. Schulten, *Protein domain movements: Detection of rigid domains and visualization of hinges in comparisons of atomic coordinates*, Proteins **29** (1997), no. 1, 1–14

[46] T. Priestley and J. A. Kemp, *Kinetic study of the interactions between the glutamate and glycine recognition sites on the N-methyl-D-aspartic acid receptor complex*, Mol. Pharmacol. **46** (1994), no. 6, 1191–6

[47] C. J. McBain, N. W. Kleckner, S. Wyrick, and R. Dingledine, *Structural requirements for activation of the glycine coagonist site of N-methyl-D-aspartate receptors expressed in xenopus oocytes*, Mol. Pharmacol. **36** (1989), no. 4, 556–65

[48] W. F. Hood, R. P. Compton, and J. B. Monahan, *D-cycloserine: a ligand for the N-methyl-D-aspartate coupled glycine receptor has partial agonist characteristics*, Neurosci. Lett. **98** (1989), no. 1, 91–5

[49] A. Sheinin, S. Shavit, and M. Benveniste, *Subunit specificity and mechanism of action of NMDA partial agonist D-cycloserine*, Neuropharmacology **41** (2001), no. 2, 151–8

[50] P. E. Chen *et al.*, *Influence of a threonine residue in the S2 ligand binding domain in determining agonist potency and deactivation rate of recombinant NR1a/NR2D NMDA receptors*, J. Physiol. (London) **558** (2004), no. Pt 1, 45–58

[51] L. C. Anson *et al.*, *Identification of amino acid residues of the NR2A subunit that control glutamate potency in recombinant NR1/NR2A NMDA receptors*, J. Neurosci. **18** (1998), no. 2, 581–9

[52] T. L. Kalbaugh, H. M. A. VanDongen, and A. M. J. VanDongen, *Ligand-binding residues integrate affinity and efficacy in the NMDA receptor*, Mol. Pharmacol. **66** (2004), no. 2, 209–19

[53] W. Maier, R. Schemm, C. Grewer, and B. Laube, *Disruption of interdomain interactions in the glutamate binding pocket affects differentially agonist affinity and efficacy of N-methyl-D-aspartate receptor activation*, J. Biol. Chem. **282** (2006), no. 3, 1863–72

[54] M. L. Mayer, A. Ghosal, N. P. Dolman, and D. E. Jane, *Crystal structures of the kainate receptor GluR5 ligand binding core dimer with novel GluR5-selective antagonists*, J. Neurosci. **26** (2006), no. 11, 2852–61

Part II

Comparison of Paclitaxel Analogs
through Molecular Dynamics Simulation

Solution Conformations of Cyclic Peptides

Chapter 6

Comparison of Paclitaxel Analogs through Molecular Dynamics Simulation

> "When the seagulls follow the trawler, it is because they think sardines will be thrown into the sea."
>
> — Eric Cantona

6.1 Introduction

The α,β-tubulin dimer plays a critical structural role throughout the cellular life cycle of eukaryotes. These individual protein units assemble into massive cylindrical polymers called microtubules (MTs), which are a cornerstone of a cell's internal cytoskeleton and play a crucial part in the cell division process. The equilibrium between unpolymerized tubulin dimers and microtubules is dynamic, and cells are able to modulate the balance between free dimer and microtubule through levels of other proteins and concentrations of other compounds such as GTP. Precise control of this dynamic equilibrium is especially critical during mitosis, where microtubules aid in formation of the mitotic spindle, a cytoskeletal element that aids in the separation of the two copies of the chromosomes. Disruption of the tubulin dimer/MT equilibrium at this phase is recognized by the cell, and can lead to programmed cell death, or apoptosis. Because of this sensitivity, compounds that alter the dynamic equilibrium have been identified as potential anticancer agents due to increased vulnerability of rapidly-dividing cells.

Paclitaxel (PTX) was the first of several compounds discovered that modulate the assembly of microtubules, and is widely used to treat breast, lung, and ovarian cancer in the clinic.[1] PTX acts to stabilize microtubules, shifting the equilibrium away from free α,β-tubulin dimer. The location of PTX binding was originally determined by

photoaffinity labeling, but the subsequent determination of the structure of the α,β-tubulin dimer through electron crystallography granted the opportunity for a more definitive determination of the binding location and conformation.[2–4] Refinement of the electron density in combination with NMR analysis of conformers in solution led to the proposition of a T-shaped conformation.[5] Figure 6.1 displays the structure of α,β-tubulin derived from electron crystallography. The lower, brown domain is α-subunit while the upper, β-subunit is colored grey. The guanidine nucleotides are colored purple, while PTX is shown in green. The M-loop, a region important for contact between neighboring tubulin dimers within a microtubule, is highlighted in red.[6–8]

6.1.1 Bridged Paclitaxel Analogs and Improved MT Assembly

An interesting feature of the activity of paclitaxel is its low nM IC_{50} in cytotoxicity assays while only having a μM apparent affinity for microtubules, and negligible binding to free α,β-tubulin.[9] This disparity is likely due to the cellular sensitivity to alteration of the equilibrium between microtubule formation and degradation. In fact, the ability of a taxoid to induce polymerization generally corresponds to its cytotoxicity, although other factors such as membrane permeability and presence of P-glycoprotein efflux pumps can modulate a compound's effect. Thus, the efficacy of these compounds is dependent on two factors: the binding of the compound to the

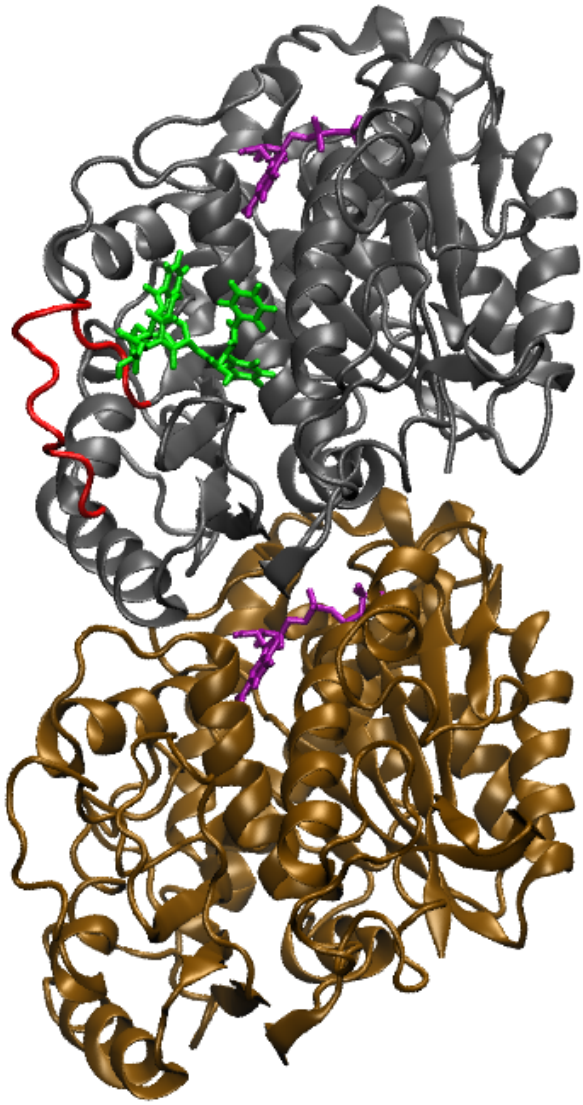

Figure 6.1 *The α,β-tubulin dimer as derived from 1JFF*

protein, and the extent to which the compound alters the protein conformation in a way to influence assembly. These can be determined separately through competition

assays to determine affinity (K_a) and measurement of the critical concentration to determine the polymerization equilibrium constant (K_p).

Many bridged derivatives of PTX have been synthesized, modified in order to be fixed in the T-conformation.[10–12] Activity of these compoounds equivalent to that of paclitaxel would be strong evidence for the validity of the T-form as the bioactive conformation. Recently, increased cyctoxicity over PTX was measured for several analogs synthesized with a linker between the C-4 acetyl and the C-3' phenyl groups.[12] Further measurements of K_a and K_p revealed an interesting discrepancy with a few of the most active ligands. While a general relationship between K_a and K_p exists, a few of the compounds have greatly increased values of K_p relative to K_a. In other words, these compounds are much more potent inducers of polymerization than their affinity would predict relative to the other compounds. The structures of two such compounds, **258** and **282**, are shown in Figure 6.2 along with the structure of PTX for reference. Both compounds have a three-carbon bridge between the moieties present on PTX: **258** containing an olefin while the bridge of **282** is saturated. In this work molecular dynamics simulations of each of these ligands bound to α,β-tubulin were performed in explicit solvent to ascertain any divergence in the behavior of PTX and the bridged analogs. Structural changes around the binding site imply this increase in polymerization may be due to modulation of cross-dimer contact.

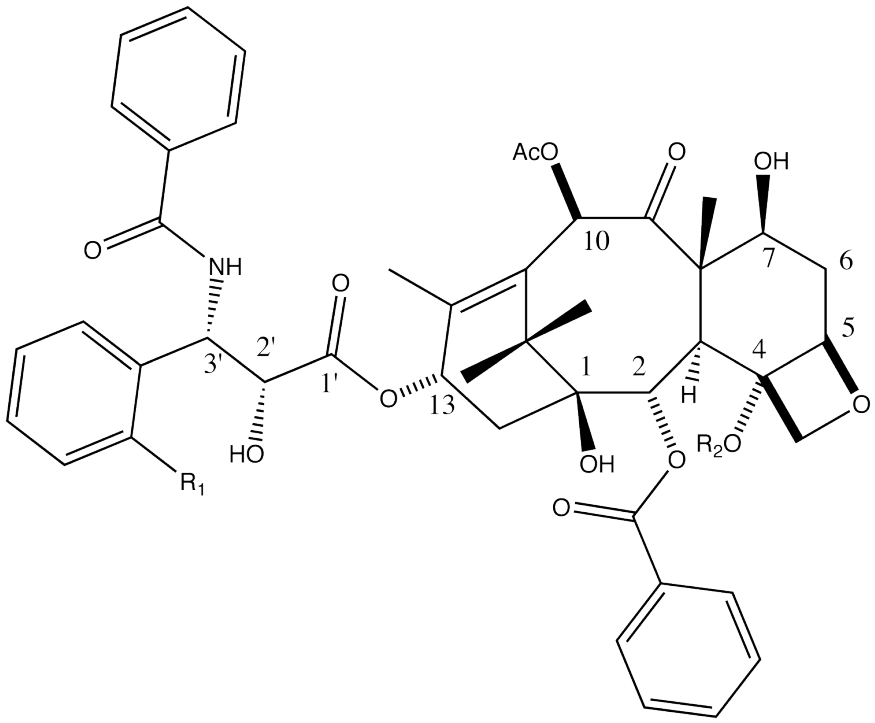

PTX, R_1: H R_2: Ac

Ligand	R_1-R_2 Linker	K_a (μM)	K_p (μM)
PTX	none	0.51 ± 0.04	55 ± 7
258	*Z*-CH_2CH-CHCO	1.22 ± 0.03	210 ± 30
282	$(CH_2)_3$-CO	1.48 ± 0.05	680 ± 100

Figure 6.2 *Structure, affinity, and polymerization data for PTX and analogs*

6.2 Methods

Complexes of α,β-tubulin with the three different ligands as well as an empty structure were all prepared from a modified protein structure based on the 1JFF structure of α,β-tubulin, which contains PTX as well as bound GTP (bound to α subunit)

and GDP (bound to the β subunit).[4] The empty structure was prepared through removal of the T-Taxol form of PTX from its binding site while leaving the GDP and GTP in place. Complexes with compounds **258** and **282** were obtained from docking results that mimicked the T-form of PTX.[13] All simulations were performed using the GROMOS96.1 force field, and all ligands were parameterized using the PRODRG topology generator.[14–15] The complexes were placed in a periodic box with 8 Å distance between protein and periodic boundary, and solvated with over 35,000 SPC water molecules.[16] Despite the presence of a magnesium cation complexed with the the phosphate groups of both GTP and GDP, 36 sodium cations were required to neutralize the overall charge of the system. All complexes were initially energy-minimized using a steepest descent algorithm. Harmonic restraints were the placed on the positions of all ligand and protein atoms, and a restrained MD simulation was run at 300K for 20 ps to allow the water and ions to equilibrate around and into the protein structure. After this solvent relaxation, the system was run unrestrained at 50K for 5 ps to allow the structure to relax in the presence of a small amount of thermal energy. The systems were then restarted at 20K, with the temperature increasing linearly to 300K over 25 ps, and then continuing on for 5 ns. Simulations of PTX-bound and empty α,β-tubulin were extended to 10 ns of simulation. A timestep of 2 fs was employed for all simulations except for the initial unrestrained simulation at 50K, which used a 1 fs timestep. NPT conditions and a Berendsen thermostat were used for all

simulations, and electrostatics were treated with PME using a 9 Å cutoff.[17–18] All simulations were performed using GROMACS v3.2.1 and visualized with VMD.[19–21] Average structures were derived from the final 1 ns of simulation. These calculations averaged slightly over 407 CPU hours per nanosecond of simulation on 2.2 GHz AMD Opteron processors.

6.3 Results

6.3.1 Ligand Positioning

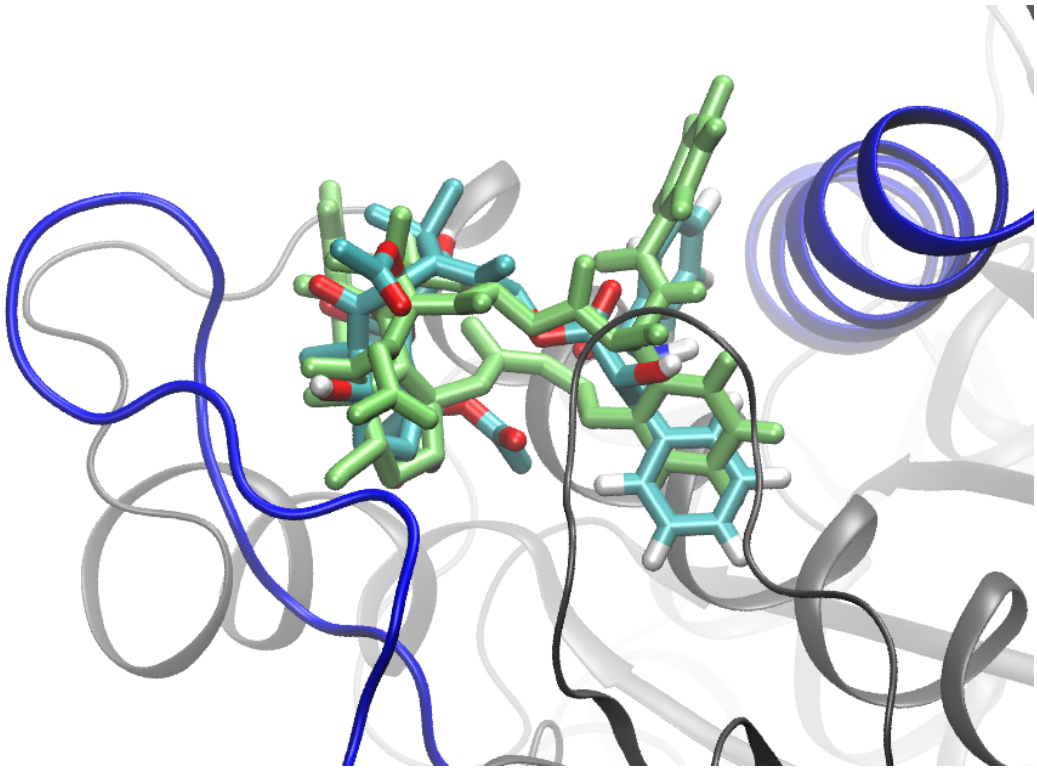

Figure 6.3 *Side view of PTX and* **258** *(green) within the binding site, with helix H1 and the M-loop colored blue*

All simulations were stable over the length of the simulations, and the ligands remained within the binding pocket of the β-subunit. Over the course of the simulation, PTX has shifted down into the binding site, leading to a deeper positioning of the C-3' phenyl group. This deeper placement is not seen in the structures of **258** and **282**, likely due to the additional steric bulk of the linker. This higher positioning of both **258** and **282** leads to a straddling of the H1 helix, a long helix that horizontally forms the inner wall of the binding pocket, by the C-3' and benzamido phenyl groups as shown in Figure 6.3. This position is stabilized by hydrogen bonds between the benzamido amide and 2'-hydroxyl and Asp26, a residue on the first turn of helix H1.[4]

Despite the similar positioning of the C-3' and benzamido groups on the inner edge of the pocket, the C-2 benzoyl phenyl group of the bridged analogs stretch out farther than that of PTX, as demonstrated in Figure 6.4. This is likely due to the spacing between the C-4 and C-3' groups induced by the three carbons inserted in **258** and **282**. The effect can be seen in distances measured from C-4 to C-3' shown in Table 6.1, where the saturated linker of **282** clearly causes a larger separation than the *Z*-olefin in the bridge of **258**. Distances are comparable to the same measurements recorded in simulations of the ligands free in solvent.[13] The extended distance of the C-2 benzoyl phenyl group from the baccatin core also corresponds to the same order as the compounds' abilities to induce polymerization.

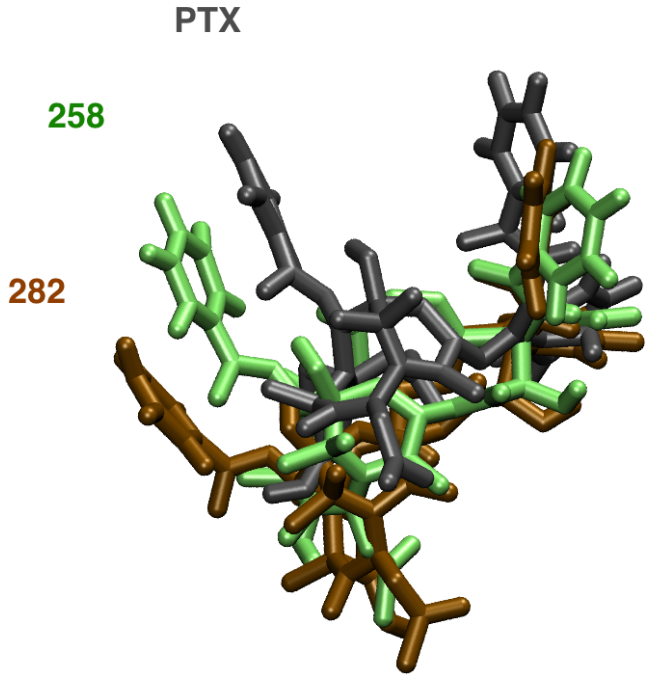

Figure 6.4 *Top-down overlay of the ligands in the pocket highlighting different positions of the C-2 benzoyl phenyl group*

Table 6.1 *C-4 to C-3' distances*

Ligand	**Distance (Å)**
PTX	5.8
258	6.1
282	7.3

6.3.2 M-loop Displacement

As shown in Figure 6.5, the conformation of the M-loop of β-tubulin varies between the different simulations. When α,β-tubulin was simulated without a ligand

present (purple in Figure 6.5), the M-loop actually moves into the region that would be occupied by PTX, and would occlude the binding pocket. This is accompanied by an upward shift of the helix directly below the M-loop. In the simulation with PTX (grey), the M-loop is clearly shifted outward by the presence of the ligand, and forms several hydrogen bonds with the outer-facing hydrophilic portion of PTX. The simulations of the bridged taxane analogs both extend the M-loop farther than occurred with PTX, with the simulation of **282** (brown) resulting in a more extended conformation than **258** (green). As seen with the ligand positioning of the C-2 benzoyl phenyl, the extent to which the M-loop conformation is extended away from the binding site correlates to the increased ability of the respective ligand to induce polymerization of the α,β-tubulin dimers to microtubules.

6.4 Discussion

Independent of the effects of the bridged taxane analogs is the repositioning of the M-loop that occurs in simulation without a ligand (see the purple loop Figure 6.5). As mentioned previously, it is known that PTX does not bind to free α,β-tubulin in solution, but rather only to polymerized α,β-tubulin.[9] The simulations performed in this work do not attempt to include effects of neighboring α,β-tubulin dimers in a microtubule, and so more directly simulate the protein as a free dimer in solution. Thus, the prediction by the empty simulation of displacement of the M-loop through

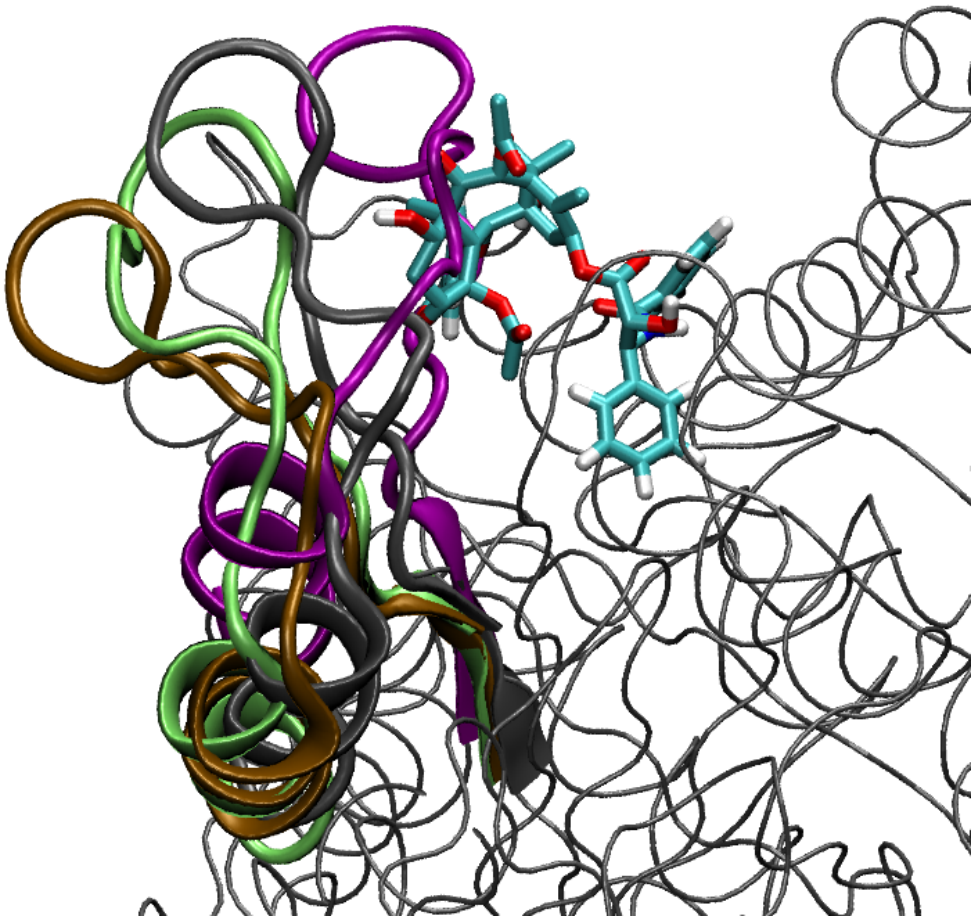

Figure 6.5 *Overlay of average structures of the M-loop region following MD simulation with PTX shown in the pocket*

the space occupied by ligand provides an explanation for the lack of PTX binding to free α,β-tubulin dimer. This movement seems to be largely driven by the sequestration of hydrophobic residues at the bottom of the taxoid binding site. Extension of the M-loop away from the center of the β-subunit, and toward the neighboring dimer reveals a deep, hydrophobic pocket into which taxanes and other ligands bind. In fact, the

T-form of PTX buries a hydrophobic region of the molecule while leaving a hydrophilic surface exposed to solvent.[5] As shown in Figure 6.6, the M-loop in the simulation without ligand performs a similar role, sliding in to cover the deep hydrophobic pocket, resulting in an overall more hydrophilic protein surface.

The simulations of α,β-tubulin with bound bridged analogs shift the M-loop in the opposite direction as seen in the simulation without ligand, with loop conformations extended farther away from the β-subunit that predicted in the simulation with PTX (see Figure 6.5). As noted previously, the bridged taxane analogs **258** and **282** sit higher in the binding pocket as shown in Figure 6.3, and place a phenyl ring on either side of helix H1, which provides a firm interior wall to the taxoid binding site. This higher positioning wedges the bridged ligands between the H1 helix and the M-loop to a greater extent than PTX. As shown in previously in Figure 6.4 the C-2 benzoyl phenyl of PTX is not extended as far as that of either bridged analog. The effect of this on the protein is detailed in Figure 6.7, which clearly shows direct contact of the C-2 benzoyl phenyl of **282** with residues of the M-loop. Thus, the extension of the C-2 benzoyl phenyl caused by the linker in the bridged analogs seems to translate to outward-shifted conformations of the M-loop. However, the inactivity of bridged analogs with 4-atom tethers implies there is a limit to the extent to which linker length translates into M-loop displacement.[12–13]

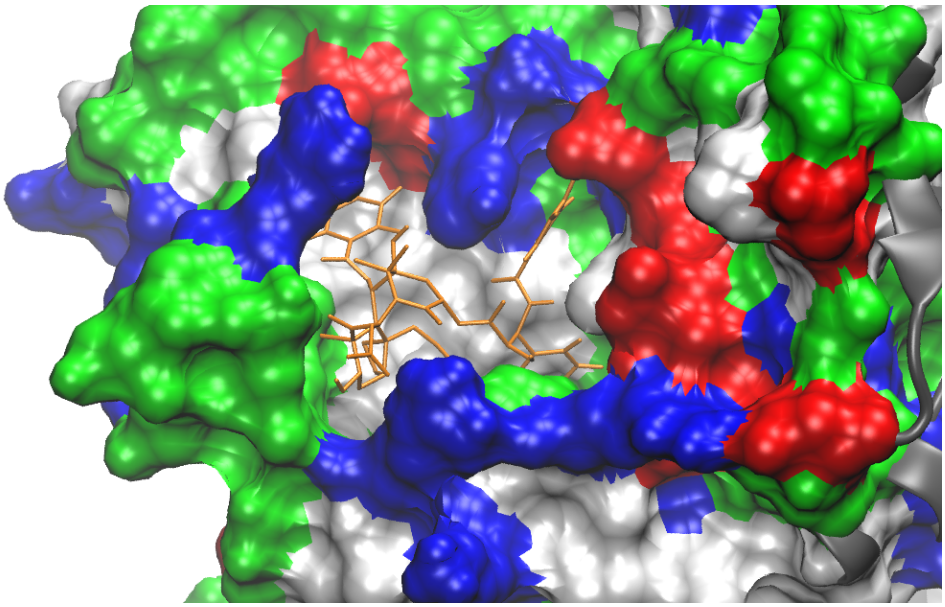

PTX-bound α,β-tubulin

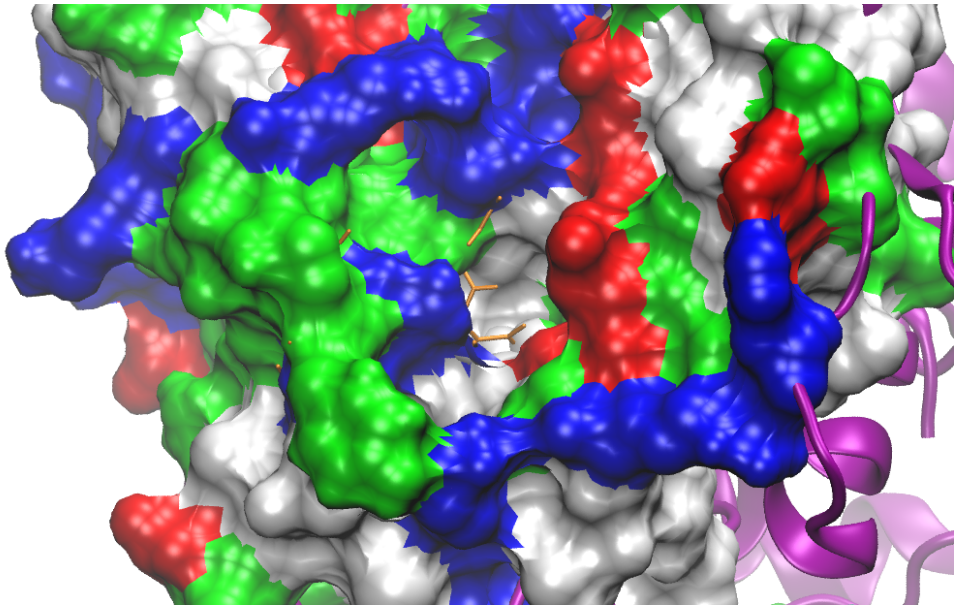

Empty α,β-tubulin

Figure 6.6 *Hydrophobic binding site residues (white) are hidden by the displacement of the M-loop into the bound position of PTX (orange)*

Although these simulations were performed on free α,β-tubulin, they require inter-

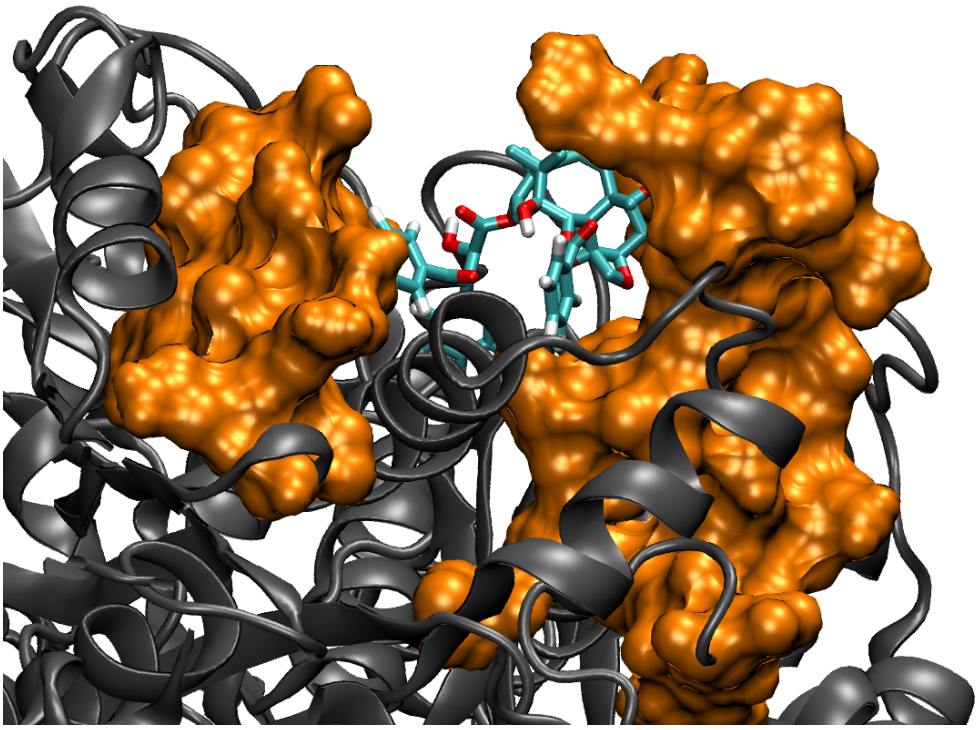

α,β-tubulin with PTX

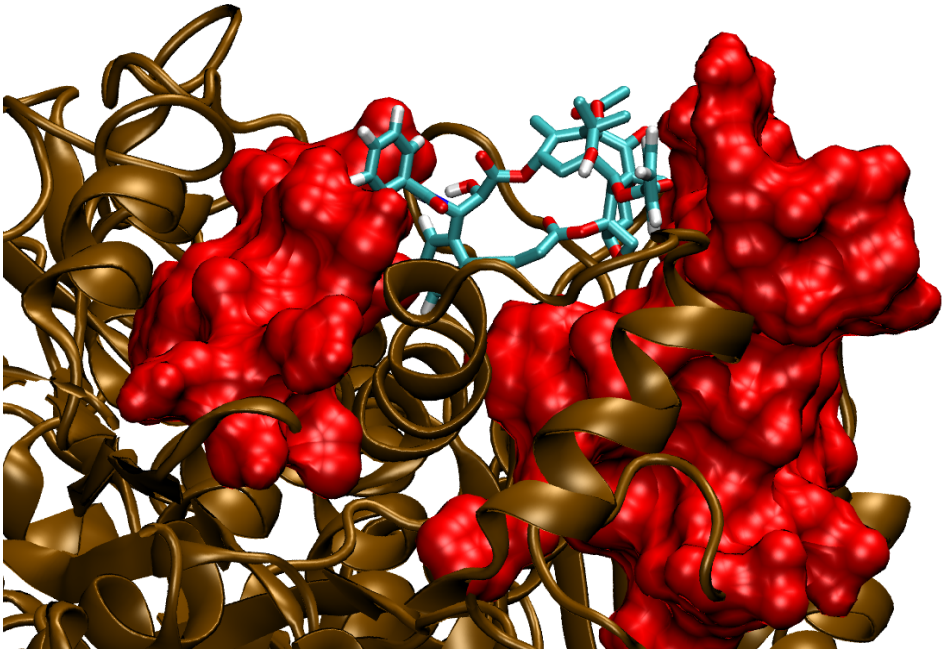

α,β-tubulin with **282**

Figure 6.7 *Positioning of ligands between helix H1 (left surface) and the M-loop (right surface)*

pretation in the context of an assembled microtubule. As the M-loop interacts with the neighboring α,β-tubulin dimer in a microtubule, it would reveal the deep hydrophobic pocket shown in Figure 6.6. The energetic cost of exposing this pocket to solvent would likely be counterbalanced by favorable interactions of the M-loop with the neighboring protein. It is likely that an equilibrium exists between the conformation with the M-loop extended to contact the adjacent dimer, and a retracted conformation obscuring the hydrophobic pocket, as predicted by the simulation without ligand. Although the conformations of the M-loop predicted in simulations with PTX, **258**, and **282** may not be realistic within the context of an assembled microtubule, they clearly induce conformations of the M-loop that would bring it into greater proximity with the neighboring α,β-tubulin dimer. In the setting of an polymerized microtubule, the effects of these ligands may manifest as a shift in equilibrium towards an M-loop conformation with favorable contacts with the protein in the adjacent protofilament.

6.5 Summary

Molecular dynamics simulations of paclitaxel and two bridged taxane analogs bound to α,β-tubulin, as well as a simulation of α,β-tubulin without a taxane ligand were undertaken to explore the curious increased polymerizing ability of these two specific analogs. Simulations predicted all three ligands to be stably bound within the binding pocket, and remain in the T-conformation. PTX slipped lower into the binding site

than the two bridged analogs, and the analogs pushed the C-2' benzoyl phenyl group farther from the opposite end of the ligands, which were braced against the H1 helix. This elongation is likely due to the linker, as evidenced by distance measurements in the region of the 3-atom bridge (Table 6.1). The conformation of the M-loop was different in each simulation as well, even in the simulation without a taxane ligand, where the loop was moved to pass through the binding site region and cover up the deep hydrophobic pocket that taxanes exploit. For the three ligands in question, the extent that C-2' benzoyl phenyl is extended correlates with both the displacement of the M-loop towards the position of an adjacent tubulin dimer in a microtubule and the enhanced ability of the ligand to induce polymerization.

These simulations suggest that the extent to which a ligand that binds in the taxoid site engenders a displacement of the M-loop towards the adjacent protofilament correlates with the capability of that ligand to induce polymerization of α,β-tubulin into microtubles. The occlusion of the taxane binding site by the M-loop in the simulation with an empty binding site also provides a structural hypothesis for the lack of PTX binding to free α,β-tubulin dimer. The potential to design ligands for favorable M-loop reorganization ahead of increased affinity raises the prospect of new molecules with high levels of anticancer activity.

Chapter 7

Solution Conformations of a Cyclic Peptide

> "Water? Never touch the stuff! Fish [make love] in it."
>
> — W. C. Fields

7.1 Introduction

Identifying the conformations of small, flexible molecules present in an aqueous environment at room temperature presents a challenging problem to both experimental and computational methods. The predominant experimental method is NMR spectroscopy, specifically 2-D NMR methods such as NOESY, that can provide geometric information about the conformation of the molecule. This information is derived from measurement of the Nuclear Overhauser Effect (NOE), which when converted provides through-space interatomic H–H distances. Separate 1-D techniques deliver a ^3J coupling constant, from which a dihedral angle can be derived. However, if transitions between conformers are fast compared to the NMR timescale, measurements become averaged and their values may not reflect any one conformation. NMR-derived information thus represents an ensemble of conformations for most small molecules. Despite the potential for averaging, the literature often erroneously selects only one conformation that best matches the NMR data as the solution conformation.[22–24]

Computational methods face linked limitations in speed and accuracy in determining conformations of small, flexible molecules in solution. For a conformational search of a flexible molecule to approach complete coverage of conformational space, large numbers of conformers must be generated and then evaluated energetically. This puts a premium on speed and limits the feasible methods for relative energy calculations

by force fields. However, it has been widely shown that force fields do not possess the level of accuracy necessary to reproduce the relative energies of conformers of complex natural products in solution.[25]

7.1.1 NAMFIS Methodology

The NAMFIS protocol addresses the conformational averaging present in NMR data by combining experimental and modeling methods. NAMFIS attempts to deconvolute averaged NMR data by finding a weighted set of reasonable conformers that as an ensemble best recreate the experimental constraints.[26] The approach is based on the proposition that force field-based conformational searches can provide accurate structures, but are unable to furnish accurate predictions of the relative energies of those conformers, especially in solution. By combining structures from a molecular mechanics conformational search with coupling constants and NOEs determined by 1D- and 2D-NMR, NAMFIS selects the subset of reasonable conformers that as an ensemble best reproduce the experimental data. However, as the conformational search was performed independent of the NMR data, the results are reasonable, low energy conformers not influenced by NMR-derived constraints. The NAMFIS protocol returns a mole fraction for each conformer in the pool, usually identifying only a handful with a mole fraction greater than 1%. Also reported is the sum of square differences (SSD), a measure of the degree to which the calculated values of the ensemble together fit

the experimental data. NAMFIS has been applied to a variety of molecules, ranging from small peptides to large bioactive compounds such as paclitaxel, laulimalide, geldanamycin, and radicicol.[11, 22, 24, 27–28]

7.1.2 D-Pro-Ala$_4$, a Cyclic Pentapeptide

Cyclic pentapeptides (CPPs) have been proposed as semi-rigid, synthetically approachable templates for drug design that can be varied easily with the use of different amino acids.[29–30] While the cyclic pentapeptide D-Pro-Ala$_4$, shown in Figure 7.1, is a simple example of a CPP, it has proved an interesting case for demonstrating the difficulty in deconvoluting NMR data by computational methods. While the NMR experiments were performed almost 15 years ago, a lengthy dispute has continued around the authors' proposals for different conformers containing a βII'-turn and a γ-turn in solution.[30–31] Later, extensive molecular dynamics simulations were performed with explicit DMSO solvent, and two stable conformations (labeled here as LitA and LitB, see Figure 7.2 below) were identified: both contained the βII'-turn and one (LitB) also contained the γ-turn.[32] Contention remained as the initial claim of a population of 15%-30% for conformations containing the γ-turn was challenged by a subsequent simulation that reported a γ-turn contribution of only 0.4% to 6.7%.[33] An altered set of solvent parameters, modified to more accurately reproduce physical characteristics, was singled out as a critical difference from the previous simulations. The authors

asserted that the presence of the γ-turn conformer was likely overestimated, and in solution D-Pro-Ala$_4$ exists almost exclusively as LitA.

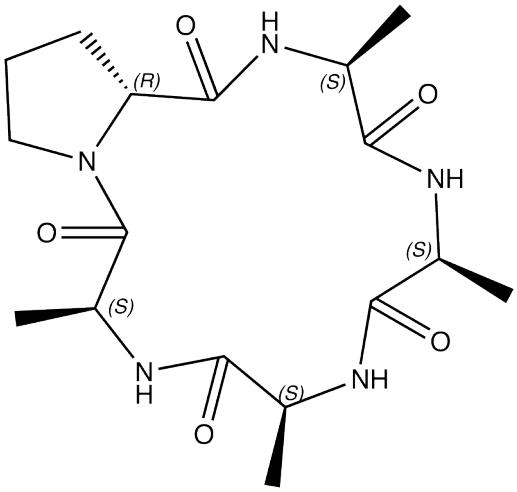

Figure 7.1 cyclo*(D-Pro-Ala$_4$)*

7.2 Methods

7.2.1 D-Pro-Ala$_4$ NMR Data

The NMR-derived distance constraints and coupling constants were obtained directly from the initial measurements of D-Pro-Ala$_4$ performed in DMSO.[31] This is the same data used in all subsequent publications and simulations by both groups. The data set is comprised of 20 NOEs and 8 ^3J coupling constants covering all α and amide protons. Error ranges for the distance constraints were also derived from the published experimental ranges. Coordinates for the structures of the two reported conformations (denoted LitA and LitB, see Figure 7.2) were obtained from supporting information.[33]

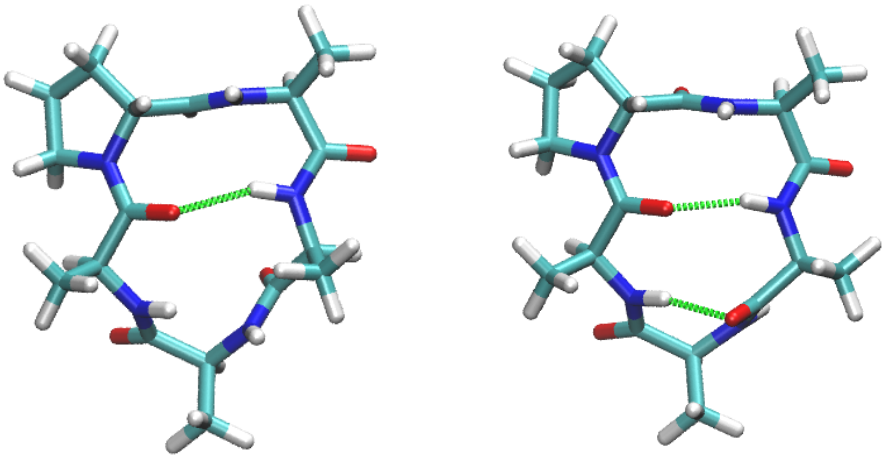

LitA LitB

Figure 7.2 *Two conformations derived from published MD simulations*

7.2.2 Conformational Searching and Clustering

The coordinates obtained for the major conformer (LitA) from the literature provided the starting structure for conformational searches in MacroModel v9.5 with three force fields (AMBER94, MMFFs, and OPLS-05) using the GBSA/H2O continuum solvation model.[34–39] In each conformational search, conformers were initially generated from 5000 steps of the Low-mode conformational search (LMCS) followed by two rounds of energy-optimization, first with 500 steps of the TNCG method, and then by 250 steps of FMNR minimization.[40–42] An energy cutoff of 25 kJ/mol was used, and a heavy-atom RMSD cutoff of 0.5 Å determined whether a conformer was considered unique. As shown in previous work, finding the global energy minimum (GEM) conformation more than 10 times is a common measure of the completeness of a

conformational search.[43] The results from these conformational searches are shown in Table 7.1. The conformer pools from each search were combined using the 0.5 Å cutoff to eliminate redundant conformers resulting in a pool of 246 unique conformers.

Table 7.1 *Results of Conformational Searches*

Force Field	**AMBER94**	**MMFFs**	**OPLS05**
# of Confs	133	273	78
E of GEM (kJ/mol)	20	176.5	-448.2
Times GEM found	63	128	189
# Confs after MultiMin	68	161	43

7.2.3 NAMFIS Calculations

NAMFIS analysis was run using the NMR constraints and conformer pool described above. The NAMFIS algorithm optimizes the mole fractions of all provided conformers to find the subset of conformations that together best reproduce the experimentally-measured geometric constraints. Multiple runs were performed with randomized initial conformer populations, all resulting in the same set of 9 conformers. Utilization of two different optimization algorithms within NAMFIS results in selection of the same 9 conformers with populations that differ by less than 1%.

7.2.4 DFT Calculations

The NAMFIS-derived conformers as well as the two previous conformers from the literature were subjected to energy minimization and analysis by density functional

theory (DFT) single-point calculation. Initially, each of the 9 conformers were minimized in the MMFFs force field. With the exception of one NAMFIS conformer (Nam5), there were no significant changes in geometry upon minimization. Torsional constraints were applied to the Nam5 conformation, which applied MMFFs bond lengths and angles while preserving torsions. A single-point energy was then calculated using a Becke3LYP/6-31G* protocol with the PBF solvation model as implemented in Jaguar.[44–48]

7.3 Results

7.3.1 MD Conformers

Although D-ProAla$_4$ has a backbone of 15 atoms, there are effectively only 9 rotatable bonds in the ring that determine the conformation of the molecule (disregarding the rotations of the alanine sidechains and conformations of the proline ring). The two conformers of the cyclic peptide presented in Figure 7.2 represent the two dominant forms of the cyclic peptide found in MD runs by both groups.[32–33] The hydrogen bond between the carbonyl of Ala5 and the amide hydrogen of Ala3, indicative of a βII'-turn, is present in both conformers. In addition, the minor conformer, LitB, also forms a hydrogen bond between the carbonyl of Ala3 and the amide proton of Ala5 forming the γ-turn. While the Kessler group indicates that the γ-turn conformation is

present in a population of 15-30%, the Marshall group suggests a contribution of LitB of 6.7% or less.

7.3.2 NAMFIS Conformers

The NAMFIS protocol identified 9 peptide conformations from the overall pool of 246 conformations that best recreate the NMR-generated geometric constraints, with individual conformation populations ranging from 3% to 27% (see Table 7.2). This set of conformers recreates the experimental NOE and coupling constants with a sum of square distances (SSD) of 7, a very small deviation from experimental values when compared to other molecules analyzed by NAMFIS. It should be remembered that this cyclic peptide has less molecular flexibility than those examined previously.

Table 7.2 *NAMFIS conformers and Relative Free Energies*

Conformer	**population (%)**	**ΔG_{boltz} (kcal/mol)**
Nam1	28	0.0
Nam2	14	0.4
Nam3	11	0.6
Nam4	10	0.6
Nam5	9	0.7
Nam6	9	0.7
Nam7	9	0.7
Nam8	7	0.8
Nam9	3	1.3

Conformations identical to both literature conformations are found within the NAMFIS set. The second most populous conformer, Nam2, matches the LitB conformation with the γ-turn, while Nam7 is essentially LitA, as shown in Figure 7.3. The highest-ranked conformation, Nam1, is very similar to LitA, however the amide proton of Ala4 is rotated towards the center, which rotates the carbonyl of Ala3 outward. This change results in a hydrogen bond between the Ala4 amide hydrogen and the Ala5 carbonyl (see Figure 7.4. Conformers Nam6 and Nam9 are very similar to Nam1, and exhibit the same two internal hydrogen bonds. A secondary run of NAMFIS on the same conformer pool augmented by the addition of the two literature conformations resulted in selection of the same conformations. None of the literature conformations were selected in place of the previously-identified similar conformations, and the population of conformers did not change appreciably.

Of the 9 conformations within the NAMFIS set, 5 conformations (representing 63% of the population) contain the hydrogen bond between the carbonyl of Ala5 and the amide hydrogen of Ala3, indicating the type II'β turn. Only one conformation, Nam2, displays the γ-turn hydrogen bond between Ala3 and Ala5, and is predicted to represent 14% of the population in solution. Several conformations exhibit different hydrogen bonds than those represented in the literature conformations. Two examples are shown in Figure 7.5, including Nam5, which reveals a contrasting γ-turn between the carbonyl of Ala2 and the amide of Ala4.

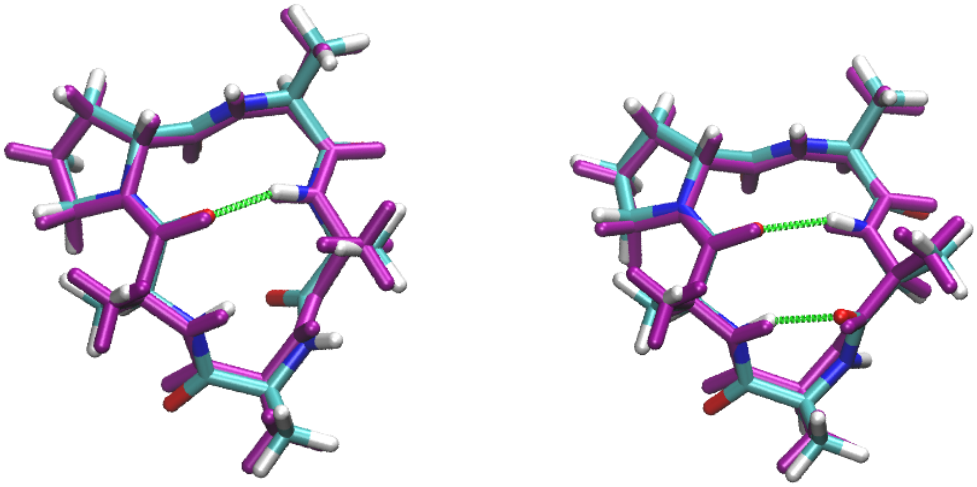

LitA and Nam7 LitB and Nam2

Figure 7.3 *Comparison of literature conformations (purple) with identical conformations selected by NAMFIS*

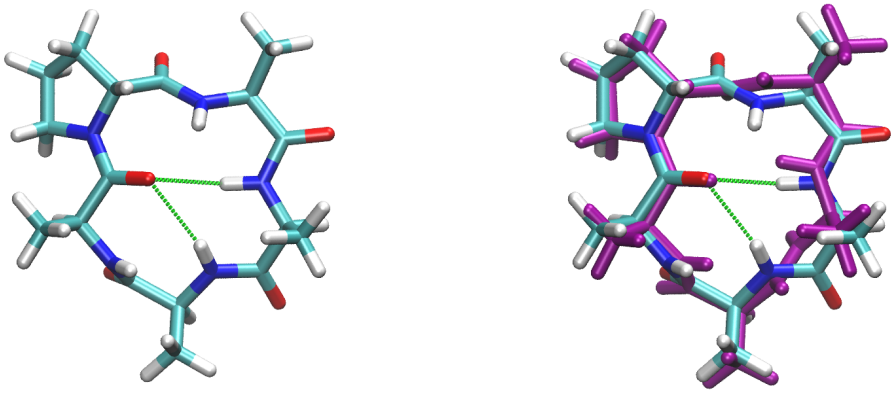

Nam1 Nam1 and LitA

Figure 7.4 *Subtle differences in amide rotation between LitA (purple) and the highest population NAMFIS conformer, Nam1*

7.3.3 Post-NAMFIS Analysis

NAMFIS selects conformers from the conformer pool based solely on geometric

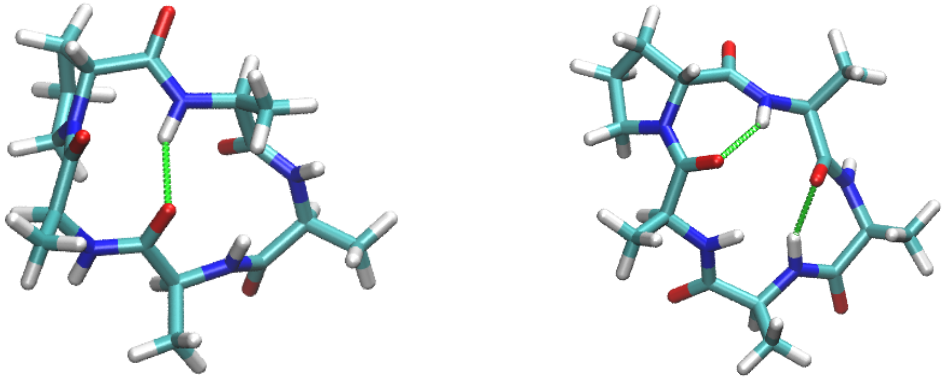

Nam4 Nam5

Figure 7.5 *NAMFIS-selected conformations unlike either literature conformation*

criteria. Only the goodness of fit between the NMR-derived constraints and the individual measurements for each conformation is considered during the optimization that results in a solution subset. Structural defects or relative energies are not evaluated. Skepticism of the accuracy of energies derived from force fields necessitates opening the energy cutoff "window" (about 6 kcal/mol in this case) wide enough to let in reasonable structures with inaccurately evaluated force field energies. However, the inclusion of poor structures with over-represented energies also increases in probability. Application of a more rigorous energy analysis is impractical on the results of a conformational search due to the large number of conformers. NAMFIS analysis reduces the number of potential conformers to a small enough subset to bring more computationally expensive energy evaluations within reason.

Post-NAMFIS analysis of the conformer energetics was conducted with DFT single-point energy calculations of a subset of the NAMFIS-selected structures. Due to similarity with the Nam1 conformer as described above, conformers Nam6 and Nam9 were removed. Conformers Nam3 and Nam8 were rejected as spurious due to relative energies of over 10 kcal/mol in comparison to the lowest energy conformer, Nam2. The remaining five conformers still provide an excellent match to the experimental data, with an SSD of 8 compared to an SSD of 7 for the set of 9 conformers. Table 7.3 provides a breakdown of the results from the DFT calculations (Becke3LYP/6-31G*//MMFFs), and a comparison to energies derived from the Boltzmann distributions reflected by the predicted populations of the remaining conformers.

Table 7.3 *Relative Energies (kcal/mol) of Reduced NAMFIS set from Boltzmann distribution and DFT Calculations (298K, Becke3LYP/6-31G*//MMFFs)*

Conformer	**population (%)**	ΔG_{boltz}	ΔE_{gas}	ΔE_{DMSO}
Nam1	40	0.0	7.0	6.4
Nam2	14	0.6	0.0	0.0
Nam4	13	0.7	12.2	5.6
Nam5	15	0.6	4.3	3.0
Nam7	18	0.5	7.1	1.0

Examination of Table 7.3 reveals several insights into the underlying energetics of these conformers. Clearly, the Boltzmann-derived relative energies (ΔG_{boltz}) and therefore the population percentages do not correlate well with the predicted enthalpies from

DFT calculations (ΔE_{gas} and ΔE_{DMSO}). This is not an "apples-to-apples" comparison, as the Boltzmann-derived energies include entropic contributions (-TΔS) while the DFT energies do not, but the lack of correspondence may also simply reflect errors within both computational methods rather than an entropic difference. Also of note is the lower energy of Nam2 to all other conformers, despite a predicted population of only 14%. This conformation with a γ-turn between Ala3 and Ala5 is lower in energy than all other conformers both in gas-phase and when a solvation term is included. As seen before the post-NAMFIS analysis, only one conformer contains the γ-turn predicted in the previously published work from both labs, and it still accounts for 14% of the conformer population. Unlike the work of other labs, conformers containing the type II'β-turn accounted for only 72% of the solution population, with two conformers without the type II'β-turn comprising the other 28%.

The energies of Nam1, Nam2, and Nam7 are of special interest due to their similarities to the conformations previously identified through molecular dynamics simulation, as detailed in Figures 7.3 and 7.4. Note that Nam1 and Nam7 differ mainly by an approximately 90 degree rotation of the amide linkage between Ala3 and Ala4 (see Figure 7.4). Their similarity is also evident in their relative gas-phase energies from our DFT calculations, shown in Table 7.3. Both Nam1 and Nam7 are about 7 kcal/mol higher in energy than Nam2 in gas-phase, but that equivalence does not occur when

solvation is taken into consideration. Nam7 is calculated to have 5.5 kcal/mol of more favorable solvation than Nam1, resulting in a large disparity between their predicted relative energies in DMSO.

Table 7.4 *Relative Energies (kcal/mol) of Literature Conformers from Boltzmann distribution and DFT Calculations (298K, Becke3LYP/6-31G*//MMFFs)*

Conformer	**population (%)**	ΔG_{boltz}	ΔE_{gas}	ΔE_{DMSO}
LitA	28	0.6	6.8	0.8
LitB	72	0.0	0.0	0.0

Conformations LitA and LitB, identical to Nam7 and Nam2 respectively, display a similar pattern of energies in DFT results, as shown in Table 7.4. Again, LitB is about 7 kcal/mol lower in energy than LitA in gas-phase, but the solvation treatment drops the difference below 1 kcal/mol. Surprisingly, when the NAMFIS conformer pool consists of only the two LitA and LitB structures, the best match to the NMR data occurs when LitB, the conformer with the γ-turn, represents 78% of the solution population, with LitA contributing only 28%. This also results in a higher SSD (33) than the SSD of 8 for the five conformations in the reduced NAMFIS set.

7.4 Discussion

The NAMFIS analysis of the D-Pro-Ala_4 cyclic peptide identified a small number of conformations which together accurately recreate the observed NMR data. Found

within this solution set are the same two conformers predicted in previous studies using other computational methods.[32–33]

7.4.1 Use of NAMFIS on small cyclic peptides

The specific case of D-Pro-Ala_4 presents a challenge for the NAMFIS methodology. The molecule is relatively inflexible, with effectively 9 dihedrals (the already somewhat restricted ϕ and ψ angles) that determine the conformation. The identity of the individual amino acids provide no added sidechain complexity, with the D-proline furnishing increased rigidity. The cyclic nature of the molecule also severely limits the range of conformations. Combination of these factors results in a restriction of conformational space available to D-Pro-Ala_4. This insures a degree of similarity between conformations, limiting the variation possible within the entire conformer pool. This is unlike most molecules to which NAMFIS has been applied in the past, as most previous molecules have at least one region with a high degree of molecular flexibility.

This lack of flexibility tests the ability of the NAMFIS methodology to discern the difference between highly similar conformations. Recall that the NAMFIS approach determines the presence of a specific conformation in solution by fit to the NMR data (via geometric criteria) alone, with no regard for energetics once the conformation is determined reasonable by the conformational search. The average RMSD over the entire conformer pool is only 1.1 Å with a maximum of 1.8 Å. However, despite

this similarity between conformers, NAMFIS allows for strong differentiation between similar conformers based on the NMR data, as evidenced in Table 7.5. Shown are the fit (SSD) of individual conformations to the NMR data.

Table 7.5 *Fit of individual conformers to NMR data*

Conformer(s)	SSD
Nam1	27
Nam2	40
Nam4	190
Nam5	87
Nam7	64
LitA	39
LitB	42
LitA and LitB	33

First, this table underscores the ability of NAMFIS to identify a subset of conformers that together provide a superior recreation of the NMR data than any one (reasonable) individual conformer. The five conformations in the reduced NAMFIS set combine for an SSD of 8, over three-fold lower than the best individual conformer. Also evident is the difference between two superficially similar conformations, LitA and Nam1 (see Figure 7.4). The sensitivity of SSD to rotation of the amide linkage between Ala3 and Ala4 is reinforced when Nam7 is included, which rotates the amide proton of Ala4 out slightly more than LitA, as shown in Figure 7.3.

The high SSD (33) of a conformer pool comprised only of LitA and LitB is conspicuous, as it implies that these two conformers alone are unable to match the NMR data to the same degree as the larger, NAMFIS-derived set (SSD of 8). In fact, when only these two conformations are included in the pool, NAMFIS predicts LitB as the dominant conformer, contrary to conclusions in the literature derived from experiment

and multiple independent MD simulations.[32–33] Detailed analysis of this result indicates the largest disagreement between the LitA and LitB NAMFIS fit and the NMR data occurs in the coupling constant (CC6) that describes the ϕ angle of Ala4, precisely the region of difference between Nam1 and Nam7/LitA. Table 7.6 displays the calculated (via the Karplus equation) coupling constant for the five conformers in the reduced NAMFIS set. It is clear from this table that a combination of the conformers Nam2 and Nam7 alone could never recreate the experimental coupling constant. The contributions of the other conformers in the reduced NAMFIS set cut the error of this specific measurement by more than half, which contributes greatly to the reduced SSD.

Table 7.6 *Calculated Values of Coupling Constant 6 for Individual Conformers*

Conformer	**CC6**
Nam1	0.1
Nam2	3.9
Nam4	0.5
Nam5	0.2
Nam7	12.4
Experiment	0.40

7.4.2 Conformation, Energy, and Solvation

In general, conformations such as LitB, which has two internal hydrogen bonds, might be expected to have lower gas-phase energies than conformers such as LitA,

which has only one. However, when solvent effects are taken into consideration, the energetic advantage of an internal hydrogen bond is often mitigated by the loss of favorable solvent interactions. This anti-correlation seems to occur in the DFT-derived energies of LitA/Nam7 and LitB/Nam2, where the differences in gas-phase energies of LitB/Nam2, approximately 7 kcal/mol lower than those of LitA/Nam7, are largely removed when the more favorable solvation of LitA/Nam7 is taken into account, reducing energy differences to 1 kcal/mol or less (see Tables 7.3 and 7.4). Further DFT calculations reveal a large difference in dipole moments of these conformations, from 5.3 debye for Nam2 to 13.3 debye for Nam7, which reinforces the stronger stabilization of Nam7 relative to Nam2 by DMSO.

The DFT energies of Nam1 present an outlier to this trend. Its gas-phase energy is similar to that of Nam7, about 7 kcal/mol above Nam2, which it largely resembles except for a rotation of the Ala3-Ala4 amide bond (see Table 7.3 and Figure 7.4). This energy parity is surprising, given that Nam1 nominally has two internal hydrogen bonds while Nam7 has only one.(Figure 7.3) However, the H–O distances in Nam1 are 0.2 Å larger than the hydrogen bond in Nam7, indicating that the hydrogen bonds may be weaker. Also, the energetic gain of a second hydrogen bond may be countered by other energetically unfavorable differences between the structures. Despite their similarity in gas-phase energy in structure Nam1 has a less favorable solvation energy by 5.5 kcal/molrelative to Nam7, which unlike the previous comparison between Nam2

and Nam7 is not correlated with the DFT-derived dipole moment (12.8 debye for Nam1, 13.3 debye for Nam7). This results in an overall energy for Nam1 that is 6.4 kcal/mol higher than Nam2, compared to an energy difference of 1 kcal/mol between Nam2 and Nam7.

7.5 Summary

The discrepancies between the DFT, NAMFIS, and NMR results are difficult to resolve. If the DFT energies are believed implicitly, then the only conformers effectively present in solution at room temperature would be LitA and LitB. However, the energy differences between these two conformations implies a 5:1 ratio of LitB to LitA, in conflict with that predicted in previous analysis as well as that performed above. Further, these two conformations alone provide an inferior fit to the experimental data when compared to expanded conformer sets. However, if NAMFIS-derived rankings are believed, Nam1 is to represent 40% of the solution conformations despite having the highest DFT-derived relative energy in solution of the conformers examined.

Despite this disagreement, valuable insights can be drawn from this work. The NAMFIS methodology was able to identify a subset of conformations that recreated the experimental NMR data to a high degree of accuracy despite the relative lack of conformational variation in D-Pro-Ala_4. This subset of conformations included both conformations predicted by groups that previously studied this molecule, yet utilized

significantly less computational time than alternative methods previously employed, such as all-atom, explicit solvent molecular dynamics simulation. Also, the importance of an accurate solvation model is highlighted by the large role that solvation energy plays in the energies of the similar conformations Nam1 and Nam7.

References

[1] P. Schiff, J. Fant, and S. Horwitz, *Promotion of microtubule assembly in vitro by taxol*, Nature **277** (1979), 665–667

[2] S. Rao *et al.*, *Characterization of the Taxol Binding Site on the Microtubule*, J. Biol. Chem. **270** (1995), no. 35, 20235–8

[3] E. Nogales, S. Wolf, and K. Downing, *Structure of the $\alpha\beta$ tubulin dimer by electron crystallography*, Nature **391** (1998), 199–203

[4] J. Löwe, H. Li, K. H. Downing, and E. Nogales, *Refined Structure of $\alpha\beta$-tubulin at 3.5 Å Resolution*, J. Mol. Biol. **313** (2001), no. 5, 1045–57

[5] J. Snyder, J. Nettles, B. Cornett, and K. Downing, *The binding conformation of Taxol in β-tubulin: A model based on electron crystallographic density*, Proc. Natl. Acad. Sci. USA (2001)

[6] E. Nogales, M. Whittaker, R. A. Milligan, and K. H. Downing, *High-resolution model of the microtubule*, Cell **96** (1999), no. 1, 79–88

[7] L. A. Amos and J. Löwe, *How Taxol stabilises microtubule structure*, Chem. Biol. **6** (1999), no. 3, R65–9

[8] H. Li *et al.*, *Microtubule Structure at 8 Å Resolution*, Structure **10** (2002), no. 10, 1317–28

[9] J. F. Díaz, M. Menéndez, and J. M. Andreu, *Thermodynamics of Ligand-Induced Assembly of Tubulin*, Biochemistry **32** (1993), no. 38, 10067–77

[10] L. Barboni *et al.*, *Synthesis and NMR-Driven Conformational Analysis of Taxol Analogues Conformationally Constrained on the C13 Side Chain*, J. Med. Chem. **44** (2001), no. 10, 1576–87

[11] T. Ganesh *et al.*, *The bioactive Taxol conformation on β-tubulin: Experimental evidence from highly active constrained analogs*, Proc. Natl. Acad. Sci. USA **101** (2004), no. 27, 10006–11

[12] T. Ganesh *et al.*, *Evaluation of the Tubulin-Bound Paclitaxel Conformation: Synthesis, Biology, and SAR Studies of C-4 to C-3' Bridged Paclitaxel Analogues*, J. Med. Chem. **50** (2007), no. 4, 713–25

[13] N. Shanker *et al.*, *Enhanced Microtubule Binding and Tubulin Assembly Properties of Conformationally Constrained Paclitaxel Derivatives*, Biochemistry **46** (2007), no. 41, 11514–11527

[14] W. F. van Gunsteren *et al.*, *Biomolecular Simulations: The GROMOS96 manual and user guide*. (Vdf Hochshulverlag, ETH Zurich, Switzerland, 1996).

[15] A. Schüttelkopf and D. van Aalten, *PRODRG: a tool for high-throughput crystallography of protein-ligand complexes*, Acta Crystallographica D **60** (2004), 1355-1363

[16] J. Hermans, H. Berendsen, and W. van Gunsteren, *A Consistent Empirical Potential for Water-Protein Interactions*, Biopolymers **23** (1984), no. 8, 1513-1518

[17] H. Berendsen, J. Postma, and W. van Gunsteren, *Molecular dynamics with coupling to an external bath*, The Journal of Chemical Physics (1984)

[18] U. Essmann *et al.*, *A smooth particle mesh Ewald method*, The Journal of Chemical Physics **103** (1995), no. 19, 8577-8593

[19] H. Berendsen, D. van der Spoel, and R. van Drunen, *GROMACS: A message-passing parallel molecular dynamics implementation*, Computer Physics Communications (1995)

[20] D. van der Spoel *et al.*, *GROMACS: fast, flexible, and free*, J. Chem. Phys. **26** (2005), no. 16, 1701–18

[21] W. Humphrey, A. Dalke, and K. Schulten, *VMD: Visual Molecular Dynamics*, Journal of Molecular Graphics **14** (1996), no. 1, 33-8, 27–8

[22] N. Nevins, D. Cicero, and J. Snyder, *A Test of the Single-Conformation Hypothesis in the Analysis of NMR Data for Small Polar Molecules: A Force Field Comparison*, J. Org. Chem. **64** (1999), no. 11, 3979–3986

[23] K. Gademann, M. Ernst, D. Seebach, and D. Hoyer, *The Cyclo-β-Tetrapeptide (β-HPhe-β-HThr-β-HLys-β-HTrp): Synthesis, NMR structure in Methanol Solution, and Affinity for Human Somatostatin Receptors*, Helv. Chim. Acta (2000)

[24] J. P. Snyder, A. S. Lakdawala, and M. J. Kelso, *On the Stability of a Single-Turn α-Helix: The Single versus Multiconformation Problem*, J. Am. Chem. Soc. **125** (2003), no. 3, 632–3

[25] A. Lakdawala *et al.*, *Calculated conformer energies for organic molecules with multiple polar functionalities are method dependent: Taxol (case study)*, BMC Chemical Biology **1** (2001), no. 1, 2

[26] D. Cicero, G. Barbato, and R. Bazzo, *NMR Analysis of Molecular Flexibility in Solution: A new Method for the Study of Complex Distributions of Rapidly Exchanging Conformations*, J. Am. Chem. Soc. **117** (1995), 1027–1033

[27] P. Thepchatri *et al.*, *Conformations of laulimalide in DMSO-d6.*, J. Am. Chem. Soc. **127** (2005), no. 37, 12838–46

[28] P. Thepchatri *et al.*, *Relationship among ligand conformations in solution, in the solid state, and at the Hsp90 binding site: geldanamycin and radicicol*, J. Am. Chem. Soc. **129** (2007), no. 11, 3127–34

[29] M. Gurrath *et al.*, *Conformation/activity studies of rationally designed potent anti-adhesive RGD peptides*, European Journal of Biochemistry **210** (1992), 911-921

[30] G. Nikiforovich, K. Kover, W. Zhang, and G. Marshall, *Cyclopentapeptides as Flexible Conformational Templates*, J. Am. Chem. Soc **122** (2000), 3262-3273

[31] D. Mierke, M. Kurz, and H. Kessler, *Peptide Flexibility and Calculations of an Ensemble of Molecules*, J. Am. Chem. Soc. **116** (1994), no. 3, 1042-1049

[32] M. Heller *et al.*, *The Conformation of cyclo(-D-Pro-Ala4-) as a model for cyclic pentapeptides of the DL4 type*, J. Am. Chem. Soc. **128** (2006), no. 42, 13806–14

[33] X. Zhang, G. V. Nikiforovich, and G. R. Marshall, *Conformational Templates for Rational Drug Design: Flexibility of cyclo(D-pro1-Ala2-Ala3-Ala4-Ala5) in DMSO solution*, J. Med. Chem. **50** (2007), no. 12, 2921–5

[34] MacroModel, *version 9.5*, Schrödinger, LLC, New York, NY (2007)

[35] W. Cornell *et al.*, *A Second Generation Force Field for the Simulation of Proteins, Nucleic Acids, and Organic Molecules*, J. Am. Chem. Soc. **117** (1995), no. 19, 5179–5197

[36] T. Halgren and R. Nachbar, *Merck molecular force field .4. Conformational energies and geometries for MMFF94*, Journal of Computational Chemistry **17** (1996), no. 5-6, 587–615

[37] T. Halgren, *MMFF VII. Characterization of MMFF94, MMFF94s, and other widely available force fields for conformational energies and for intermolecular-interaction energies and geometries*, Journal of Computational Chemistry **20** (1999), no. 7, 730–748

[38] G. Kaminski, R. Friesner, J. Tirado-Rives, and W. Jorgensen, *Evaluation and Reparametrization of the OPLS-AA Force Field for Proteins via Comparison with Accurate Quantum Chemical Calculations on Peptides*, Journal of Physical Chemistry B **105** (2001), no. 28, 6474–6487

[39] W. C. Still, A. Tempczyk, R. C. Hawley, and T. Hendrickson, *Semianalytical treatment of solvation for molecular mechanics and dynamics*, J. Am. Chem. Soc. **112** (1990), no. 16, 6127–6129

[40] I. Kolossvary and W. Guida, *Low Mode Search. An Efficient, Automated Computational Method for Conformational Analysis: Application to Cyclic and Acyclic Alkanes and Cyclic Peptides*, J. Am. Chem. Soc. **118** (1996), no. 21, 5011–5019

[41] I. Kolossavary and W. Guida, *Low-Mode Conformational Search Elucidated: Application to C39H80 and flexible Docking of 9-deazaguanine Inhibitors into PNP*, Journal of Computational Chemistry **20** (1999), no. 15, 1671–1684

[42] J. Ponder and F. Richards, *An efficient newton-like method for molecular mechanics energy minimization of large molecules*, Journal of Computational Chemistry **8** (1987), no. 7, 1016–1024

[43] G. Chang, W. Guida, and W. Still, *An Internal Coordinate Monte Carlo Method for Searching Conformational Space*, J. Am. Chem. Soc. **111** (1989), 4379-4386

[44] A. Becke, *Density-functional thermochemistry .3. The role of exact exchange*, Journal of Chemical Physics **98** (1993), no. 7, 5648–5652

[45] P. Stephens, F. Devlin, C. Chabalowski, and M. Frisch, *Ab-Initio Calculation of Vibrational Absorption and Circular Dichroism Spectra Using Density Functional Force-Fields*, J. Phys. Chem. **98** (1994), no. 45, 11623–11627

[46] D. J. Tannor *et al.*, *Accurate First Principles Calculation of Molecular Charge Distributions and Solvation Energies from Ab Initio Quantum Mechanics and Continuum Dielectric Theory*, J. Am. Chem. Soc. **116** (1994), no. 26, 11875–11882

[47] B. Marten *et al.*, *New Model for Calculation of Solvation Free Energies: Correction of Self-Consistent Reaction Field Continuum Dielectric Theory for Short-Range Hydrogen-Bonding Effects*, J. Phys. Chem. **100** (1996), no. 28, 11775–11788

[48] Jaguar, *version 7.5*, Schrödinger, LLC, New York, NY (2008)